ANNUAL REPORT

July 1983 - June 1984

NIKHEF

NIKHEF-section K--83/84

NATIONAL INSTITUTE FOR NUCLEAR PHYSICS AND HIGH-ENERGY PHYSICS AMSTERDAM

NIKHEF-K

ANNUAL REPORT

July 1983 – June 1984

Oosterringdijk 18
P.O. Box 4395
1009 AJ Amsterdam
Tel. 020 - 5919111
Telex 11538 - NL

CONTENTS

PREFACE

This report covers the scientific and technical progress of the section Nuclear Physics of NIKHEF in the period July 1983 - June 1984. Although these activities constituted the major effort of the institute, two topics - characterized by the keywords evaluation and future - required also attention.

As a result of the much improved reliability of accelerator operation, particularly at high energies, experiments on high-momentum components and proton-hole states could be performed successfully. Particularly noteworthy is the detection of the $3s_{1/2}^{-1}$ ground state of ^{207}Tl through the proton knock-out reaction on ^{208}Pb. Due to the high missing-energy resolution of the spectrometer pair the excitation of this state could be observed at low as well as at high missing momentum. This demonstrates that one may determine the $3s_{1/2}$ proton wave function which peaks in the nuclear interior. Another highlight concerns the measurements on two-body break up of ^{3}He. Both proton and deuteron knock-out reactions were studied, sometimes simultaneously. By also detecting the reaction product (^{2}H) recoil momenta up to 480 MeV/c could be covered. This is interesting since for momenta larger than 300 MeV/c one expects a strong cross-section enhancement due to final-state interactions and meson-exchange currents. The study of excitations to 0^{+} states in ^{26}Mg and ^{58}Ni has revealed the necessity of including core-polarization contributions, i.e. of 2 $\hbar\omega$ one particle - one hole excitations. On the inclusion of only a few percent (intensity) of such giant monopole resonance-like excitations an almost perfect description for the E0 transitions was obtained.

The pion and muon physics programme has also benefitted from the available higher primary electron energies. This has led to higher fluxes for the secondary particle beams. Pionic-atom X-ray studies on Mg and Al showed again, but now for the $2p \rightarrow 1s$ transitions, that the final-state widths are appreciably smaller than those predicted by the 'standard' optical potential. It seems that these and previous results may be explained by further increasing the repulsive s-wave part of the interaction, rather than by decreasing the imaginary (absorptive) part. The installation of beam hodoscopes in the pion channel together with the higher available fluxes have enabled us to perform elastic pion-scattering experiments with sufficient resolution. The first results hold promise for experiments at kinetic energies as low as 15 MeV.

The description of the nuclear electromagnetic current in the σ-ω model appears to yield quite different results from that in the standard impulse approximation. The model is being extended to describe the nucleon knock-out reaction. This may prove to be important in the analysis of proton knock-out reactions. The Δ-hole model has been extended to inclusive electron scattering above the pion-production threshold. The new table of atomic masses has been completed and is accepted for publication in Nuclear Physics.

With the opening of the new chemistry building, named after the late professor Aten, the chemists now have a well-equipped 'hot' laboratory at their disposal. There is a steadily growing activity in the exploration of radionuclide production with MEA. The longest-lived radioisotope of copper (^{67}Cu) for instance could be readily produced through the (γ,p) reaction on a ZnO target. It was shown that quantities of millicuries can be obtained. This isotope has a clear potential for biological applications. Detailed information on dynamical properties of the muonic radical of a chlorobutene has been obtained from μSR experiments at SIN.

The implementation of the 4 MW mode of operation of the accelerator klystrons caused at first severe difficulties. These problems have been overcome so that since the beginning of 1984 400 MeV beams are routinely available, though with a duty factor of 1 % to secure reliability.

Several evaluations took place in the past year. As part of the nuclear physics community, the institute was visited by a panel of experts from abroad whose task was to review the present scientific work and to give recommendations for future developments of nuclear physics in the Netherlands. The institute's activities were also considered by a Dutch committee set up by the Minister of Science and Eduation to review all physics in the country. The third evaluation of different nature - the objective being an increase of efficiency - was imposed on the institute by the same Ministry. Finally the future programme for radiochemistry has been reviewed by an external committee.

A plan for upgrading the accelerator to an almost 100 % duty factor facility has been briefly outlined in the previous annual report. Such an upgrading appeared to be the major recommendation of the nuclear physics review panel. Meanwhile this plan has been worked out into a formal proposal for UPDATE MEA that was put forward on July 1st, 1984. This proposal contains an extensive scientific motivation and the result of a feasibility study for a pulse-stretcher ring and modifications of MEA to increase the

duty factor and maximum energy of external electron beams to 90 % and 700 MeV, respectively.

Amsterdam, October 1984

Ger van Middelkoop
(scientific director)

1 ELECTRON SCATTERING

(Groupleader: C. de Vries)

1.1 Introduction

A large variety of experiments has been started and/or completed. Especially gratifying is that, besides the on-going high-resolution single-arm electron-scattering program, the experiments requiring coincidences between the scattered electron and knocked-out particles (protons, deuterons) have been quite successful. In particular, the missing-energy resolution could be made to be in the order of 100 keV, which is a major step forward compared to the resolution obtained so far elsewhere. Even for heavy nuclei (e.g. ^{208}Pb) the (e,e'p) reaction showed, under those circumstances, to be a powerful tool for the study of valence and deep-hole states.

At the other side of the periodic table the study of high-momentum components of the proton in ^{3}He has been successfully completed up to recoil momenta of $p_r \approx 500$ MeV/c. This could be achieved mainly due to the detection of the outgoing deuteron (instead of the proton) in coincidence with the scattered electron. It should be mentioned here that the liquid ^{3}He target especially designed for this purpose by Professor H. Postma and his collaborators from the T.H. Delft fulfilled all the tight specifications.

The (γ,π^-) reaction could also be employed with success due to the large suppression factor for electrons obtained with the detection telescope in the focal plane of the QDQ spectrometer.

The collaboration with Dutch universities (VU, RUU, TH (Delft)) is still growing and interest from outside users continues to be strong. As a result, about half of the present experiments is carried out by internationally composed research teams.

In the realm of the NIKHEF-K tradition a miniconference was held in November 1983 on 'Coincidence reactions with electromagnetic probes'.

1.2 Single-arm electron-scattering experiments

1.2.1 Nuclear structure and models

Monopole and other transitions in ^{26}Mg and ^{58}Ni

(H. Blok, H.P. Blok, J.F.A. van Hienen, G. van der Steenhoven and H. de Vries, in collaboration with Northwestern University and M.I.T.)

The analysis of the transitions to excited 0^+ states in ^{26}Mg and ^{58}Ni has yielded some quite interesting results. The outcome of shell-model calculations in a 1 $\hbar\omega$ model-space disagrees completely with the measured monopole form factors (see fig. 1.1). This can be understood from the form of the monopole transition operator, which shows that the predictions, especially at low q, are very sensitive to admixtures from outside the 1 $\hbar\omega$ model space, i.e. core polarization contributions. Particle-hole components in the ground state from outside the model space cannot explain the data. A rather good description of the data is obtained (see fig. 1.2) by including 2 $\hbar\omega$ 1p - 1h, i.e. giant monopole resonance like, excitations.

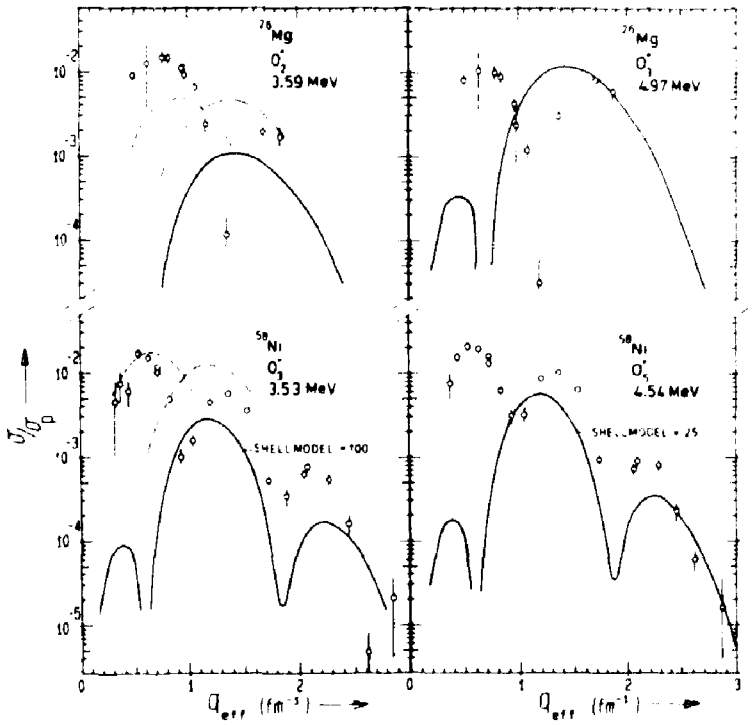

Fig. 1.1 Measured monopole form factors for ^{26}Mg and ^{58}Ni (the data taken at different incident energies have been recalculated to 361 MeV. Also shown are the shell model prediction (solid line) and the shape of a 2^+ and 4^+ form factor (dashed and dot-dashed curve).

The amplitudes squared of these admixtures in the wave functions are only a few percent. Extracted M(E0) matrix elements show that the contribution of these low-lying 0^+ states to the energy-weighted sum rule is also only a few percent. These results have been submitted for publication.

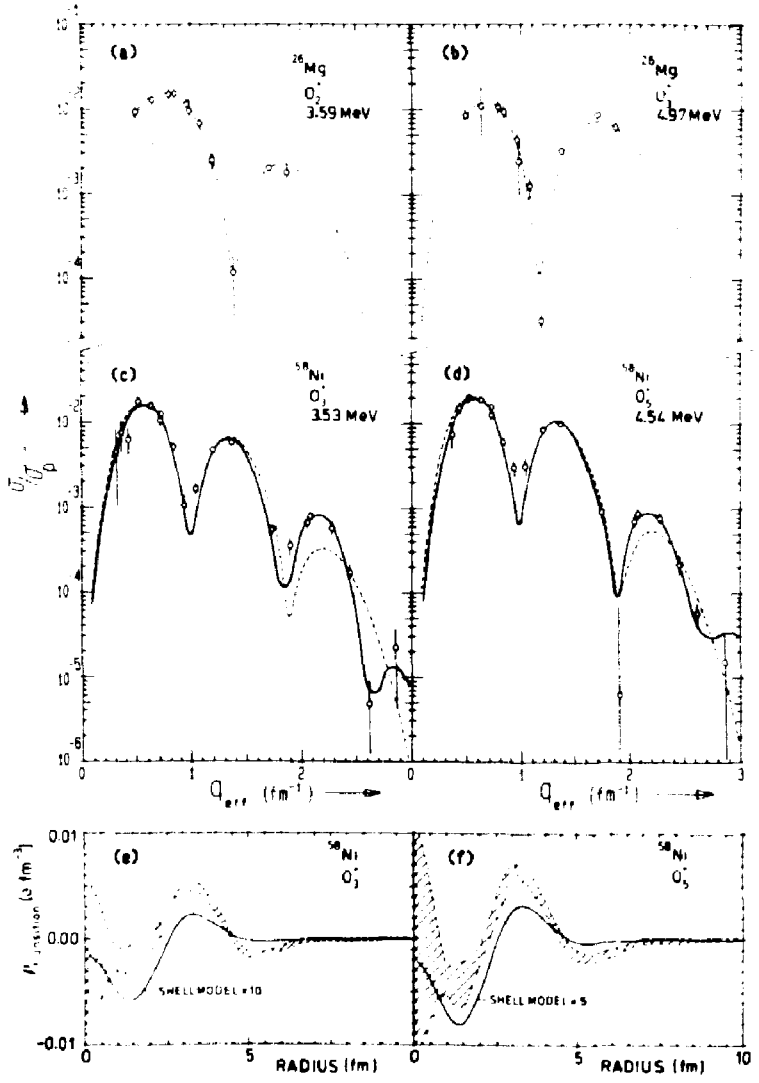

Fig. 1.2 (a-d) Fits to the measured form factors by the shell-model including a 2 $\hbar\omega$ admixture (dashed line) and from a Fourier-Bessel analysis (solid line).
(e,f) Transition densities as determined from the Fourier-Bessel analysis (shaded area) and as predicted by the shell model calculation without admixture (solid line).

For ^{26}Mg, the measured 2^+ and 4^+ form factors obtained at forward scattering angles show good agreement with shell-model calculations. A comparison with the results obtained from proton scattering resulted in numerical values for transition matrix elements for both protons and neutrons. The existing data set has recently been extended with measurements taken at higher q values (q = 1.8 - 2.8 fm^{-1}). A proposal to further extend this experiment with measurements at 154^o in order to perform a longitudinal/transverse separation, has been approved by the PAC.

The measurements for ^{58}Ni are nearly completed and the theoretical analysis of the measured form factors has been started.

Inelastic electron scattering from ^{50}Ti

(A.M. Selig, P.K.A. de Witt Huberts, I.E. Zacharov)

The aim of this experiment is to study effective electric and magnetic operators of different multipolarity. A comparison between form factors for electric and magnetic transitions provides a test of correlations between EL and M(L+1) operator pairs as predicted by e.g. schematic models [1], the shell model [2] and core-polarization calculations [3].

Electric excitations. Form factors have been determined from high-resolution spectra measured at forward scattering angles in the range of momentum transfer q = 0.6 - 2.2 fm^{-1} for the $J^\pi = 0^+_1$, 2^+_1, 4^+_1, 6^+_1 levels $((1f_{7/2})^2$ quadruplet). The form factors calculated in the shell model (inert ^{40}Ca-core) do not reproduce the present data. Additional effective proton charges $\delta e_{eff}(C\lambda)$, different for each multipole order λ, are needed to match the enhanced form factors: $\delta e_{eff}(C2) = 0.6(1)$, $\delta e_{eff}(C4) = 0.5(1)$, $\delta e_{eff}(C6) = 0.2(1)$. In the framework of core polarization with the Michigan 3-range Yukawa interaction [4] these additional effective charges are calculated to be $\delta e_{eff}(C2) = 0.20$, $\delta e_{eff}(C4) = 0.19$ and $\delta e_{eff}(C6) = 0.10$, in disagreement with the experimental values. It should be noted, however, that the typical trend of a decreasing additional effective charge as a function of multipole order is reproduced by the core-polarization calculation. At present the effect of different types of residual interactions on the effective charges is being investigated.

Magnetic excitations. A systematic survey of transverse excitation strength is performed by a Rosenbluth separation of the form-factor data. Transverse strength has been observed at $E_x = 4.892(6)$ MeV for q = 0.7 - 2.0 fm^{-1}. From the ^{49}Ti(n,γ)^{50}Ti, the ^{49}Ti(d,p)^{50}Ti reactions [5,6] and the shape of the experimental form factor - which corresponds to a $(1f_{7/2} \rightarrow 2p_{3/2})$ M5 transition - we conclude that this level has spin-parity $J^\pi = 5^+$. The shell-model calculation predicts the yrast 5^+ level at $E_x = 4.98$ MeV. Most of the strength of this level comes from the neutron $(1f_{7/2} \rightarrow 2p_{3/2})$ transition. The experimental form factor is reduced by a factor of $(0.8)^2$ with respect to the shell-model prediction. This indicates the presence of polarization effects. At present core-polarization calculations are being performed for M5 transitions.

Tests of the IBA for $^{104-110}$Pd and ^{196}Pt

(A.J.C. Burghardt, C.W. de Jager, J.B. van der Laan, H. de Vries, in collaboration with KVI, Groningen)

In the analysis of the Pd spectra approximately 30 levels are observed in each nucleus up to an excitation energy of 3 MeV. From these data the form factors for the first and second excited 2^+ states have been extracted. In all isotopes the transition charge density for the second 2^+ state peaks much more inside the nucleus than the surface peaked first 2^+ state, as is shown for ^{110}Pd in fig. 1.3. With the matrix elements, calculated by Van Isacker and Puddu [7], IBA-1 boson quadrupole structure functions $\alpha_2(r)$ and $\beta_2(r)$ were determined. This allowed a prediction for the form-factor behaviour of the third 2^+ state; this is consistent with the data. Up till now such a state has only been observed in ^{110}Pd.

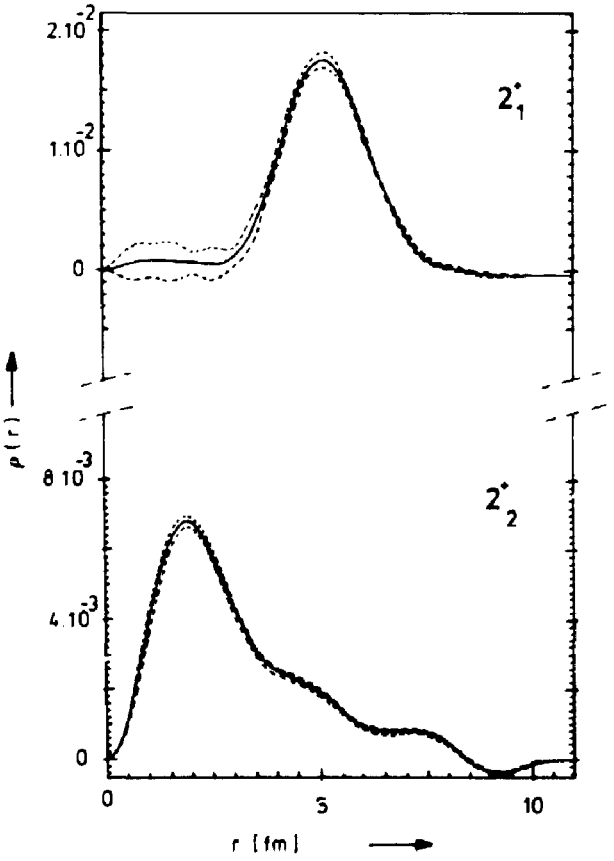

Fig. 1.3

Transition-charge densities for the first and second excited 2^+ state in ^{110}Pd. The density for the 2^+_1 peaks at the nuclear surface, that for the 2^+_2 is much more concentrated inside the nucleus.

In ^{196}Pt the excitation of three 3^- and three 4^+ states of comparable strength was observed. A reaonable description of the transition

strength and density of the 4^+ states is obtained by assuming separate hexadecapole structure functions $\beta_4(r)$ for proton and for neutron bosons. The 3^- excitations necessitate the introduction of an f-boson. A preliminary analysis successfully explains both the excitation energy and the transitions strength of all three 3^- states.

Study of the transitional nuclei ^{198}Hg and ^{204}Hg

(A.J.C. Burghardt, C.W. de Jager, H. de Vries, in collaboration with University of Virginia, Charlottesville)

Ground-state and transition densities of several nuclei in the transition region are being studied at several laboratories, especially the family of W-Os-Pt isotopes. An interesting extension of such measurements is the study for Hg isotopes, for which the intrinsic shapes range from oblate to spheroidal. The present investigation deals with ^{198}Hg (oblate) and ^{204}Hg (spheroidal).

By measuring both elastic and inelastic cross sections over a large momentum-transfer range, the ground-state and transition densities may be extracted in a model-independent way. An attempt will then be made to describe the collective states in terms of the IBA-model.

To perform this experiment targets have been constructed, composed of Li-amalgam covered by two thin Be foils. Since the targets are being rotated during beam exposure, fairly high beam currents (up to 40 μA) can be used.

Recently the first measurements have been performed at 340 MeV with a resolution of better than 10^{-4} in a momentum-transfer range of q = 0.9 - 2.2 fm^{-1}.

Measurement of longitudinal form factors in ^{15}N

(J.W. de Vries (University of Utrecht), C.W. de Jager, H. de Vries, in collaboration with the Universities of Glasgow and Massachusetts)

For the electron-scattering study of ^{15}N a room-temperature gas target was constructed, consisting of a 50 mm high cylinder with a 40 mm diameter and 40 μm wall thickness.The material used was a special aluminium alloy (2024T3) which guaranteed a high tensile strength at elevated temperatures. The target cells filled with 5 atmosphere gas, were demonstrated to withstand beam currents of 60 μA for a whole week. The diameter was chosen such that the QDD spectrometer would not 'see' scattering from the walls at

scattering angles between 40^{o} and 140^{o} without the use of internal collimators.

Data have been taken at 300 MeV and 19 scattering angles between 40^{o} and 90^{o}, thus covering a momentum transfer region of $q = 1.0 - 2.3$ fm^{-1}. For normalization purposes an identical cell filled with ^{4}He was used. The resolution obtained was 90 keV.

1.2.2 Magnetic scattering from nuclear ground states

The ground-state magnetic form factor of ^{19}F

(A.J.H. Donné, L. Lapikás, J. de la Mar, G. van Middelkoop)

The measurement of magnetic scattering from the ground state of ^{19}F at 180^{o} was completed with data taken at 126 and 137 MeV in the low-energy station LEF [8] and at 154^{o} for energies between 137 and 272 MeV in the 500 MeV station (EMIN). The targets used for the second series were teflon $(CF_2)_n$ and polyvinylidenefluoride $(CF_2CH_2)_n$. The PVDF targets could stand beam currents up to 35 μA (teflon 5 μA).

The charge-scattering contribution to the measured cross sections was determined from a Fourier-Bessel fit to the longitudinal cross sections measured at Bates [9]. The deduced magnetic ground-state form factor for ^{19}F is given in fig. 1.4 in which preliminary data from Williamson [9] are also shown.

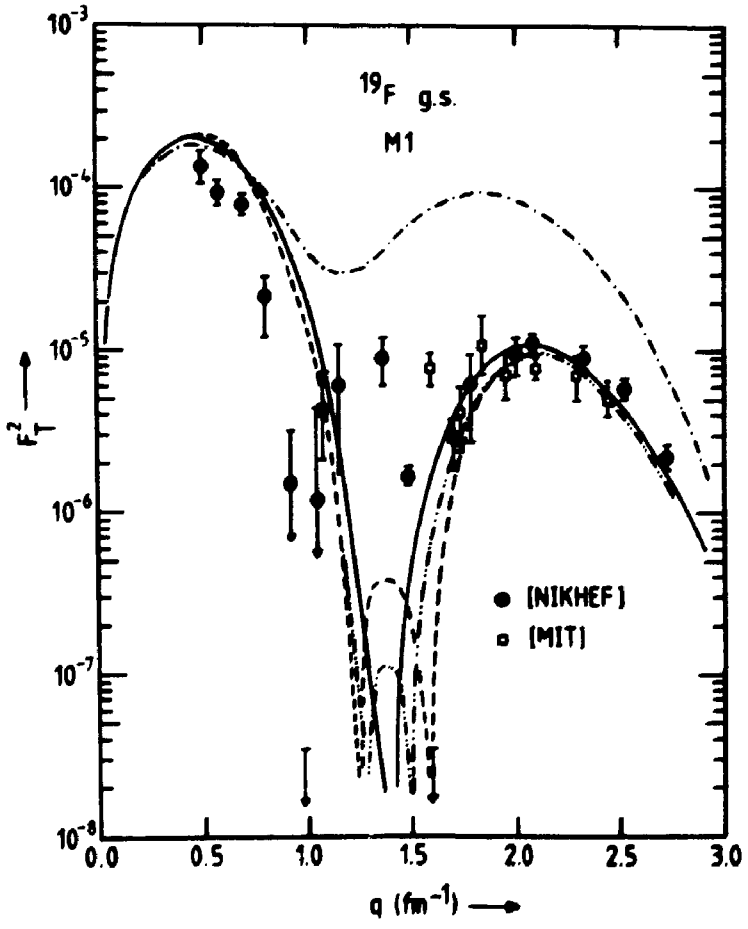

Fig. 1.4

Experimental data for the magnetic elastic form factor of ^{19}F compared with some full sd-shell model calculations: by BCWI [11] (——), MSDI [12] (---) and BCWI [12] (-.-.-.-). An extreme single-particle prediction $(\pi 2s_{\frac{1}{2}})^1$ (·-·-·) is also shown.

There is an obvious disagreement between experiment and existing shell-model calculations. Earlier full sd-shell model calculations predict only one form-factor minimum around 1.4 fm^{-1} [10,11]. Shell-model calculations performed recently by Glaudemans *et al.* [12] with the modified surface delta interaction (MSDI) and with an earlier Brown, Chung and Wildenthal interaction (BCWI) do show two minima, but the experimental behaviour between 0.9 and 1.6 fm^{-1} is still not described properly.

Recently Suzuki [13] performed a core-polarization calculation (M3Y) based on a shell-model calculation by Inoue [10] which improved the agreement with experiment considerably (see fig. 1.5). An extension of this calculation with meson-exchange currents and Δ-hole excitations results in a correct description of the experimental data for the first and second form factor maxima; the position of the third maximum is predicted at a slightly too large a momentum transfer.

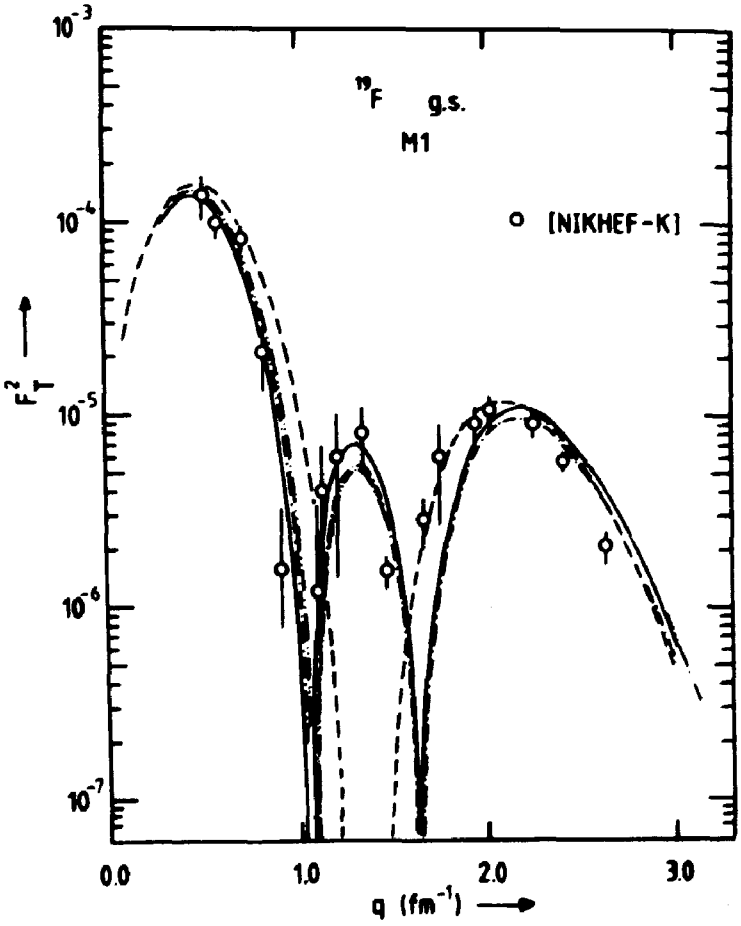

Fig. 1.5 Experimental data for the magnetic elastic form factor of ^{19}F compared with the sd-shell model calculation by Inoue *et al.* [10] (---) and with core-polarization calculations performed by Suzuki [13] (-·-·-) shell model + core polarization (M3Y), (-···-) shell model + core polarization (M3Y) + exchange currents (pair + pionic), (——) shell model + core polarization (M3Y) + exchange currents (pair + pionic) + Δ-hole excitations (π+p).

Core polarization of ^{49}Ti

(L. Lapikás, A.M. Selig, T. Suzuki, P.K.A. de Witt Huberts, in collaboration with C.E.N. Saclay)

Cross sections have been determined for magnetic scattering from the $J^{\pi} = 7/2^-$ ground state of ^{49}Ti. The deduced form factor is shown in fig. 1.6. The observed strength is considerably less than calculated for a single $1f_{7/2}$ neutron (heavy dashed curve). Shell-model calculations with an inert ^{40}Ca-core have been performed by Zybert, Mooy and Glaudemans [14]. The calculation reproduces both the experimental value of the dipole moment and the high-q M7 form-factor data of Platchkov *et al.* [15], but overshoots the present intermediate-q form-factor data.

As a next step beyond the shell-model prediction the core-polarization (CP) effect has been evaluated [16]. Three different mechanisms have been taken into account:

- Nucleonic core polarization (NCP) with the Michigan 3-range Yukawa (M3Y) residual interaction (dot-dashed curve),
- NCP + pion + pair meson exchange currents (MEC) (thin full curve),
- NCP + MEC + Δ_{33}-isobar currents (heavy full curve).

The decomposition of the calculated total (NCP + MEC + Δ_{33}) form factor (heavy full curve) in its individual multipoles (light dashed curve) is also shown in fig. 1.6.

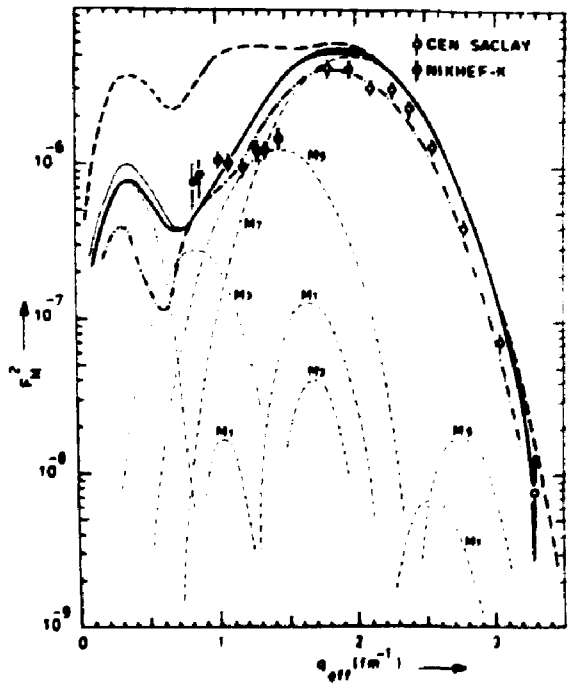

Fig. 1.6

The elastic magnetic form factor for ^{49}Ti. For explanation of the curves see text.

The calculation comes very close to reproducing the large quenching of the form-factor data at intermediate q. In comparison with the shell-model calculation this improvement is mainly due to the interfering effect of MEC and NCP which appears to reduce the second lobe of the M1 form factor by a factor of seven. It should be noticed that the influence of Δ_{33}-isobar currents is negligible relative to the NPC and MEC effects in the momentum-transfer range of this experiment. The data which cover M1, M3, M5 and M7 multipoles therefore constitute a severe test for the NCP and MEC mechanism and in particular for the residual interaction used in the calculation.

1.2.3 Magnetic dipole transitions

An 1-forbidden M1 transition in ^{39}K

(C.W. de Jager, P.H.M. Keizer, E.A.J.M. Offermann)

The study of orbital-momentum forbidden M1 transitions yields a sensitive measure for subnuclear effects such as meson exhange and Δ-isobar currents [17]. For that purpose the $1d_{3/2} \rightarrow 2s_{1/2}$ M1 (+E2) transition in ^{39}K leading to the 2.53 MeV state has been studied. The B(M1) value obtained from this work, B(M1) = (0.014 ± 0.006) μ_N^2 is in good agreement with earlier findings [18]. The best available calculation that includes isobar and meson-exchange currents as well as second-order core polarization [19] underestimates the strength by a factor of six. The measured transverse form factor (M1 + E2) can also not be reproduced theoretically [20]. The E2 form factor alone already comes out too high at the first maximum; the same calculation, however, does reproduce the Coulomb form factor.

Electro-excitation of the 1^+ state at E_x = 3.486 MeV in ^{88}Sr

(L.T. van der Bijl, H. Blok, H.P. Blok, R. Ent, P.K.A. de Witt Huberts, in collaboration with University of New Hampshire and Technische Hochschule Darmstadt)

The differential cross section for excitation of the 1^+ state at E_x = 3.486 MeV in ^{88}Sr by inelastic electron scattering has been measured for values of the momentum transfer q between 0.22 and 2.57 fm^{-1}. Both nuclear core polarization and Δ-hole polarization seem to be necessary to describe the observed reduction of the B(M1)-value and data at low q and the behaviour of the cross section at intermediate values of q (see fig. 1.7). The results have been published [21].

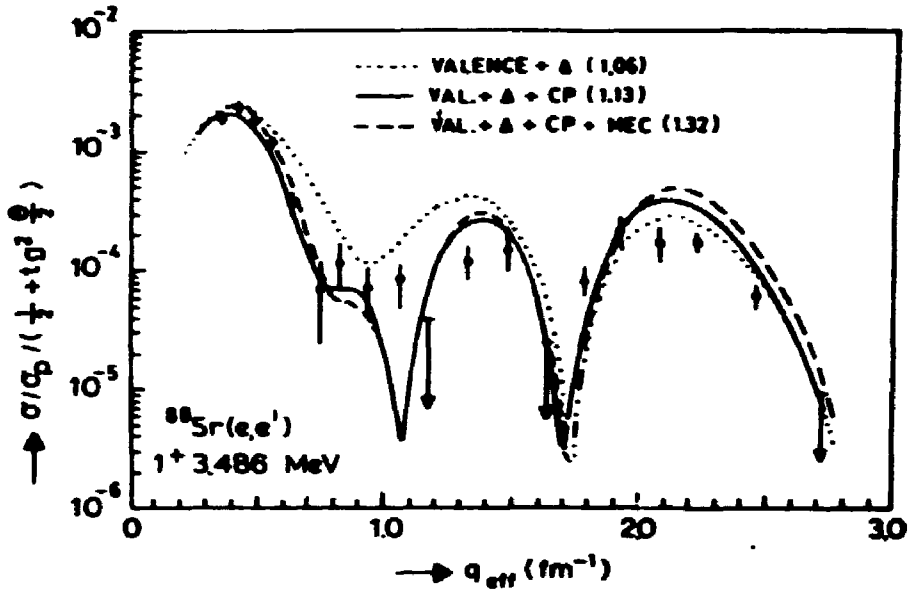

Fig. 1.7 Measured M1 form factor for the 1^+ state at 3.486 MeV in ^{88}Sr compared to calculations in-including the effects of the Δ(1232). The numbers in brackets are the corresponding B(M1)-values (in units of μ_N^2).

The 1^+ state at 5.846 MeV in ^{208}Pb

(H. Blok, H.P. Blok, C.W. de Jager, H. de Vries, in collaboration with Technische Hochschule Darmstadt)

The analysis of the spectra taken at 77 and 91 MeV confirmed the presumed isoscalar character of the M1 transition to the 5.846 MeV level. The shape of the form factor can be explained correctly by RPA calculations [22] that include tensor correlations from π and ρ exchange; the absolute size, however, is underestimated (see fig. 1.8). Three more spectra have been measured at 154^0 and energies of 105, 120 and 138 MeV. At the corresponding q_{eff}-values (1.2 - 1.5 fm^{-1}) one expects to see the influence of 1-forbidden particle-hole components.

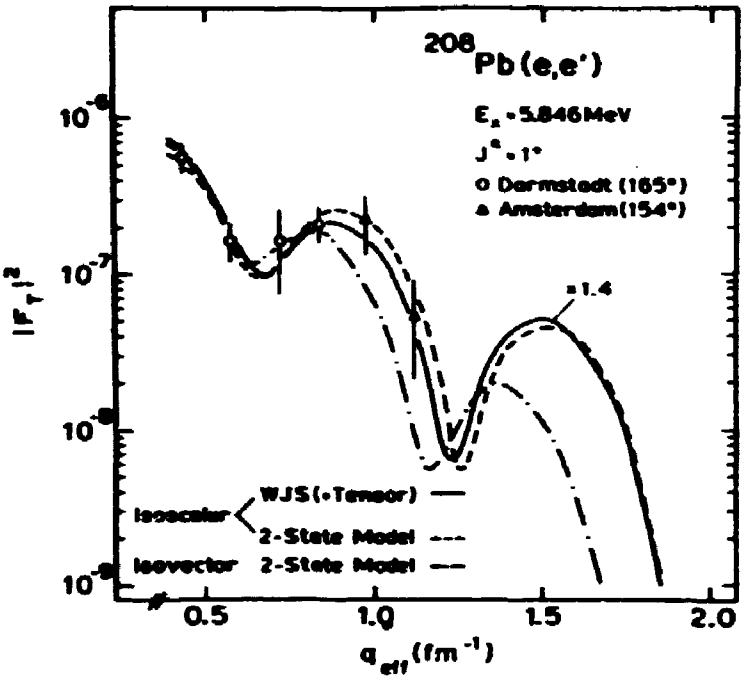

Fig. 1.8

Comparison of the experimental form factor of the $J^\pi = 1^+$ state to various theoretical predictions. The solid line shows the results of a DBWA calculation using wave functions of ref. 22. The dashed and dash-dotted lines result from two-state model wave functions assuming an isoscalar and isovector mode, respectively.

1.2.4 High-spin stretched configurations

Electro-excitation of 8^- states in ^{52}Cr

(R. Ent, J.F.A. van Hienen, C.W. de Jager, H. de Vries, in collaboration with Argonne National Laboratory and University of Birmingham)

The experimental study of the electron-induced excitation of high-spin states in ^{52}Cr has been completed. Spectra of electrons scattered through 154^0 have been taken at incoming electron energies of 170, 200, 230 and 260 MeV. Together with measurements taken at 90^0 and 115^0 at 260 MeV this will allow for a unique identification of 8^- states. A preliminary analysis reveals some seven 8^- states. The data will be compared with results obtained with hadronic probes (proton and pion scattering on ^{52}Cr and (^{3}He,d) on ^{51}V).

Stretched-spin states in ^{116}Sn

(C.W. de Jager, H. de Vries, in collaboration with KVI, Groningen)

Forward-angle electron-scattering experiments have been performed for q-values between 1.4 and 2.8 fm^{-1}. The analysis of stretched and nearly stretched states in ^{116}Sn in conjunction with that of hadronic measurements

($^{116}Sn(\vec{p},p)^{116}Sn$, $^{115}In(\alpha,t)^{116}Sn$, $^{115}In(^{3}He,d)^{116}Sn$ and $^{115}In(\alpha,t\gamma)^{116}Sn$) is in progress. The results will be compared with extensive shell-model calculations, in which two quasi-particles are allowed relative to the BCS ground state of ^{116}Sn.

1.2.5 Dispersive effects

Investigation of the first diffraction minimum in elastic electron scattering from ^{12}C

(C.W. de Jager, E.A.J.M. Offermann, in collaboration with Technische Hochschule Darmstadt and University of Illinois)

This experiment should provide data of sufficient accuracy to permit an experimental test of the contribution of dispersive effects in elastic electron scattering and should assist in the extension of ^{12}C as a reference standard for electron scattering to momentum transfers well above 1 fm^{-1}.

Because the trace of a detected electron through the spectrometer is known, the scattering-angle acceptance (4.6^{o} for the QDD, 8.0^{o} for the QDQ) can be subdivided into bins. In this way the analysis of one spectrum results in cross sections at several scattering angles. If the bins are sufficiently small, no solid angle unfolding procedure is needed to interpret the data.

Test-runs are performed with both spectrometers: QDD (Ω = 5.6 msr) and QDQ (Ω = 17.2 msr). Spectra were measured at E = 299 MeV and $\theta = 74^{o}$, 78^{o} and 82^{o}, covering the elastic form factor from the first minimum up to about the second maximum. With a natural ^{12}C target (93 mg/cm^2) the resolution ($< 2.5 \times 10^{-4}$) in the QDD was such that the elastic ^{13}C- and ^{12}C-peaks are resolved. In the analysis of the QDQ data some problems arose, which are probably due to incorrect backtracing elements for converting focal-plane angles to target angles. Measurements to determine these backtracing elements more accurately will be performed shortly.

1.3 Coincidence (e,e'X) experiments

(H.P. Blok, J.F.J. van den Brand, J.W.A. den Herder, E. Jans, A. Kaarsgaarn, P.H.M. Keizer, L. Lapikás, E.N.M. Quint, G. van der Steenhoven, P.K.A. de Witt Huberts)

The two-spectrometer set-up in the EMIN hall has been subjected

to a number of test measurements, in order to establish the fine tuning of the apparatus. This investigation, which concerned the determination of optimum beam dispersion and spectrometer matrix elements, has led to a further improvement of the missing-energy resolution to 100 keV (FWHM) for thin ($\lesssim$ 10 mg/cm^2) targets.

To improve on the possibilities for particle identification by means of pulse-height discrimination a supplementary 1 mm thick scintillator has been installed on the QDQ spectrometer. Together with the already existing detection system the set-up is now able to discriminate between protons and deuterons of momenta ranging from 380 to 500 MeV/c. For 435 MeV/c particles this is shown in fig. 1.9.

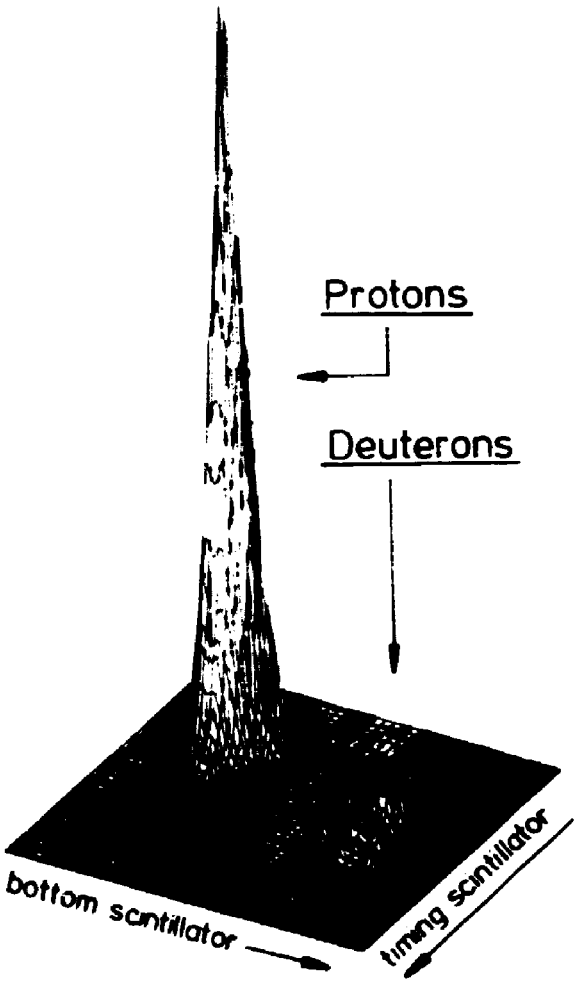

Fig. 1.9
Correlation plot of pulse-height information of the bottom (0.3 cm) and timing scintillators (1.0 cm) for 435 MeV/c particles.

In order to calculate the distortion in (e,e'p) reactions of the knocked-out proton due to its interaction with the residual nucleus, a version of the Saclay program PEEP has been implemented. The exact solution of the Schrödinger equation for a proton moving in an optical potential is decomposed into partial waves (typically 20 to 30). For this optical

potential the usual Woods-Saxon form has been chosen to which a Coulomb part is added. The effect on the $3s_{\frac{1}{2}}$ momentum density distribution in ^{208}Pb when passing from PWIA to DWIA is shown in fig. 1.10 for 150 MeV protons. Due to absorption the low momentum part is suppressed by a factor of two. The calculation also exhibits a filling in of the minima together with a shift of strength towards lower momenta.

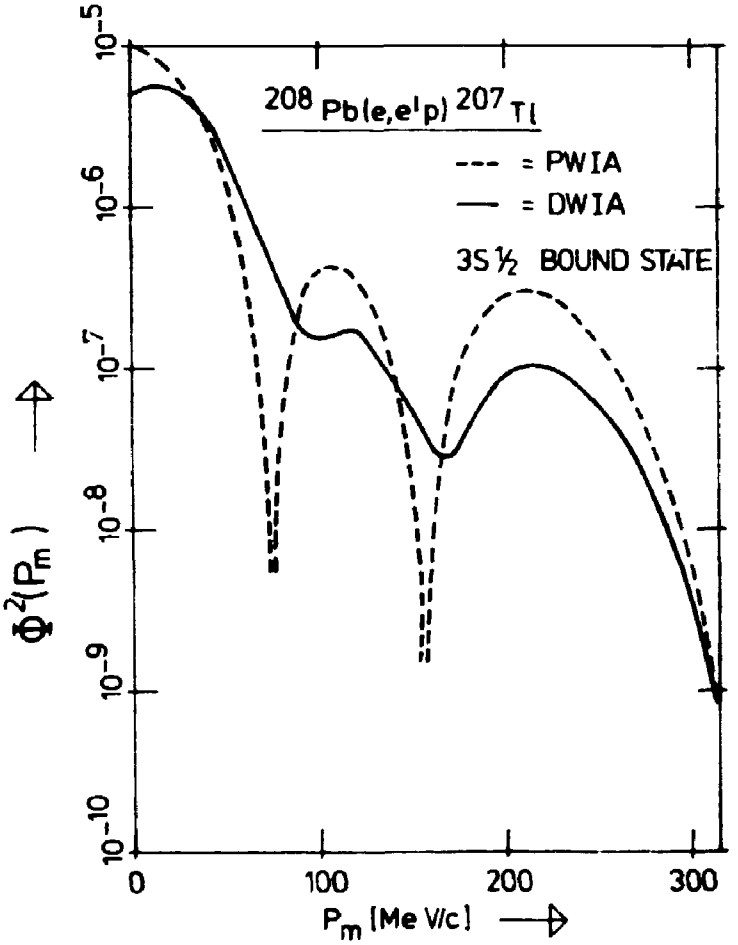

Fig. 1.10 Momentum-density distribution of the $3s_{\frac{1}{2}}$ proton-hole state in ^{208}Pb, calculated for 150 MeV protons in plane wave impulse approximation (PWIA) and distorted wave impulse approximation (DWIA). The variation in p_m is obtained in parallel kinematics ($\vec{q}//\vec{p}$) by varying $q(|q|<|p|)$ while keeping $|p|$ constant (T_p = 150 MeV).

So far data have been taken for a number of nuclei ranging from mass A = 3 to A = 208, the results of which are presented below. These experiments have been performed at a duty factor of typically 0.5 - 0.7 % and average beam currents of 20 - 35 μA. In combination with the coincidence timing resolution of 0.9 ns this has led to overall real-to-random ratios of greater than unity. For individual peaks this ratio may be higher by one or two orders of magnitude.

1.3.1 The ground state of ^{3}He studied with (e,e'p) and (e,e'd) reactions

The experimental information on the two-body breakup process of ^{3}He, obtained with electron scattering, consisted up to now of a single-arm experiment performed at SLAC [23] and a (e,e'p) coincidence experiment performed at Saclay [24]. From these experiments contradictory information on the ground-state wave function was obtained. The inclusive experiment indicated the need for more high-momentum components in the Faddeev three-body wave function. In contrast to this the coincidence data fall slightly below the theoretical curve. The range of recoil momenta involved was p_r = 0 - 500 MeV/c for the single-arm experiment and p_r = 0 - 300 MeV/c for the coincidence experiment.

The present experiment was devoted to the study of a number of different aspects of this three-nucleon system. The measurements were performed on a liquid ^{3}He target with a primary electron energy of 390 MeV. The duty factor was about 0.6 %. The detection efficiency for protons and deuterons was determined from measurements on CH_2 and CD_2 targets mounted in the cryostat.

In order to extend the existing data set, data were taken with the (e,e'p) and (e,e'd) reactions. The recoil momentum range covered in the (e,e'p) experiments was p_r = 0 - 350 MeV/c. The lowest recoil momenta were measured in parallel kinematics. The kinematics for the higher recoil momenta were determined by fixing both the three-momentum transfer and the energy transfer. In this way the effect of final-state interactions could be treated in a consistent way. The momentum and energy transfer are kept at q = 250 MeV/c and ω = 113 MeV, resulting in a center-of-mass energy of 92 MeV in the final (p,d) system. Recent calculations [25] show a strong enhancement due to the effect of final-state interactions and meson exchange currents at recoil momenta p_r > 300 MeV/c. Data were taken at p_r = 390, 420 and 480 MeV/c to study this phenomenon. For this purpose the reaction product (deuteron), instead of the proton was detected in coincidence with the scattered electron. Particle identification with the aid of the pulse-height information from a stack of scintillators in the hadron detection system allowed a large improvement of the real-to-random ratio. The p_r = 350 MeV/c (e,e'p) and p_r = 390 MeV/c (e,e'd) data were measured simultaneously. This could be done by selecting the kinematics such that the phase space for both reactions overlapped.

Data were also taken at p_r = 100 MeV/c at different values of

the center-of-mass energy to study the effect of final state interactions at low recoil momentum.

At fixed three-momentum transfer q = 380 MeV/c the direct knock-out of deuterons was observed. For that purpose parallel kinematics were chosen to minimize the contribution of recoil deuterons coming from the ^{3}He(e,e'p)d channel. Here, the recoil momentum range p_r = 0 - 200 MeV/c was covered. The preliminary result is shown in fig. 1.11, where the experimental deuteron momentum density distribution is plotted as a function of the primary deuteron momentum. The curve represents the proton spectral function for the two-body breakup obtained from the Paris potential using the

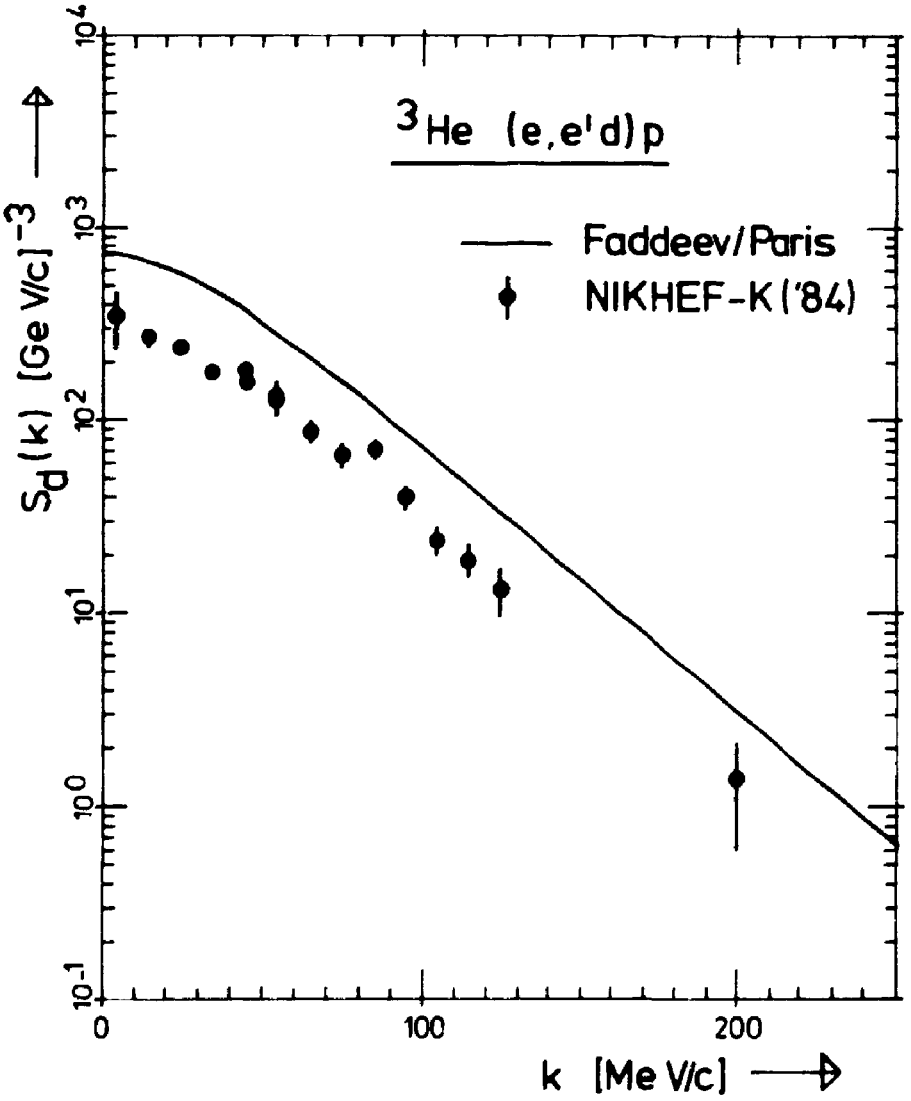

Fig. 1.11 Preliminary data on the knock-out of deuterons from ^{3}He. Plotted are fivefold differential cross sections divided by the elastic deuteron cross section, which corresponds to an experimental momentum distribution for the deuteron in ^{3}He. The curve is the result of a Paris potential Faddeev calculation.

Faddeev technique. The data were analysed under the assumption that the virtual photon couples to a deuteron which is subsequently knocked out and detected. The electron deuteron cross section needed to extract this momentum density distribution has been derived from elastic electron deuteron scattering [26].

It is apparent that the momentum distribution derived in this way has the same shape as the theoretical proton-momentum density. This indicates that the proton-momentum density can be used to study the off-shell form factor for the deuteron bound in the ^{3}He nucleus by performing (e,e'd) experiments at various momentum transfers in a restricted recoil-momentum region. Such a measurement was carried out at q = 350, 380 and 450 MeV/c for a recoil momentum p_r = 60 MeV/c.

1.3.2 The $^{12}C(e,e'p)^{11}B$ reaction

The principal motivation of this experiment is to study the structure of the $1/2^+$ state at E_x = 6.79 MeV in ^{11}B also with the direct proton-knock-out reaction (e,e'p). This state is of great interest to assess the role of excited states of the ^{4}He-core in 1p-shell nuclei. The excitation of the state could, however, also be due to $2s_{\frac{1}{2}}$ components in the wave function of the ^{12}C ground state.

Since the spectral function peaks at p_m = 0 MeV/c for states with angular momentum l = 0, measurements of the proton knock-out cross section have been performed at low values of the missing momentum (10, 30, 60 MeV/c). Due to the good missing-mass resolution of 200 keV the state has been clearly observed in all spectra (see fig. 1.12a). A preliminary analysis (see also fig. 1.12b) indicates a predominant $2s_{\frac{1}{2}}$ character with a relatively small contribution of $1s_{\frac{1}{2}}$ components for this state.

Surprisingly the spectra also show the presence of a peak at 9.87 MeV excitation energy. According to the literature [27] this level should be identified as a $3/2^+$ state. However, such a state would show a l = 2 character and should not be seen at low p_m. The results of this experiments will be compared with recent shell-model calculations, performed in an almost complete configuration space which includes ^{4}He-core excitations [28].

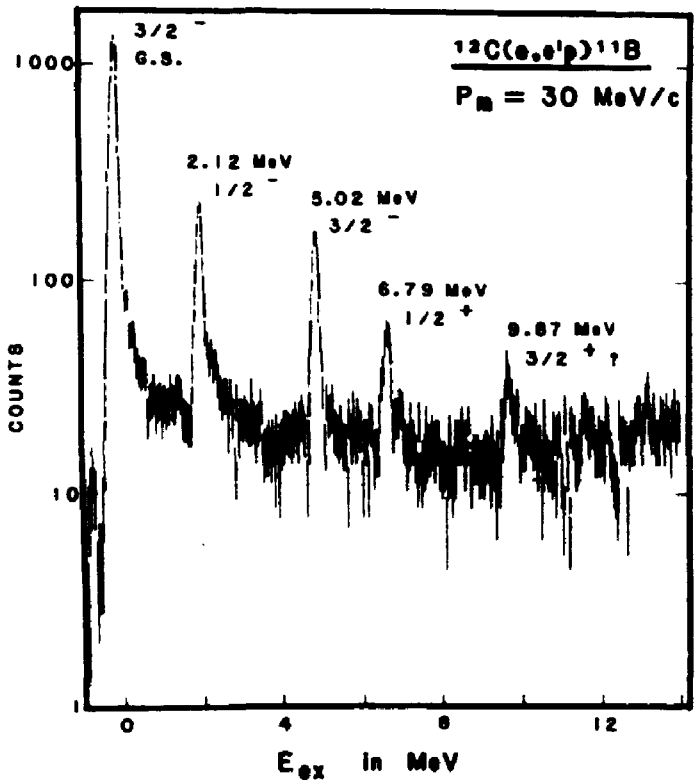

Fig. 1.12a Missing-energy spectrum for the $^{12}C(e,e'p)$ reaction at p_m = 30 MeV/c. The data are neither corrected for accidental coincidences nor radiatively unfolded.

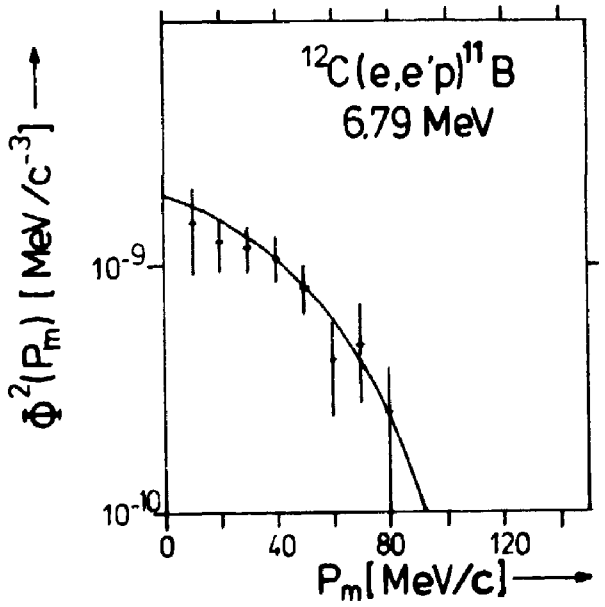

Fig. 1.12b Momentum distribution for the $1/2^+$ state at 6.79 MeV in ^{11}B. The curve is a DWIA calculation with a 2s HO bound state wave function. The spectroscopic factor (C^2S) for this calculation is taken 0.01.

1.3.3 Study of valence and deep-hole states in ^{51}V, ^{90}Zr and ^{208}Pb

In the quasi-elastic proton knock-out experiment on ^{51}V and ^{90}Zr the spectral function is studied in the excitation energy range E_x = 0 - 20 MeV and for missing momenta p_m between - 50 and 300 MeV/c ($\vec{p}$ parallel to $\vec{q}$). Data taking, including two runs at higher E_x (20 - 40 MeV) and a few reaction-mechanism tests (perpendicular kinematics, proton-energy dependence), is nearly completed. A typical missing-energy resolution of 150 keV has been obtained (see fig. 1.13).

In the $^{51}V(e,e'p)^{50}Ti$ spectra the ground state, 1.56 (2^+), 2.68 (4^+), 3.21 (6^+), 4.42, 5.44, 5.85, 6.10 (4^-) and 6.46 MeV peaks are clearly observed. The expected l = 3 behaviour of the momentum distributions for the 0^+, 2^+, 4^+, 6^+ quadruplet ($(1f_{7/2})^2$ configuration) is confirmed by this experiment. A preliminary analysis of the p_m dependence of the 5.44 and 5.85 MeV states (see fig. 1.14) shows a strong l = 0 admixture which was so far not observed in hadronic reactions [29]. However, a recent high-resolution (d,^{3}He) experiment, carried out at KVI also indicates the presence of l = 0 strength at these excitation energies.

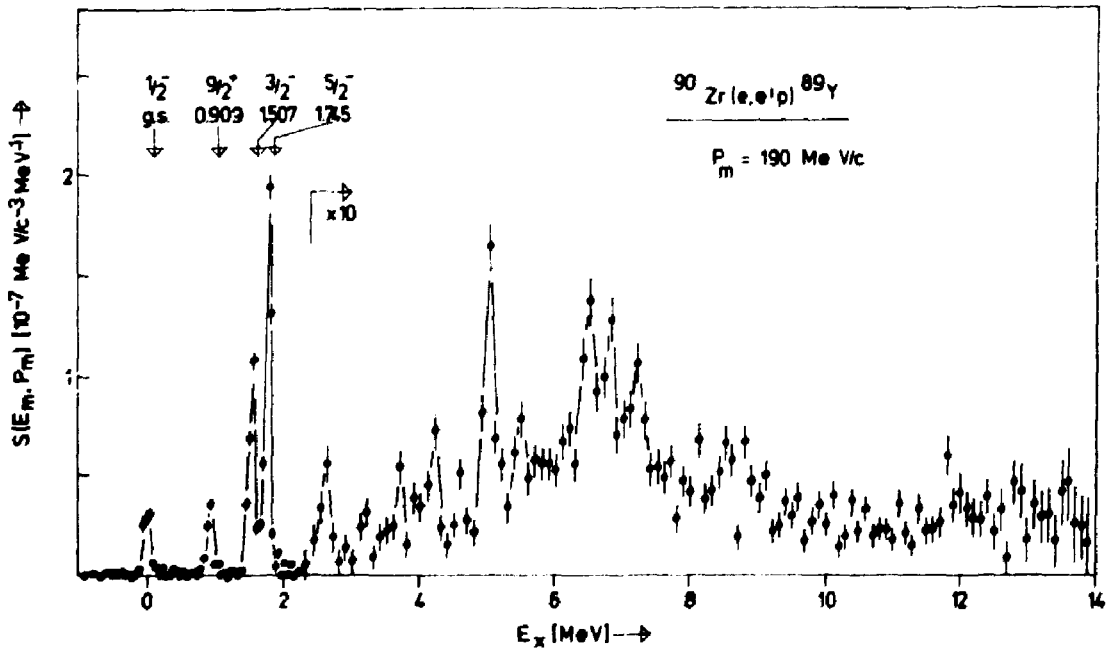

Fig. 1.13 Excitation-energy spectrum for the reaction $^{90}Zr(e,e'p)^{89}Y$ at p_m = 190 MeV/c. The data are corrected for radiative effects.

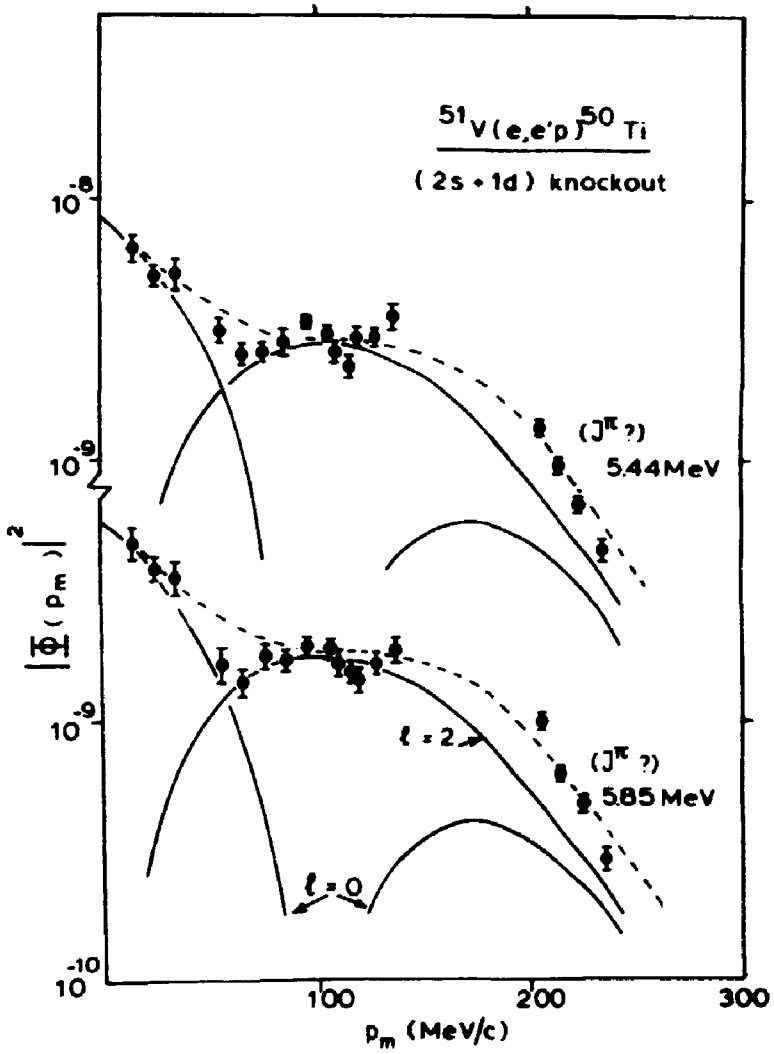

Fig. 1.14

Momentum-density distribution for the 5.44 and 5.85 MeV levels in ^{50}Ti with l = 0 and l = 2 components.

In the analysis of the $^{90}Zr(e,e'p)^{89}Y$ reaction the valence states at 0 ($1/2^-$), 0.90 ($9/2^+$), 1.51 ($3/2^-$), 1.75 MeV ($5/2^-$) are well resolved (see fig. 1.13). Their relative spectroscopic factors agree within 20 % with those obtained from ($\vec{d}$,^{3}He) reactions [30]. In addition a multiplet of states around 6.8 MeV has been observed at high missing momenta (p_m > 70 MeV/c). The spectroscopic factor (assuming a l = 3 behaviour, as found by the ($\vec{d}$,^{3}He) experiment) and the width are much smaller than those of the giant-resonance-like structure observed in this hadronic reaction. The experimental momentum distribution of 2p and 1f holes is shown in figs. 1.15 and 1.16, respectively, together with DWIA predictions. The 2p transitions measured with T_p = 70 and 100 MeV can clearly not be described simultaneously. However, such a discrepancy is absent in the case of 1f (and also 1g) holes. This might be due to the fact that the 2p wave function is located much more inside the nuclear medium, but the optical potential parameters have been determined from elastic proton scattering data, which

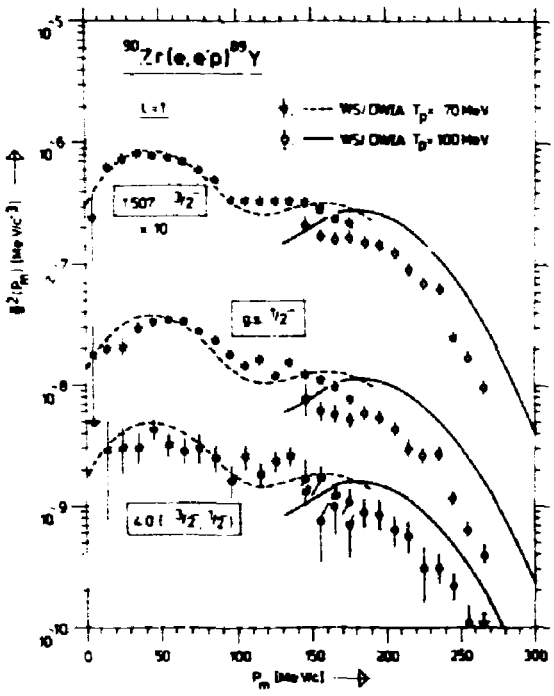

Fig. 1.15

Experimental momentum distributions $\phi^2(p_m)$ for 2p hole states observed in the reaction $^{90}Zr(e,e'p)^{89}Y$. The curves are calculated in DWIA for WS bound state wave functions, their normalization is chosen to reproduce the first maximum. Data and theory are plotted for protons of outgoing energy T_p = 70 MeV (asterisks and dashed curves) and T_p = 100 MeV (open circles and solid curves).

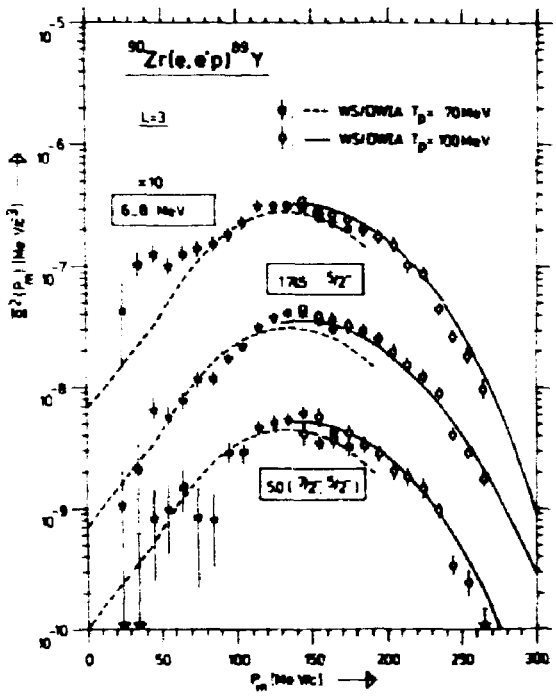

Fig. 1.16

Same as fig. 1.15, but for 1f hole states.

are primarily sensitive to the nuclear surface.

For the first time the (e,e'p) reaction has been applied to the doubly magic nucleus ^{208}Pb. Experimental information on the structure of this nucleus is of fundamental importance in e.g. self-consistent many-body calculations. It will also be interesting to compare the proton-hole structure as derived from this electromagnetic reaction with that from hadronic reactions. The experiment was performed on a 14 mg/cm^2 ^{208}Pb target mounted in a rotating frame, which could stand an average beam current of 25 μA.

So far measurements have been carried out at missing momenta 10, 70 and 160 MeV/c (see fig. 1.17). The knock-out of $3s_{1/2}$ protons leading to the ground state of ^{207}Tl and $2d_{3/2}$ and $2d_{5/2}$ protons leading to states

at 0.35 MeV and 1.67 MeV, respectively, is observed in all spectra. At p_m = 160 MeV/c the known higher l states show up at 1.35 MeV ($1h_{11/2}$) and 3.48 MeV ($1g_{7/2}$). For the rather narrow peaks ($\Gamma \leq 175$ keV) at 4.05 MeV and 5.05 MeV a comparison will be made with similar structures observed in a recent (d,^{3}He) experiment at 108 MeV [31].

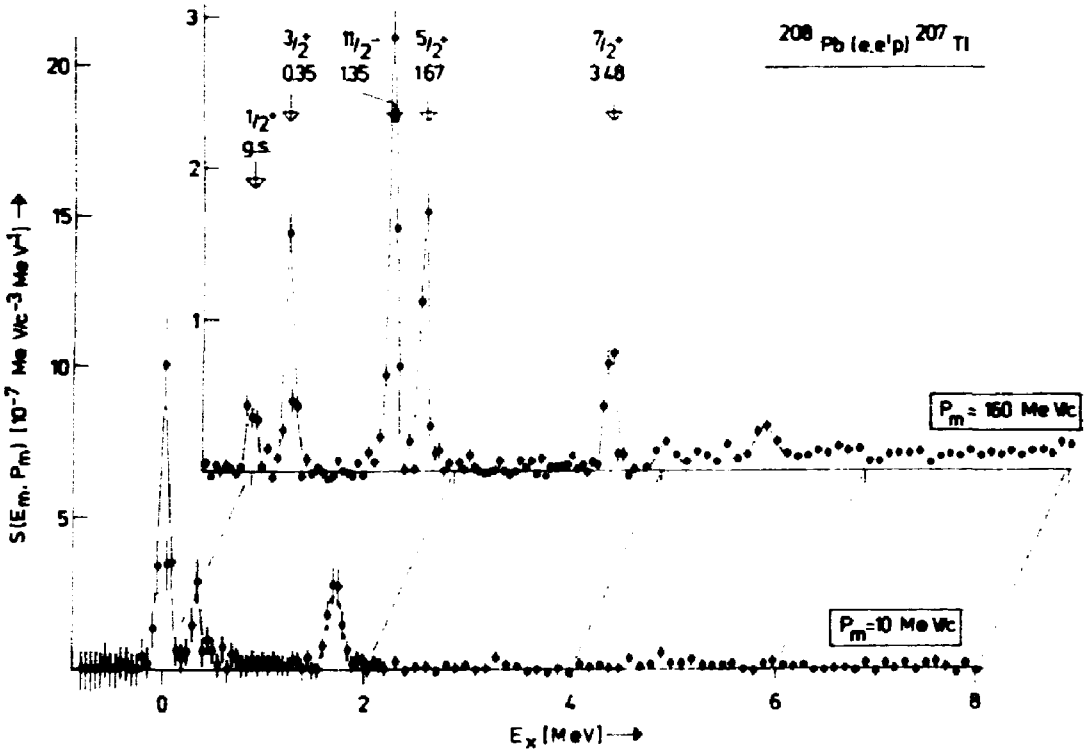

Fig. 1.17 Missing energy spectra for the reaction ^{208}Pb(e,e'p)^{207}Tl at missing momenta of 10 and 160 MeV/c.

1.4 Pion production experiments

1.4.1 The reactions $^{13}C(\gamma,\pi^-)^{13}N$ and $^{11}B(\gamma,\pi^-)^{11}C$

(A. Kaarsgaarn, J.H. Koch, P.K.A. de Witt Huberts, in collaboration with University of Mainz, Rensselaer Polytechnic Institute and C.E.N. Saclay)

A modestly-sized program of charged pion production experiments with the virtual photon end point is being carried out. At present, in charged photopion production there is a conspicuous lack of reliable negative-pion production data.The instrumental problems related with the large

electron background in (γ,π^-) experiments have been solved by installation of an aerogel Cerenkov detector in the QDQ detector assembly [32]. The present experience with this electron noise suppression system indicates that cross sections up to a pion energy of 200 MeV can be measured at angles as small as 45^o.

The differential photoproduction cross sections for the reactions $^{13}C(\gamma,\pi^-)^{13}N$ (g.s.) and $^{11}B(\gamma,\pi^-)^{11}C$ (g.s.) have been measured. Part of the experiment was to determine the angular distribution of the pion production cross section. The present data confirm that the cross section is low, but is appreciably larger than earlier data at a production angle $\Theta_\pi = 90^o$ [33]. The data also show that the angular distribution is rather flat in the angular range $\Theta_\pi = 65^o - 125^o$.

The main interest of the experiment is to study the role of the Δ resonance in the (γ,π) reaction. A value of $q \approx 1$ fm^{-1} is chosen for the momentum transfer in order to emphasize the resonant part of the π-production process. While keeping q constant the pion kinetic energy is varied across the delta-resonance region. Data points have been taken at a pion kinetic energy of 50, 130 and 220 MeV for both the $^{13}C(\gamma,\pi^-)^{13}N$ (g.s.) and the $^{11}B(\gamma,\pi^-)^{11}C$ (g.s.) reaction.

For the $^{13}C \rightarrow {}^{13}N$ (g.s.) transition one expects that the cross section should rise with increasing pion energy due to the increased role of the Δ-resonance in the reaction. In contrast, the $^{11}B \rightarrow {}^{11}C$ (g.s.) transition is dominated by non-resonant processes and one therefore expects a slowly varying cross section with increasing pion energy. These effects are indeed observed in our data.

The angular distribution of 48 MeV pions from the $^{13}C(\gamma,\pi^-)^{13}N$ reaction [34] is shown in fig. 1.18 together with various theoretical DWIA calculations of the process. It is remarkable that especially the small-angle cross section is much lower than the calculated values.

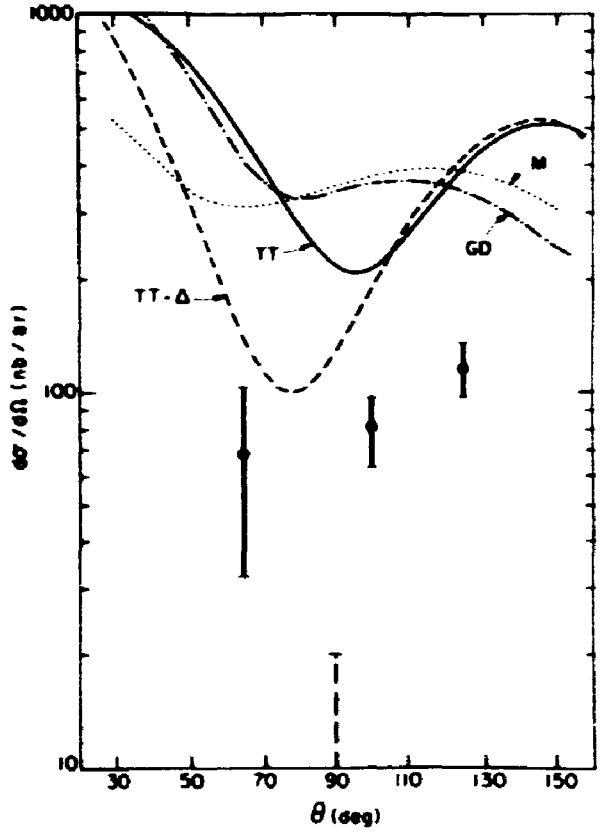

Fig. 1.18

The measured differential cross sections for the ground state transition compared with the theoretical results of Toker and Tabakin (TT) (——) and Giraud and Delorme (GD) (-·-·-). The result of TT omitting the delta from the BL operator is also shown (---). Both calculations use non-local operators. The result of the local calculation of Maleki (M) is denoted (...). The measurement of LeRose at T_π = 42 MeV is shown as a vertical hatched line.

1.5 References

1. L. Zamick, Phys. Rev. Lett. 40 (1978) 381
2. L. Zybert, R.B.M. Mooy, P.W.M. Glaudemans (Utrecht),to be published
3. T. Suzuki (NIKHEF), private communication
4. G. Bertsch *et al.*, Nucl. Phys. A284 (1977) 399
5. J. Ruyl, thesis, University of Utrecht (1983)
6. Nucl. Data Sheets 19 (1976)
7. P. van Isacker, G. Puddu, Nucl. Phys. A348 (1980) 125
8. A.J.H. Donné *et al.*, Nucl. Instr. and Meth. 224 (1984) 97
9. C.F. Williamson (MIT, Boston), private communication
10. T.T. Inoue *et al.*, Nucl. Phys. 5º (1965) 1
11. B.A. Brown *et al.*, Phys. Lett. 133B (1983) 5
12. P.W.M. Glaudemans (Utrecht),private communication
13. T. Suzuki (NIKHEF), private communication
14. L. Zybert, R.B.M. Mooy, P.W.M. Glaudemans (Utrecht),private communication
15. S.K. Platchkov *et al.*, Phys. Rev. C25 (1982) 2318

16. T. Suzuki (NIKHEF), private communication
17. A. Richter, Proc. Int. Conf. on Nuclear Physics, Florence, Italy (1984)
18. Th.Grundey *et al.*, Nucl. Phys. A257 (1981) 269
19. I.S. Towner, F.C. Khanna, Nucl. Phys. A399 (1983) 334
20. H. Sagawa, B.A. Brown, to be published
21. L.T. van der Bijl *et al.*, Nucl. Phys. A423 (1984) 365
22. J. Wambach *et al.*, Nucl. Phys. A348 (1980) 221
23. D. Day *et al.*, Phys. Rev. Lett. 43 (1979) 1143
24. E. Jans *et al.*, Phys. Rev. Lett. 49 (1982) 974
25. J.M. Laget (Saclay), private communication
26. G.G. Simon *et al.*, Nucl. Phys. A364 (1981) 285
27. F. Ajzenberg-Selove, Nucl. Phys. A248 (1975) 1
28. P.W.M. Glaudemans (Utrecht), private communication
29. E. Newman, J.C. Hiebert, Nucl. Phys. A110 (1968) 336
30. E. Stuirbrink *et al.*, Z. Physik A297 (1980) 307
31. H. Langevin-Joliot, XIV Masurian Summerschool, Poland, Sept. 1983
32. P.C. Dunn, Nucl. Instr. Meth. 224 (1984) 106
33. J.J. LeRose *et al.*, Phys. Rev. C25 (1982) 1702
34. P. Stoler *et al.*, Phys. Lett. B, 143 (1984) 69

1.6 Approved proposals for electron scattering experiments

84-E2 Study of valence and deep-hole states in (medium) heavy nuclei,
H.P. Blok *et al.*

84-E3 Measurement of transverse form factors to high momentum transfer,
R.P. Singhal *et al.*

84-E4 Electron scattering off ^{11}B (provisionally approved),
P.W.M. Glaudemans *et al.*

84-E5 High-resolution electron scattering from mercury isotopes,
R. Altemus *et al.*

84-E6 A study of the transverse excitation of ^{26}Mg by inelastic electron scattering,
H. de Vries *et al.*

2 PHYSICS WITH PIONS, MUONS AND ANTIPROTONS

(Groupleader: R. van Dantzig)

2.1 Introduction

After the initial beam tests in the first half year of 1983, a year of almost 'routine' operation of the pion-muon facility has passed. In total, eight weeks of running time were alotted to the PIMU-group, during which always two experiments were simultaneously performed, one at the pion channel and one at the muon channel. Often there were parasytic experiments in addition. Apart from a temporary problem with the liquid helium refrigeration system for the superconducting solenoid of the muon channel, no major failures have occurred.

Following the initial increase in pion/muon fluxes, the tune-up of the facility has temporarily reached a plateau. Further increase of flux is expected. This will partly come from an improvement of accellerator performance (higher peak current and pulse repetition rate) and partly from a higher pion-production efficiency.

A water cooled pyrolytic graphite pion-production target with an electron-photon converter in front is in the final stage of development. It will ensure an increase in pion flux of at least a factor of two and at the same time a reduction of the electron contamination of the beams by a factor of three to four.

The secondary beam channels have been subject to various improvements. At the pion channel the focal spot size has been reduced. At the muon channel a new wide gap bending magnet has been installed, replacing a magnet earlier obtained from SREL (Virginia). An extension of the extraction beam line for the same channel is under construction.

The scientific program is steadily coming into shape. Pionic X-ray work had a successful start with measurements of hadronic shifts and widths of the up to now lowest observable pionic states. This work will shortly benefit from funds that have been allocated to a joint project of KVI at Groningen, VU at Amsterdam and NIKHEF-K, in which a large solid angle detection system is to be realised. This system will contain at least four germanium spectrometers with BGO compton-suppression shields, suitable for pionic and muonic X-ray and gamma-ray measurements as well as for in-beam nuclear spectroscopy at the three laboratories.

Other studies, largely of an exploratory nature, are in progress.

Elastic scattering of low energy pions on lithium,carbon and ^{208}Pb, measurements of total absorption cross sections and double (and single) charge exchange for stopped negative pions are examples of these. In collaboration with a French institute on metallurgical chemistry a pilot study on muon spin rotation is in progress. A large solid angle multi-detector time-of-flight facility to measure neutrons (and protons) suitable for the study of nuclear capture reactions of pions in flight and pions or muons at rest is in development.

This year the first proposals have been submitted to the NIKHEF-K program advisory commission, most of which met approval.

In addition to the in-house research, members of the group have participated in experiments in CERN (LEAR) and SIN. These experiments continue to give a valuable supplement to the local activities.

2.2 Pionic and muonic atoms

2.2.1 Pionic Mg and Al

(J.B.R. Berkhout, W. Duinker, W.H.A. Hesselink, P.J. van den Hoek, T.J. Ketel, J.H. Koch, J. Konijn, C.T.A.M. de Laat, G. van Middelkoop, W. Poeser, T. Prins, A. Taal, A.H. Wapstra; J.F.M. d'Achard van Enschut, C.W.E. van Eijk, W. Lourens (TH-Delft))

Earlier measurements [1] on strong interaction shifts (ε_0) and widths (Γ_0) of 3d levels in pionic Pt and Au have shown that the values are systemtically much smaller than predicted by standard pion-nucleus optical potentials. Recent calculations [2] indicate that a strong enhancement of the repulsive s-wave (local) interaction inside the nucleus - as compared to the conventionally assumed strength - could explain this effect. Measurements of the deeply bound pionic 1s level (well populated only for light nuclei) for which the s-wave interaction dominates, are from this point of view of interest.

The pionic atoms of Mg and Al were studied at the NIKHEF-K pion-muon facility. The weak $2p \rightarrow 1s$ transition could be observed in both cases by using a combination of compton suppression and time-of-flight techniques, thereby discriminating against background induced by pion capture neutrons. The muonic $2p \rightarrow 1s$ transition for Al is close to the pionic one. In this case measurements were made both at the pion and at the muon channel (with different pion to muon ratios) thereby minimizing possible systematic errors in the unfolding. The raw anti-compton spectrum for Mg as a function of

time delay with respect to the pion/muon-stop is given in fig. 2.1a. In fig. 2.1b the resulting spectrum in the energy region of the 2p → 1s transition in pionic Mg is shown together with the obtained fit.

The response function of the detector was studied by using the 344.28 keV line of ^{152}Eu. The analysis of the data is made in the same way as for Pt and Au [1]. The results for ε_0 and Γ_0 are given in table 2.1. The observed widths are about a factor of 1.5 smaller than theoretical predictions using standard optical potentials [3,4].

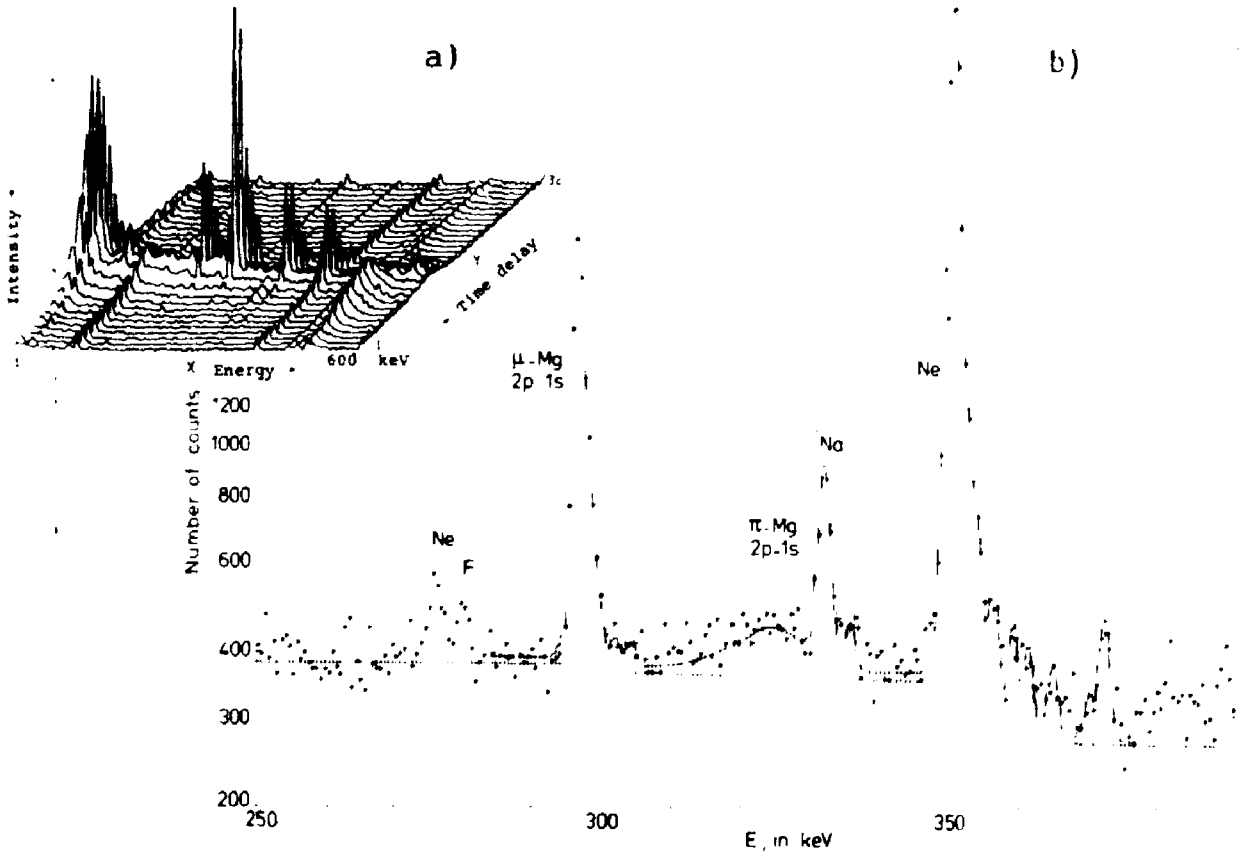

Fig. 2.1 The energy region of the 2p → 1s transition in the pionic (and muonic) X-ray spectrum for Mg.
a) time correlation with pion/muon-stop; neutron-induced (time-delayed) gamma-rays are distinguished from prompt peaks by their appearance in ridges and can be filtered out numerically.
b) final spectrum with fit including identified background lines.

Table 2.1 Preliminary results for the strong interaction monopole shifts (ε_0) and widths (Γ_0) for pionic 1s levels. The shifts are with respect to the theoretical point-nucleus values without vacuum polarisation.

	ε_0 (keV)				
	experiment	theory			
		I	II	III [3]	IV [4]
Mg	81.6 ± 1.0	79.0	76.7	79.1	77.9
Al	114.6 ± 2.3	109.0	109.3	110.1	112.3
	Γ_0 (keV)				
	experiment	theory			
		I	II	III [3]	IV [4]
Mg	16.9 ± 2.4	23.85	25.60	23.93	21.36
Al	21.4 ± 3.3	30.04	30.98	30.91	28.2

2.2.2 Single and double charge exchange in pionic atoms

(J.B.R. Berkhout, W. Duinker, W.H.A. Hesselink, P.J. van den Hoek, T.J. Ketel, J. Konijn, C.T.A.M. de Laat, G. van Middelkoop, W. Poeser, A. Taal, A.H. Wapstra; J.F.M. d'Achard van Enschut, C.W.E. van Eijk, W. Lourens (TH-Delft))

Experiments which aim at the measurement of double charge exchange (DCX) in pionic atoms have been proposed [5]. Only for few nuclei these processes are energetically possible. From these investigations information on the isovector and on the isotensor part of the pion-nucleus interaction can be obtained. Calculations have been made for DCX and SCX (single charge exchange) reactions on ^{58}Ni and ^{96}Ru. In contrast to earlier objections [6] it appears that for the latter the DCX transition can populate the first-excited 2^+ state in ^{96}Mo and that this state might even be favoured over the ground state [7]. This is because the pion is predominantly captured from an orbit with angular momentum $l = 2$ while the π^+ is preferentially emitted with angular momentum zero due to its low energy. A new

point of interest for these experiments is provided by a recent calculation[8] and data [9] for ^{14}C at 50 MeV which indicate that DCX at forward angles is strongly enhanced with respect to a two-step (second order in SCX) process. As suggested in ref. 8 the ratio between SCX and DCX probability may be sensitive to the quark structure of nuclei.

A first SCX test experiment, $^{27}Al(\pi^-,\pi^0)^{27}Mg$, has been done parasytically during the pionic Al measurements (section 2.2.1). Measurements on ^{96}Ru are in progress. The π^0 and π^+ are detected through their decays. The measurements include pionic X-rays and gamma-rays for specific final nuclear states. The gamma-rays from π^0 decay are detected with NaI(Tl) detectors and the π^+ is identified through its decay chain $\pi^+ \rightarrow \mu^+ \rightarrow e^+$ with an electron telescope covering almost 4π sr.

2.2.3 An in-beam Ge-BGO compton suppression spectrometer (NIKHEF-VU-KVI collaboration)

A germanium photon spectrometer equipped with a BGO compton suppression shield has been developed and tested. It is in use for the pionic and muonic X-ray work at this institute. The construction has been optimized with respect to compactness to allow it to be placed close to the target (large detection solid angle) along with several other, similar detectors.

A detector array containing up to four such spectrometers is under construction. With this system it will be possible to measure singles X-rays of low intensity as well as coincident X-rays from pionic and muonic cascades. The multi-detector setup has been designed (and will be used) in close collaboration with the Free University (VU) and the Nuclear Physics Accelerator Laboratory (KVI) at Groningen. The BGO detector shield shown in fig. 2.2 served as a prototype for this joint project. It has been manufactured by Harshaw Chemie Netherlands. The axis of the BGO-crystal is perpendicular to the incident beam direction. This geometry permits an optimum shielding. The unshielded part - where the photo tube is mounted - is at the far end as viewed from the beam. The Ge-detector is placed asymmetrically in the BGO detector in order to reach an optimum suppression for muonic X-ray spectra up to 9 MeV. At the front-end of the BGO shield a NaI(Tl) crystal is mounted to take care of low-energy backward-scattered photons. The overall compton-suppression factor obtained in this way is 5.5.

The spectrometer in this system is a single n-type intrinsic germanium detector with an efficiency of 28 % and a resolution of 1.9 keV at 1.33 MeV (^{60}Co).

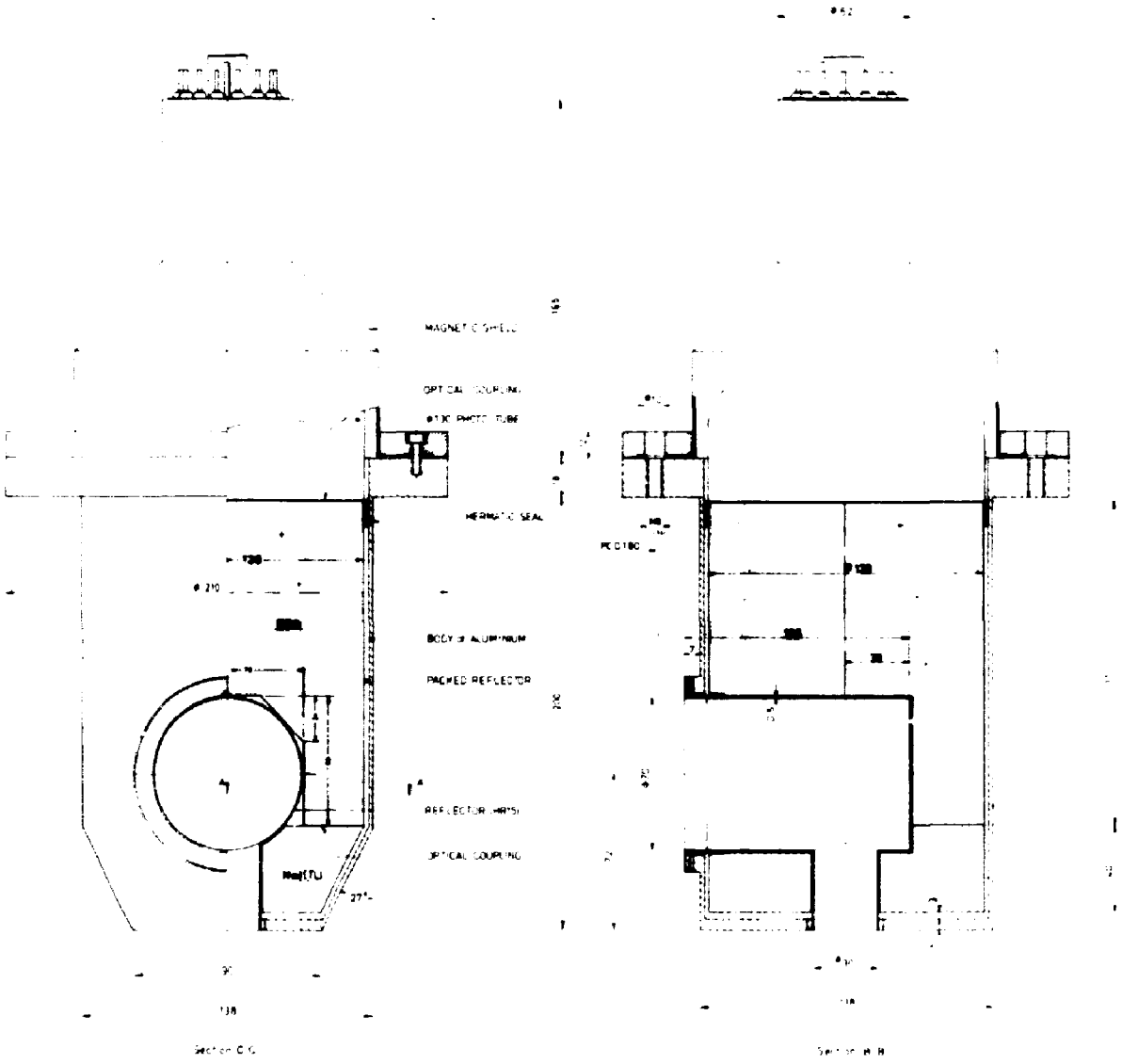

Fig. 2.2 BGO compton suppression detector shield.

2.3 Low energy pion scattering and pion absorption

(J.B.R. Berkhout, H. van Groen, R. Hamers, W.H.A. Hesselink, W. Heubers, T. Jansen, E. Kappert, T.J. Ketel, G. van Middelkoop, R.K.J. Sandor, P.H.M. Schoonejans, M. de Vries, H. Verheul, P. Verzijden, in collaboration with the TH-Delft)

Pion scattering at low energy provides a possibility to study the pion-nucleon interaction inside a nuclear medium, i.e. in the presence of nuclear binding, nucleon-nucleon correlations and Pauli blocking, while Δ_{33} resonance contributions are of less importance than at higher energies. In this respect a study of the lightest closed shell nucleus ^{4}He is particularly attractive since medium effects in this case have been evaluated theore-

tically. Moreover at pion energies below the one-nucleon knock-out threshold at about 20 MeV only the true pion absorption channel is open in addition to the elastic channel.

Other contributions to the pion-nucleus interaction can be studied for ^{3}He. In particular isospin and spin dependent terms, which are relatively large for this nucleus, can be investigated through their interference with the scalar contributions and by comparing π^+ and π^- scattering.

With the above motivation, an experimental program to measure elastic scattering of π^+ and π^- on both He isotopes at 45, 30 and 15 MeV has been initiated. A first test experiment has been performed applying pion scattering off a ^{208}Pb target. Scattered pions were detected with a scintillation range telescope obtained on-loan from CEN-Saclay. The results agree with recent data from LAMPF except for a 20 % systematic deviation which can be due to uncertainty in the absolute normalization.

In a 1 m diameter scattering chamber test experiments have been performed with positive pions scattered off a ^{12}C target at 40 and 50 MeV and a ^{208}Pb target at 50 MeV. These experiments served primarily to check the experimental equipment, in particular two scintillation hodoscopes and four telescope detectors.

The hodoscopes, constructed at the Free University, consist both of typically 30 (X) and 12 (Y) scintillator (NE 110) strips of 5 mm width with thicknesses of 0.7 mm and 1 mm, respectively (see fig. 2.3). The first hodoscope is positioned near a dispersive intermediate focus in the pion channel to determine the momentum of any incoming pion. The second hodoscope,placed 40 cm upstream of the target, serves for reconstruction of the direction of the incoming pions. Pulse-height and time-of-flight discrimination on the hodoscope signals permit a strong reduction of the background from beam contaminants (see fig. 2.4). The hodoscopes performed in general satisfactorily; some improvements on double-pulse resolution have been taken up.

The four telescope detectors inside the scattering chamber are used to measure the direction and energy of scattered positive pions. Each of them consists of a low pressure (200 torr) MWPC and a drift chamber in front of a stack of solid state detectors (30 mm diameter) cooled to liquid nitrogen temperature. The front detector of the stack is a 1 mm thick Si detector that serves as ΔE detector for particle identification. The other detectors, made of intrinsic germanium and with thicknesses of 10 and

Fig. 2.3 Scintillation hodoscope in the construction phase. The light from each of the NE 110 strips (at the left) is detected in one of the 42 Philips 1911 photo tubes (at the right).

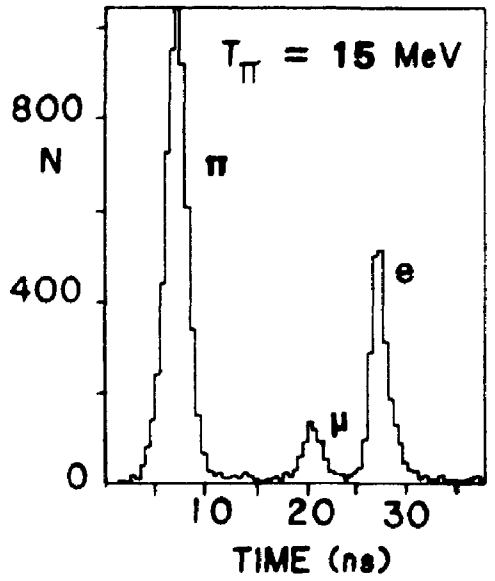

Fig. 2.4 Time-of-flight spectrum for 15 MeV negative pions which shows the possibility to distinghuish these from electrons and muons. In the spectrum the last two peaks are already suppressed by pulse height discrimination.

15 mm, are stacked together such as to stop the pions. The detectors have each a resolution of typically 40 keV for 9 MeV alpha particles. The full experimental energy resolution for 31 MeV pions has been measured to be 1.8 MeV (see fig. 2.5). This figure is mainly determined by the momentum resolution of the pion channel.

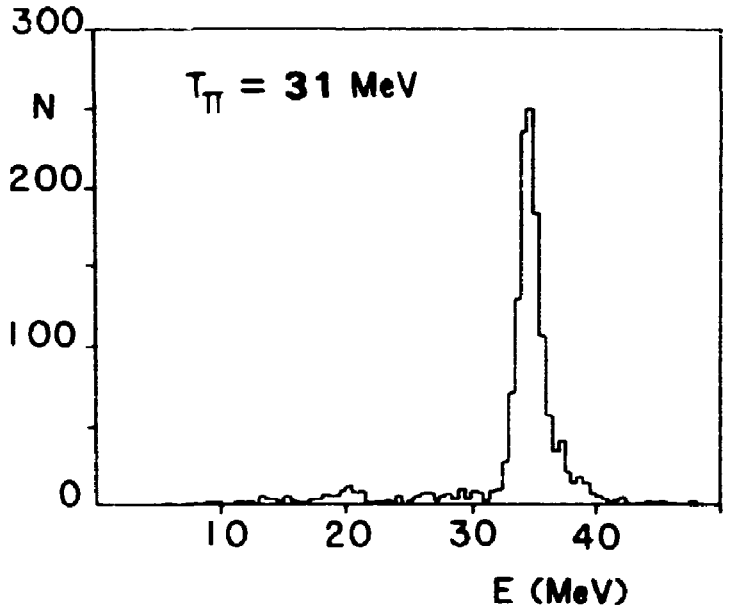

Fig. 2.5 Energy spectrum for 31 MeV positive pions stopped in a germanium telescope. The measured energy signal includes the 4.2 MeV of the decay muon from the stopped pion. The width of the peak corresponds to a momentum spread in the beam of about 3 %.

For the low-energy experiments the pion flux and the muon/electron contamination of the beam is of crucial importance. With the present Cu pion production target, the pion yield as a function of energy is shown in fig. 2.6. The steep drop towards low energies is due to a reduction in the momentum acceptance ($\Delta p/p$ = constant) of the channel as well as to an increase in decay probability of the pions in the channel. At 15 MeV only 5 % of the pions accepted at the entry of the channel survives at the target.

In addition to the above experiments, tests have been performed for different detector configurations to be used in total cross section and exclusive pion absorption (π^+,2p) experiments. For the latter experiments the same setup as for the pion scattering experiments will be used. The telescope detectors are suitable for the detection of protons up to

125 MeV. These experiments may therefore be performd to some extent simultaneously with the elastic scattering measurements.

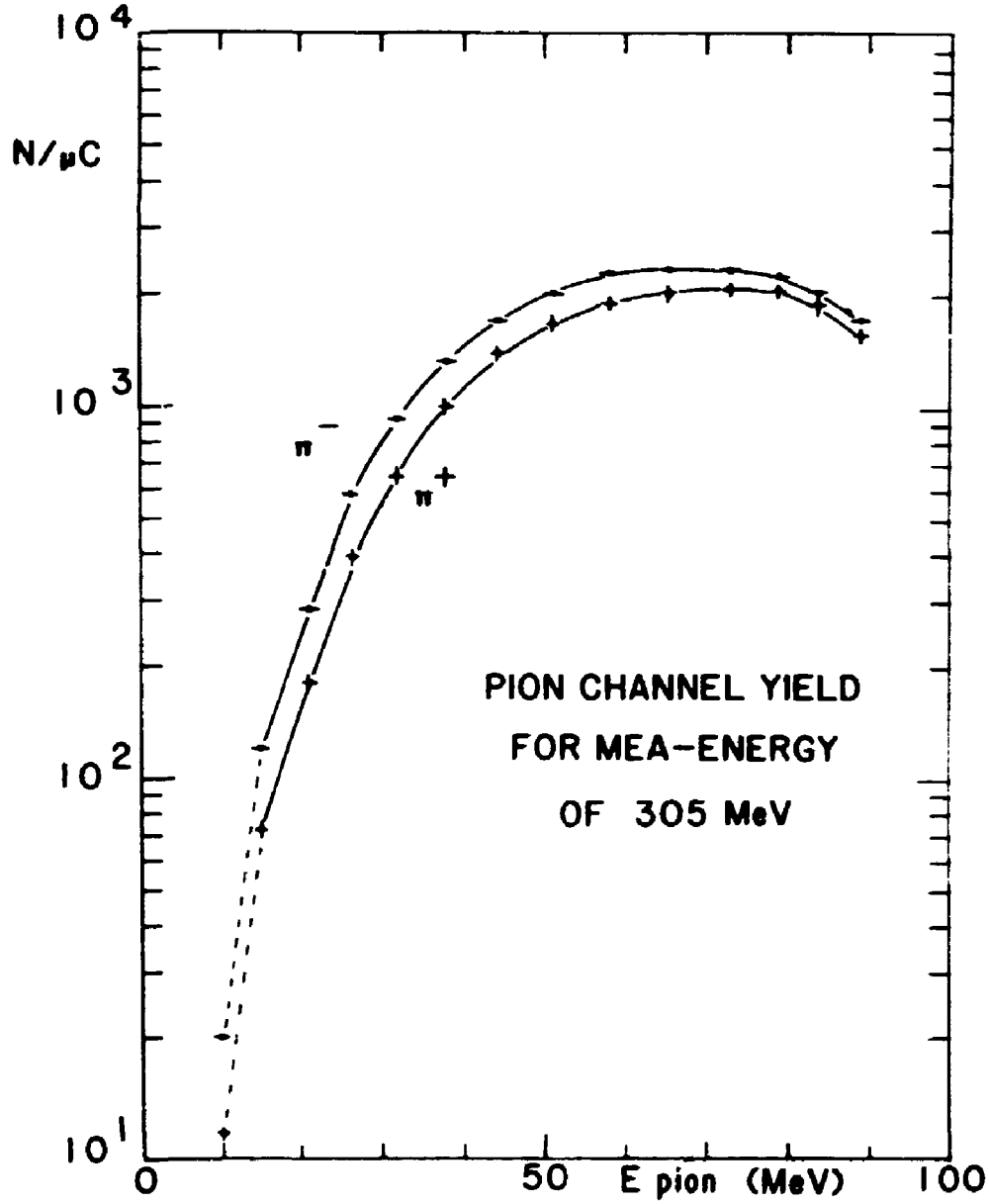

Fig. 2.6 Yield curve of pions from the pion channel for relatively low primary electron energy (305 MeV). At 400 MeV and with the new pion production target the yields are expected to be at least a factor four higher.

2.4 Nuclear pion and muon capture

(H. Arnold, W.A. Beugeling, R. van Dantzig, J. van Goudoever, E.W.A. Lingeman, H.P.J. Veerman)

An array of 16 large scintillator blocks of dimensions 100 x 18 x 18 cm^3 equipped with photo tubes at both ends has been installed in the muon channel area. The scintillators made by the University of Bologna, have been

obtained from CERN. The blocks can be arranged in a variety of ways dependent on the experimental requirements. The purpose of the detection system in its present form is to measure neutrons emitted following nuclear capture of pions, stopped or in flight, and of stopped muons. Due to the large solid angle subtended by the system it is especially suited for coincidence measurements.

The position of impact of a particle along the longitudinal direction of the blocks can be determined with an accuracy of typically 5 cm using the time difference between the two read-out signals. This position should be known to determine the actual flight path for each neutron, particularly when the detectors are placed at relatively short distance from the target. By replacing the single, common veto detector for neutrons by individual ΔE scintillation counters in front of the blocks, the setup can in the future be upgraded and become suited for detection of protons over a large solid angle as well.

With the detection system two test experiments have been made. In the first one, pion capture neutrons from ^{27}Al were measured parasytically. This allowed a study of single neutron spectra at different flight paths (3 and 5 m). The second experiment concerned the measurement of coincident neutrons from pion capture at rest in ^{12}C.

2.5 Muon spin rotation

(H. Arnold, W.A. Beugeling, R. van Dantizg, J. van Goudoever, E.W.A. Lingeman, H.P.J. Veerman with P. Bouteilloux, P. Dassonvalle, R.I. Grynszpan (Centre d'Etudes de Chimie Métallurgique (CNRS), Vitry-sur-Seine, France)

Muon-spin rotation (μSR) experiments with an exploratory character are in progress. Muon diffusion in nickel samples, pure and with dopes at the percent level, are studied in a zero field setup. The shift of the precession frequency due to a change in the local field for platinum doped nickel has been measured at room temperature to be - 1.3 % per atomic percent impurity, in agreement with similar measurements performed at SIN. At 77 K the shift was found to be twice the value at room temperature (reported in ref. 10). A dipole magnet with vertical poles for transverse μSR measurements has been equipped with a helium cryostat.

2.6 Experiments at other facilities

2.6.1 Pionic and muonic X-ray studies of ^{237}Np and muon induced fission

(W. Duinker, J. Konijn, C.T.A.M. de Laat; J.F.M. d'Achard van Enschut (TH-Delft); P. David, J. Hartfield, H. Janssen, T. Mayer-Kuckuck, R. von Mutius (Institut für Strahlen- und Kernphysik, Universität Bonn); T. Krogulski (University of Warsaw); C. Petitjean, H.W. Reist (Sin, Villigen); S.M. Polikanov (GSI, Darmstadt); C. Gugler, L.A. Schaller, L. Schellenberg (Institut de Physique Université de Fribourg)

An NpO_2 target, containing about 10 g of ^{237}Np has been used for various investigations at SIN, Villigen, with stopped pions and muons. Electromagnetic and strong interaction parameters were obtained from measurements of the pionic and muonic X-ray spectra.

From the muonic 5g → 4f complexes (fig. 2.7a) a value for the nuclear spectroscopic quadrupole moment Q = 3.65 ± 0.02 (statistical error) has been deduced. This value is in good agreement with previous measurements [11], but has an order of magnitude better accuracy.

From the muonic 2p → 1s, 3d → 2p and 4f → 3d complexes it is observed that several low-lying excited nuclear states belonging to the [642]↑ rotational band are mixed appreciably with the muonic 3d and 2p states. Various E2 matrix elements are being determined independently from these data (see fig. 2.8). A fit of the ^{237}Np nuclear charge distribution parameters to the muonic X-ray spectrum is in progress. An accurate energy calibration for this fitting procedure is needed. To accomplish this a ^{208}Pb target was inserted in the muon beam during the Np experiments. By comparing the intensities of the lower part of the muonic cascade for ^{237}Np and ^{208}Pb the probability for the 2p → 1s radiationless transition in ^{237}Np has been estimated and found to be in agreement with results obtained by others [12] for the near-by nuclei ^{238}U and ^{239}Pu.

As has been shown in the case of ^{238}U [13] prompt muon-induced fission is predominantly caused by the radiationless 3d → 1s quadrupole transition in the muonic cascade. To determine the probability for the 3d → 1s radiationless transition in muonic ^{237}Np an experiment was performed in which the 2p → 1s radiative transition was measured in coincidence with the other transitions in the cascade to determine its missing strength. A preliminary analysis indicates a similar result as for ^{238}U. A search for

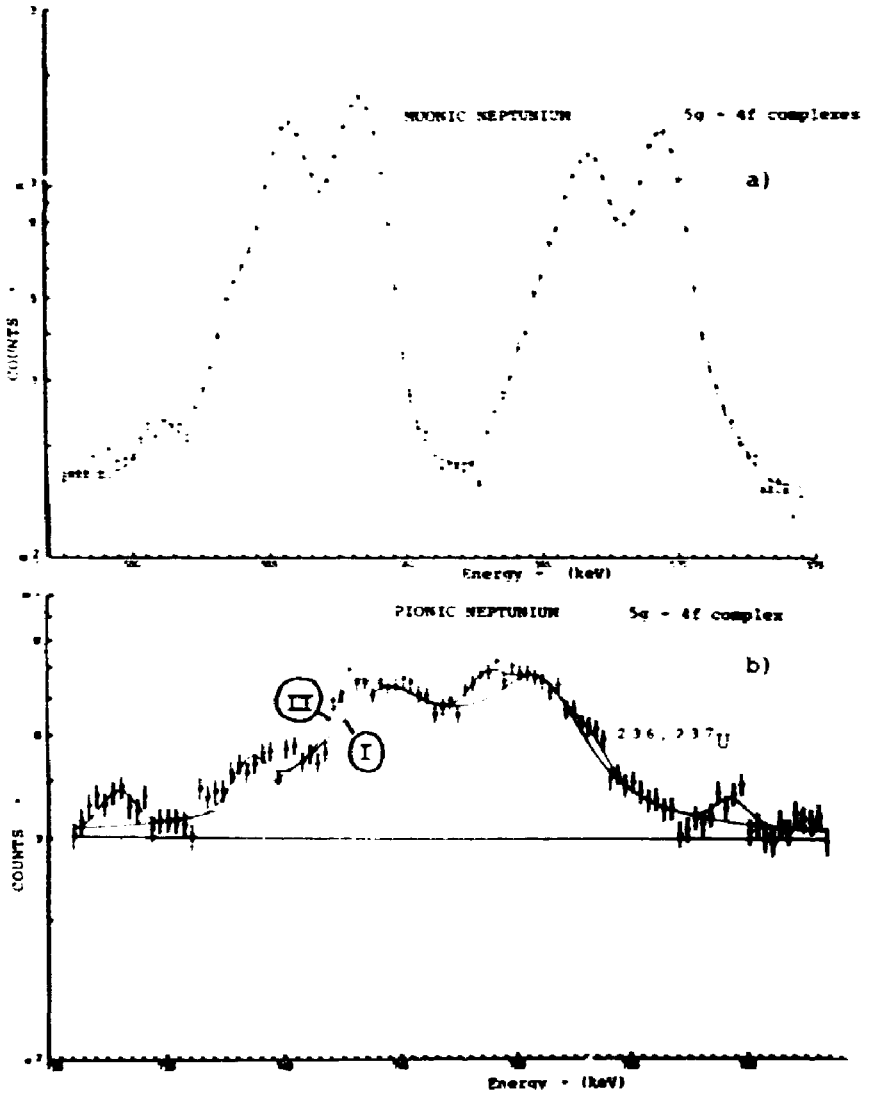

Fig. 2.7 a) Fit to the muonic ^{237}Np 5g → 4f hyperfine complexes.
b) The pionic ^{237}Np 5g → 4f complexes (calculated: curve I) with background from transitions in ^{236,237}U. Curve II has been obtained upon including known strong transitions in these nuclei.

the possible population of a 45 ns fission isomer[14] in muonic transitions for the heavy actinides has been extended to ^{237}Np. A determination of the muon induced fission half-life for this nucleus, which has the highest prompt to delayed fission ratio, is in progress. A search for gamma-rays coming from back-tunneling is also included in this work.

For the pionic ^{237}Np 5g → 4f complex (fig. 2.7b) the splitting has been compared with the corresponding muonic complexes in order to determine the strong interaction monopole and quadrupole shifts, ε_0 and ε_2, of the 4f level. A value for ε_0 of the pionic 4f state has been extracted from the data (see table 2.2). For ε_2, there is no good agreement with theoretical calculations as has been observed previously also for other deformed nuclei [15,16] (see table 2.3).

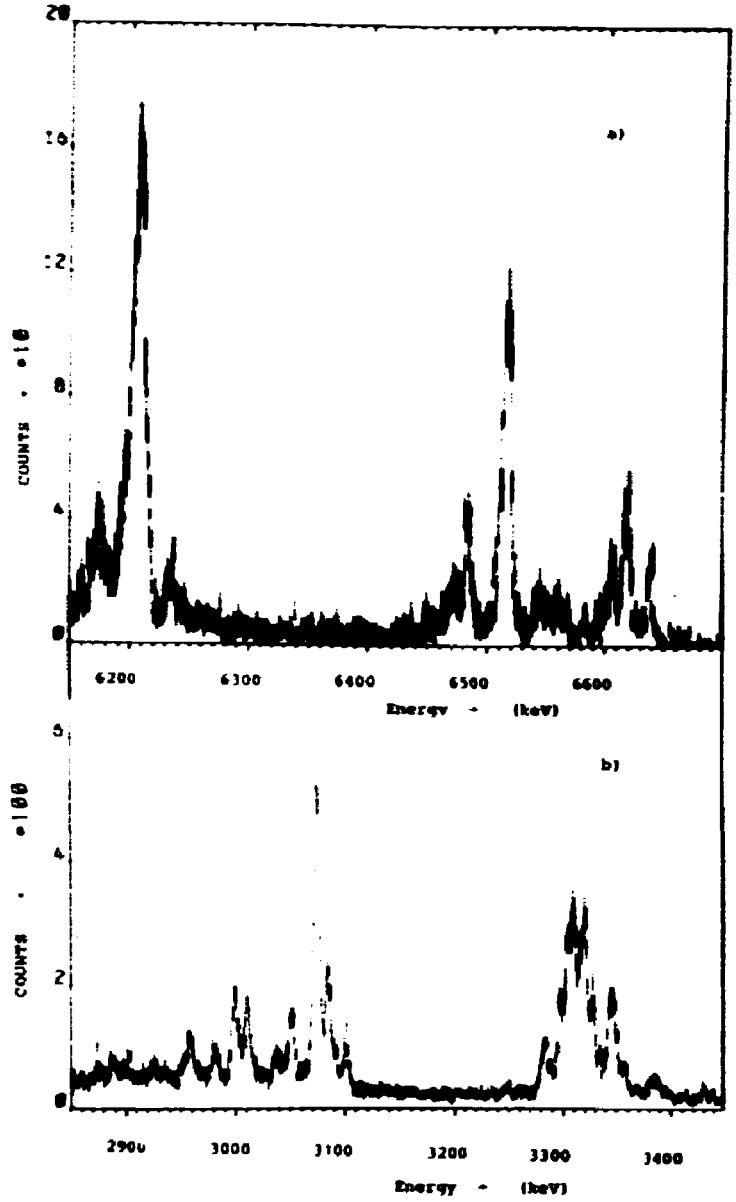

Fig. 2.8 The low-lying X-ray complexes in muonic ^{237}Np; a) 2p → 1s b) 3d → 2p. The spectra reveal significant mixing between muonic and nuclear levels.

Table 2.2 The strong interaction monopole shift (ε_0) and width (Γ_0) in keV for the 4f level in pionic ^{237}Np.

	Experiment	Theory [3]			
		I	II	III	IV
ε_0	5.75 ± 0.14	4.74	4.62	3.35	3.24
Γ_0	3.88 ± 0.26	4.10	4.00	2.53	3.87

2.6.2 Experiments with antiprotons at LEAR (CERN)

The group participates in three experiments at the Low Energy Antiproton Ring (LEAR) at CERN.

Table 2.3 The strong interaction quadrupole shifts (ε_2) of the 4f level in pionic ^{237}Np and in several other deformed nuclei. The values are obtained using the effective electric hyperfine constant (A_2^{eff}) as indicated.

Nucleus	A_2^{eff} (exp) (keV)	ε_2 (theory) [3] (keV)	ε_2 (exp) (keV)
^{165}Ho [14]	1.392 ± .029	- 0.022	- 0.061 ± .029
^{175}Lu [14]	1.694 ± .029	- 0.032	- 0.100 ± .029
^{181}Ta [15]	1.750 ± .016	- 0.036	- 0.112 ± .016
Re [15]	1.163 ± .010	- 0.026	- 0.059 ± .010
^{237}Np	3.73 ± .08	- 0.10	+ 0.46 ± .08

(i) Study of $\bar{p}$H, $\bar{p}$D and $\bar{p}$He X-rays (PS 174)
(E.W.A. Lingeman in the Amsterdam - Birmingham - Rutherford-William & Mary collaboration)

The strong interaction shift (ε_{2p}) and width (Γ_{2p}) for the 2p-level and the width (ε_{3d}) for the 3d level have been measured for antiprotonic helium atoms. As the shifts and widths are quite small an energy calibration (using a ^{75}Se source) was made continously during the measurements.

The values obtained for the 2p level are ε_{2p} = - 7.4 ± 4.9 eV and Γ_{2p} = 35 ± 15 eV. For Γ_{3d} a value of 2.4 ± 0.5 meV was obtained from the measured relative yield Y = 0.37 ± 0.05 of the 3 → 2 transition with respect to the transitions feeding the n = 3 state, by using a value of 1.44 mev for the radiative width.

The results for $\bar{p}$H and $\bar{p}$D can be summarized as follows. In H_2 and D_2 gas at 30 K and 1 atm about 10^9 antiprotons were stopped. In the $\bar{p}$p spectrum a peak containing L X-ray lines is observed as well as a broad structure in the energy region expected for the K X-rays. In the $\bar{p}$d spectrum the L_α line is present but with the present statistics no structure in the K series region has been observed.

(ii) $\bar{p}p$ reactions and scattering (PS 172)
(R. van Dantzig, J. van Goudoever, H.P.J. Veerman; K. Bos, J.C. Kluyver (NIKHEF, section High Energy Physics))

Within the framework of the Switzerland - Italy - The Netherlands - Great Britain (SING) collaboration a mini-hodoscope with 20 scintillators of 1 x 1 x 6 mm^3, read-out from both ends with fibre optic light guides has been tested with antiprotons. In the momentum range from 200 - 600 MeV/c the efficiency comes down from 99 to 89 %. Details on the design and on the test results are reported in ref. 17.

(iii) Search for heavy hypernuclei (PS 177)
(J. Konijn in the Amsterdam - CERN - Darmstadt - Grenoble- Saclay - Warsaw - Uppsala - Orsay collaboration)

In 1984 two short running periods were assigned to the experiment. A first measurement was done at $p_{\bar{p}}$ = 600 MeV/c to investigate beam conditions and backgrounds. A number of heavy target nuclei, among which Bi and U, have been investigated by measuring the angular distribution of the fission fragments arising from prompt antiproton induced fission at angles near 180^o. In a second run at $p_{\bar{p}}$ = 200 MeV/c thin targets of ^{238}U (300 $\mu g/cm^2$ and 30 $\mu g/cm^2$) and ^{209}Bi (30 $\mu g/cm^2$) were investigated using the recoil distance fission-in-flight method. Accurate beam alignment was necessary since both the beam and the target diameter were 2 mm. The analysis of the data is in progress.

2.7 References

1. J.F.M. d'Achard van Enschut *et al.*, Phys. Lett. 136B (1984) 24
2. J.G. Olivier, M. Thies, J.H. Koch, to be published in Nucl. Phys.
3. J.H. Koch, F. Scheck, Nucl. Phys. A340 (1980) 221
4. R. Seki, K. Masutani, Phys. Rev. C27 (1983) 2799
5. J. Konijn *et al.*, NIKHEF-K experimental proposal 84-PM2
6. NIKHEF-K Program Advisory Committee, private communication
7. M.D. Hasinoff, M. Salomon, A. Reitan, Can. J. Phys. 55 (1977) 1561
8. G.A. Miller, contribution E42 to PANIC conference (Heidelberg), F. GÜttner, B. Povh, G. zu Putlitz (Eds) 1984
9. I. Navon *et al.*, Phys. Rev. Lett. 52 (1984) 105
10. P. Bouteilloux, Diplôme d'Etudes Approfondies, Univ. de Paris P & M Curie, Sept, 1984

11. B.D. Dunlap *et al.*, Phys. Rev. 171 (1968) 316 and 186 (1969) 1296
12. M.Y. Balats *et al.*, Sov. Phys. JETP 11 (1960) 1239 and 22 (1966) 4
13. T. Johansson *et al.*, Phys. Lett. 116B (1982) 402
14. E. Migneco *et al.*, Phys. Rev. C16 (1977) 402
15. P. Ebersold *et al.*, Nucl. Phys. A296 (1978) 493
16. J. Konijn *et al.*, Nucl. Phys. A326 (1979) 401
17. H.P.J. Veerman, doctoraalscriptie Universiteit van Amsterdam NIKHEF-K report, PIMU840828

2.8 Approved proposals for pion and muon experiments

84-PM2 Measurement of the cross section of double-charge exchange reactions in pionic atoms (provisionally approved),
J.F.M. d'Achard van Enschut *et al.*

84-PM3 Muonic and pionic X-ray studies of even mass mercury isotopes,
J.F.M. d'Achard van Enschut *et al.*

84-PM4 Nuclear reactions with low-energy pions of 15, 30 and 45 MeV on ^{3}He and ^{4}He,
J.B.R. Berkhout *et al.*

3 THEORY

(Groupleader: J.H. Koch)

3.1 Coulomb sum rules

(T. de Forest, Jr.)

Previous work [1] on the Coulomb sum rule is extended to a field theoretical derivation. Relativistic effects obtained in this approach are shown to be equivalent to those obtained by relativistic corrections to the usual non-relativistic sum rule.

3.2 Electromagnetic interactions in the σ-ω model

(T. de Forest, Jr.)

The prediction of the σ-ω model for the electromagnetic current are explored and found to be quite different than those given by the standard impulse approximation. In particular large variations in the inclusive quasi-elastic electron scattering cross section are found, depending on the operator chosen for the current [2]; see also fig. 3.1. At present, the σ-ω model is extended to the description of the (e,e'N) reaction. Results will be presented at the MIT-Bates Workshop.

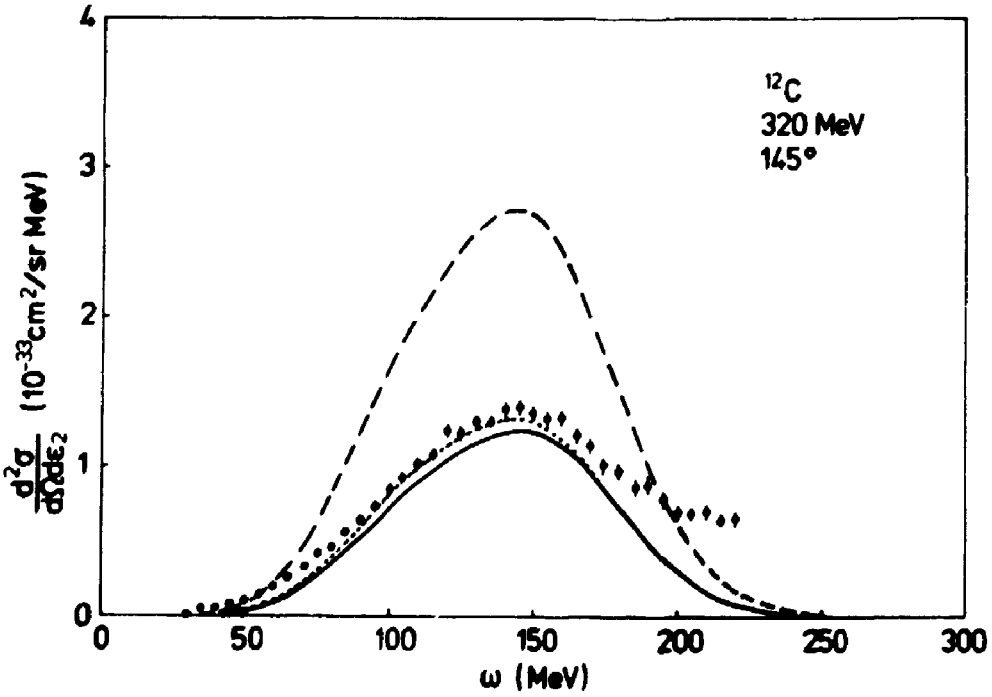

Fig. 3.1 Inclusive electron scattering cross section: – – – impulse approximation, --- and ——: predictions of the sigma-omega model.

3.3 Inclusive electron scattering from light nuclei at intermediate energies

(J.H. Koch and N. Ohtsuka (University of Mainz))

The Δ-hole approach, which has been applied previously to pion- and photon-induced reactions [3], is extended to the description of inclusive electron scattering from nuclei above the pion production threshold. Comparison with recent measurements on ^{4}He, ^{12}C and ^{16}O is made; see fig. 3.2 for the case of ^{12}C (submitted for publication to Nuclear Physics).

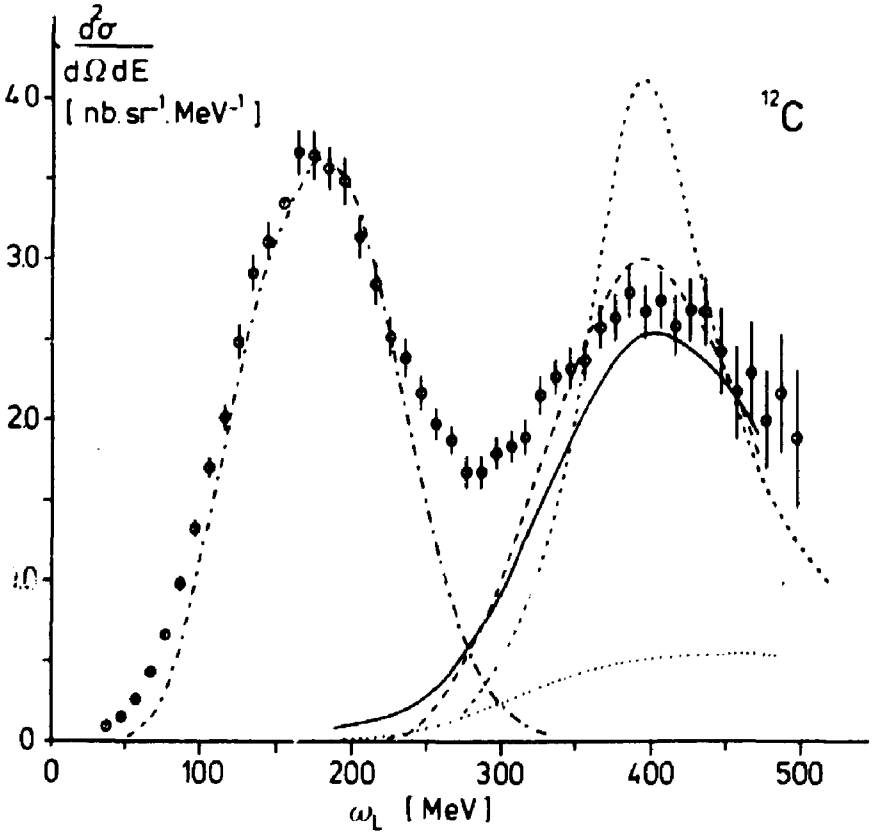

Fig. 3.2 Inclusive electron scattering cross section for ^{12}C at E = 620 MeV, θ = 60° as function of laboratory energy transfer. Data from P. Barreau et al. [4]. Solid curve: full calculation; long dashes: Fermi gas calculation; dotted: sum of non-resonant contributions; short dashes: sum of single nucleon cross sections; dash-dot: quasi-free nucleon knock-out cross section obtained by T. de Forest, Jr.

3.4 Pion photoproduction in the Δ-resonance region

(J.H. Koch, T. Suzuki, T. Takaki)

The production of neutral and charged pions is studied in the Δ-approach. Particular attention is paid to the structure of the Δ-nucleus interaction. Non-resonant production terms are included in a distorted wave approach.

3.5 Anomalous widths in pionic atoms

(J.H. Koch with J.G.J. Olivier, M. Thies (Free University, Amsterdam))

An attempt is made to relate the anomalously small widths observed in the 3d-levels of heavy pionic atoms to properties of the phenomenological pion-nucleus optical potential. Qualitatively, a strong enhancement of the repulsive s-wave potential inside the nucleus is required (Nuclear Physics, in press).

3.6 Core polarization and meson exchange current effects in nuclear electron scattering

(T. Suzuki)

Core polarization and meson exchange currents (including the Δ-isobar contribution) are studied for the magnetic form factors of ^{19}F and ^{49}Ti. These effects are found to be able to explain the enhancement of the second peak of the M1 form factor of ^{19}F and the suppression of the M3 form factor in ^{49}Ti. At present, the influence of core polarization on the charge form factors of ^{50}Ti is being investigated.

3.7 Atomic masses

(G. Audi, K. Bos, A. Hoekstra, A.H. Wapstra)

The calculation of a new table of atomic masses, to replace our 1977 tables, was completed by the end of 1983. The '1983 Tables of Atomic Masses' is accepted for publication in Nuclear Physics B. The tables have been typeset directly from magnetic tapes prepared by the computer; editing was only needed to display nuclide symbols, greek type, etc. in a correct way. Organizing this display caused rather more delay than expected.

A problem in the masses around Hg is caused by a 20 keV difference between the reported very precise absolute mass spectrometric measure-

ments on Hg (± 1 keV) and similar results for neighbouring elements combined with reaction data. Since differences between the mass spectrometric Hg results did not agree with dependable neutron capture spectroscopy results, we decided not to use the Hg mass spectroscopy. This is the only remaining serious problem.

The nuclear spectroscopy check on masses around ^{146}Gd mentiond in the previous Annual Report gave a value for the electron-capture decay energy of ^{147}Gd somewhat higher than the value adopted in our calculation, which was derived from a measurement on the ^{144}Sm(^{12}C,^{9}Be)^{147}Gd reaction. Very recently, a measurement of the (p,d) reaction on (α-radioactive, $t_{\frac{1}{2}}$ = 98 y) ^{148}Gd proved the spectroscopy result to be nearly correct. Thus, the mass values in the 1983 tables following from this decay energy are slightly over 100 keV low.

The collection of new data and their evaluation in combination with old data is being continued.

3.8 References

1. T. de Forest, Jr., Nucl. Phys. A414 (1984) 347
2. T. de Forest, Jr., Phys. Rev. Lett (in press)
3. J.H. Koch, E.J. Moniz, N. Ohtsuka, Ann. Phys. 154 (1984) 99
4. P. Barreau *et al.*, Nucl. Phys. A402 (1983) 515

4 RADIO- AND NUCLEAR CHEMISTRY

4.1 Introduction

The construction of the new chemistry laboratory, situated near the electron accelerator MEA, was completed in October. It was named after the late Professor dr. A.H.W. Aten Jr., who was the first director of the Chemistry Department and who served the Institute in this capacity from 1949 until 1970.

The period under review is characterized by a steadily increasing amount of beam time available for research on the new accelerator. The study of the reactions of radioactive isotopes from nuclear recoil formed the major research effort, with emphasis on reactions of ^{34m}Cl and ^{11}C with arenes. This recoil work is related to investigations dealing with the reactions of muonium carried out in similar systems.

Radiation chemical studies were undertaken on systems similar to those examined in recoil atom studies. This is necessary in order to obtain an understanding of the degree of interference due to the considerable dose received by samples during irradiation with Bremsstrahlung.

There was an intensified effort to produce radionuclides for applied research.

4.2 Hot-atom chemistry

4.2.1 Reactions of Cl atoms

(G.A. Brinkman, B.W. van Halteren, J.Th. Veenboer)

Earlier experiments with 1 : 1 : 1 mixtures of ortho, meta and para C_6H_4ClX compounds (X = Cl, F, CH_3) have shown that Cl-for-Cl exchange by thermal ^{34m}Cl and ^{38}Cl atoms is very selective with a strong preference for chlorine in ortho and para positions. This seems in accordance with the ortho, para directing effect on electrophilic Cl-for-H substitution of electron donating substituents of the type X. A CF_3 group has a meta directing effect on Cl-for-H substitution by virtue of its electron withdrawing nature. If electrophilic H substitution and homolytic Cl exchange are similar in nature there must be a preference for Cl-exchange in the case of meta-$C_6H_4ClCF_3$. Table 4.1 shows that this is indeed the case.

Table 4.1 Thermal ^{34m}Cl or ^{38}Cl-for-Cl exchange in 1 : 1 : 1 mixtures of ortho, meta and para-C_6H_4ClX

Compound	Isotope	Relative yields		
		ortho	meta	para
$C_6H_4Cl_2$	^{38}Cl	42 ± 2	2 ± 2	56 ± 2
$C_6H_4Cl_2$	^{34m}Cl	28 ± 1	14 ± 6	57 ± 5
C_6H_4ClF	^{38}Cl	55 ± 4	1 ± 2	44 ± 3
$C_6H_4ClCH_3$	^{38}Cl	55 ± 6	6 ± 2	39 ± 4
$C_6H_4ClCF_3$	^{34m}Cl	27 ± 7	42 ± 6	31 ± 4

The relative rate of chlorine exchange has been measured in mixtures of two different chlorobenzenes. Results for mixtures of C_6H_5Cl and ortho-$C_6H_4ClCF_3$ are shown in fig. 4.1. From these data one finds that $k_1/k_2 \approx 10$, where k_1 and k_2 are the thermal exchange rates of ^{34m}Cl atoms with C_6H_5Cl and $C_6H_4ClCF_3$, respectively.

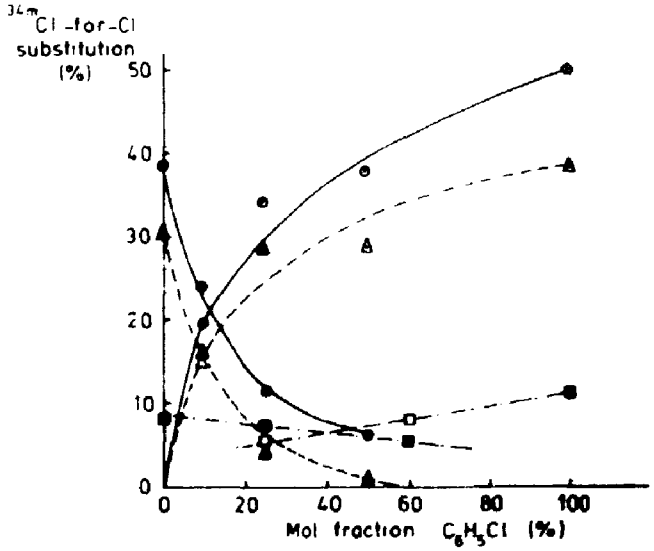

Fig. 4.1 ^{34m}Cl-for-Cl substitution yields in o-$C_6H_4ClCF_3$/C_6H_5Cl mixtures. o-$C_6H_4{}^{34m}ClCF_3$: open symbols, $C_6H_5{}^{34m}Cl$: filled symbols. (——): without scavenger, (-·-·): with 2 % I_2 (hot yields), (---): difference (thermal yields).

The radiation enhanced ^{34m}Cl-for-Cl exchange was previously ascribed to a radiation-induced neutralization of $^{34m}Cl^-$ ions, as this increase occurred at the expense of the inorganic ^{34m}Cl yield. This hypothesis is supported by the outcome of the following experiments. First $^{39}Cl^-$ ions were produced by the $^{40}Ar(\gamma,p)^{39}Cl$ reaction. Chlorobenzene in the presence of $^{39}Cl^-$ ions was then irradiated to produce ^{34m}Cl recoil atoms. Subsequent analysis showed that (61 ± 2) % of the ^{34m}Cl activity was in the form of $C_6H_5{}^{34m}Cl$ and that (84 ± 6) % of the $^{39}Cl^-$ activity was converted to $C_6H_5{}^{39}Cl$.

4.2.2 Reactions of recoil ^{11}C atoms

(G.A. Brinkman, P. Kuipers, G.A.J. Leurs)

The reactions of recoil ^{11}C atoms - produced via $^{12}C(\gamma,n)^{11}C$ - with liquid aromatic compounds were further investigated. It has been suggested that ^{11}C-toluene and ^{11}C-cycloheptatriene (CHT) could be formed from benzene through the reaction of intermediate $^{11}CH_2$ radicals. Addition of 2 - 5 % hexene, however,(as a possible scavenger for these radicals) had no significant effect on the yields of these products.

The ^{11}C product spectrum in benzene as brought about by high performance liquid chromatography (μBondapak C_{18} column, length 30 cm, diameter 3.9 mm, gradient elution from 50/50 CH_3CN/H_2O to 100 CH_3CN) is given in fig. 4.2.

4.2.3 Muonium chemistry

(G.A. Brinkman, P.W.F. Louwrier in collaboration with E. Roduner, University of Zürich)

(i) Reactions of Mu with chlorobutenes

The hyperfine coupling constant (A_μ) was measured as a function of temperature for the muonic radical of 4-chloro-butene-1: $H_2MuC - \dot{C}H - CH_2 - CH_2Cl$. The results are displayed in table 4.2.

Table 4.2 Hyperfine coupling constants A_μ versus temperature

T (K)	172	233	295	334
A_μ (MHz)	353.2	328.5	310.3	304.4

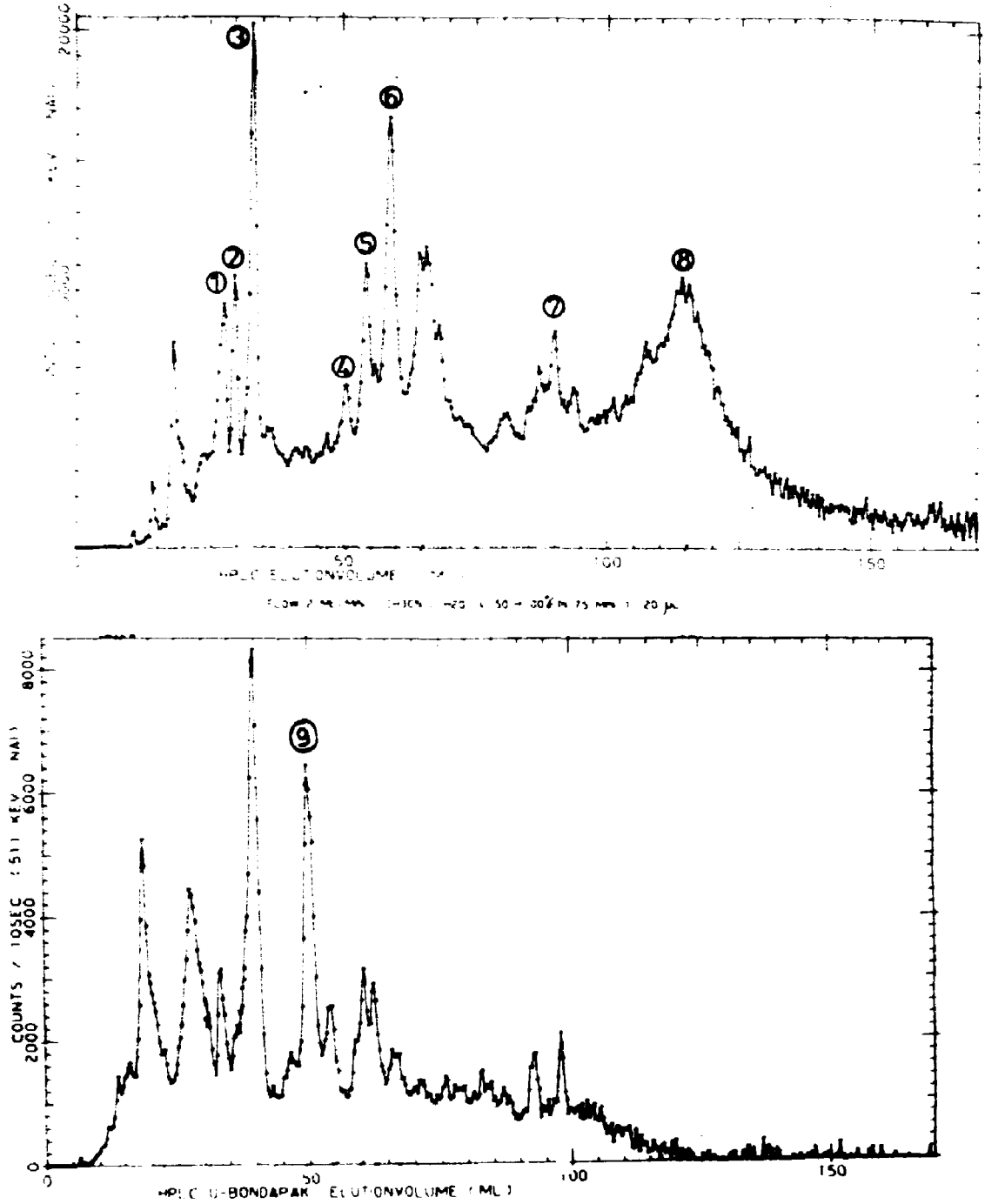

Fig. 4.2 HPLC separation from ^{11}C -labelled products formed by the reactions of recoil ^{11}C atoms with benzene. Upper curve: pure C_6H_6, lower curve: with 2 % I_2. 1: benzene, C_6H_6; 2: phenylacetylene, $C_6H_5C{\equiv}CH$; 3: toluene, $C_6H_5CH_3$ and cycloheptatriene, C_7H_8; 4: biphenyl, C_6H_5-C_6H_5 ; 5: diphenylmethane, $(C_6H_5)_2CH_2$; 6: phenyltoluene, C_6H_5-$C_6H_4CH_3$ and phenylcycloheptatriene, C_6H_5-C_7H_7 (?); 7: trimers; 8: tetramers; 9: iodobenzene, C_6H_5I.

The data are similar to those previously determined by Roduner *et al.* [1] for isobutene, $(CH_3)_2 = CH_2$. They indicate that the barrier for rotation about the $H_2MuC - \dot{C}H$ bond is higher than for the corresponding radicals containing H instead of Mu. This is caused by the larger zero-point vibration amplitudes for Mu, resulting in a larger effective Van der Waals radius.

Similar results were obtained with 2-chloro-butene-2.

(ii) Reactions of Mu with dimethylbutadiene (DMBD)-benzene mixtures

In mixtures of DMBD and C_6H_6 there is a preference for addition of Mu to DMBD. This amounts to a factor of four for a mol ratio of 1 : 4, whereas for pure C_6H_6 the extrapolated value is six.

To gain further information regarding hot or thermal addition of Mu, experiments with 1 : 4 mixtures diluted with CCl_4 were performed, but within experimental accuracy no effect was found.

(iii) Reactions of muonic cyclohexadienyl radicals

Reaction rates of muonic cyclohexadienyl radicals with benzo- and duroquinone were measured (table 4.3). It was assumed that the reaction proceeds by electron transfer from the radical to the oxydant:

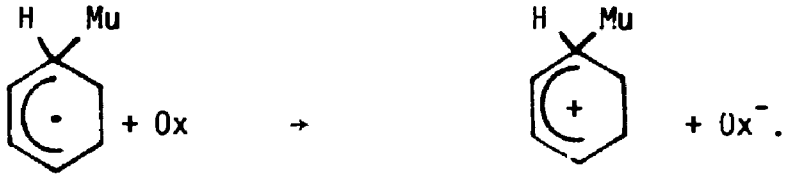

If this is correct, the reaction rate may be influenced by polair solvents. Experiments with 1 : 1 mixtures of benzene and anisol with methanol did show a small increase of the rate constant.

Table 4.3 Rate constants for the reactions of muonic cyclohexadienyl radicals with duroquinones

System	k (10^8 $M^{-1}s^{-1}$)
Benzene	0.62 ± 0.09
o-anisol	1.2 ± 0.3
m-anisol	0.66 ± 0.08

(iv) Addition of Mu to N=N bonds

Apart from the addition of Mu to C=C bonds, addition was also observed to C≡C in $C_6H_5C{\equiv}CH$, C=O in CH_3COCH_3 and N=O in $C_6H_5NO_2$. For the first time the addition of Mu to a N=N bond in azobenzene, C_6H_5-N=N-C_6H_5, was observed. The hyperfine coupling constant is 21.2 MHz; no addition to

the benzene ring (with a coupling constant in between 400 and 500 MHz) was found.

(v) Reaction rate for addition of Mu to C_6H_6

In extremely pure hexane the yield of Mu is some 20 % (in commercial hexane muonium reacts very rapidly with impurities, e.g. hexene). In dilute mixtures of benzene with purified hexane, the rate constant for addition of Mu to C_6H_6 has been determined by measuring the relaxation rate as a function of the C_6H_6 concentration; see fig. 4.3. The extracted rate constant was found to be $k = 1.36 \times 10^{10}$ dm^3 mol^{-1}s^{-1}.

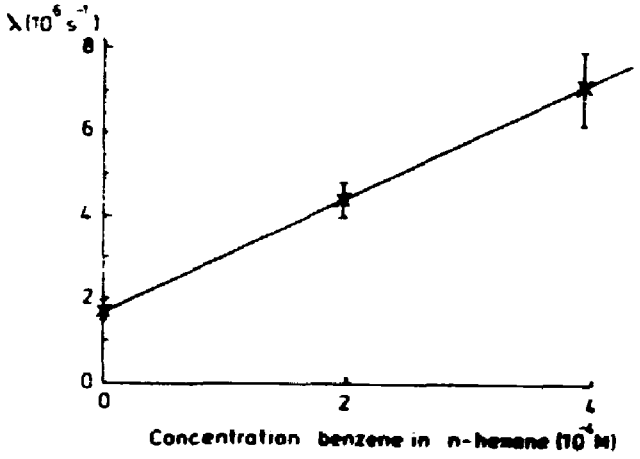

Fig. 4.3 Relaxation rate (λ) for the reaction of Mu with C_6H_6.

4.3 Radiation chemistry

(C.N.M. Bakker, P.W.F. Louwrier)

The radiation chemistry of liquid C_2Cl_4 was further investigated. Measured G-values are given in table 4.4. The reactions leading to the observed compounds are:

$$C_2Cl_4 \xrightarrow{\gamma} \cdot C_2Cl_3 + Cl$$

$$Cl + C_2Cl_4 \rightarrow \cdot C_2Cl_5$$

$$Cl + \cdot C_2Cl_5 \rightarrow C_2Cl_6$$

$$\cdot C_2Cl_5 + C_2Cl_4 \rightarrow C_2Cl_6 + \cdot C_2Cl_3$$

$$\cdot C_2Cl_3 + \cdot C_2Cl_3 \rightarrow C_4Cl_6$$

$$Cl + \cdot C_2Cl_3 \rightarrow C_2Cl_4$$

$$\cdot C_2Cl_5 + \cdot C_2Cl_5 \rightarrow C_4Cl_{10}$$

$$Cl + C_4H_9OH \rightarrow HCl + \cdot C_4H_8OH$$

$$\cdot C_2Cl_5 + C_4H_9OH \rightarrow C_2HCl_5 + \cdot C_4H_8OH$$

In the presence of I_2 several iodinated compounds were observed, but no G-values were measured.

Table 4.4 G-values for compounds formed by irradiation of C_2Cl_4 with and without additives.

	-	I_2	0.5 mol C_4H_9OH	0.5 mol C_2H_5OH
$G(C_2Cl_6)$	0.77 ± 0.03	0.19 ± 0.05	0.36 ± 0.05	0.67 ± 0.02
$G(C_4Cl_6)$	1.74 ± 0.14	0.11 ± 0.01	0.45 ± 0.01	0.26 ± 0.01
$G(C_4Cl_{10})$	0.43 ± 0.03	0.08 ± 0.01	0.14 ± 0.02	
$G(C_2HCl_5)$			2.14 ± 0.16	
$G(H^+) = G(Cl^-)$			8.5	≈ 4

4.4 Dosimetry

A matter of concern for the hot atom chemistry experiments at MEA is the high radiation dose. This dose depends on the nature and the thickness of the target (build up). Chlorobenzene was chosen as a dosimeter, closely resembling the compounds investigated. This dosimeter consists of a mixture of H_2O (40 ml), CH_3OH (860 ml) and C_6H_5Cl (100 ml). During the irradiation H^+ and Cl^- are formed, both with a G-value of 4.75. The amounts of H^+ and Cl^- are then titrated with 0.01 N NaOH and 0.01 N $AgNO_3$, respectively.

The doses were measured for four different tungsten converters at an electron energy of about 115 MeV. The results are given in table 4.5. Most of the samples for hot atom chemistry experiments were irradiated during 5 min using converter 4, with typical electron currents of 60 - 100 μA. This implies doses in the order of 100 kGy.

Table 4.5 Dose rates at the irradiation facility at 115 MeV

W-converter Nr	mm	Dose rate Gy $min^{-1}\mu A^{-1}$	Dosis (rel)	f (%)	f (%)
1	0.05	100	100	5.5	100
2	0.125	150	149 ± 17	8.6	157
3	0.25	200	197 ± 17	10.35	188
4	0.50	250	254 ± 9	13.50	245

The irradiation position is 57 cm away from the converter. Samples have a diameter of 13 mm. The fractions f of the Bremsstrahlung beams that pass through the samples can be calculated (table 4.5). The relative f-values closely correspond to the relative dose rates.

4.5 Radionuclide production

(L. Lindner, P. Polak)

Because of the steadily improving performance of the new electron accelerator, a more detailed exploration of the potential for radionuclide production with MEA was started. The high energies available make it possible to produce a number of difficult to obtain exotic radionuclides of interest for own use and for applications in other disciplines. The consideration of the future use of waste beams, presently dumped in beam-stoppers, is of particular interest in this respect.

The main difficulty specific for radionuclide production with high energy Bremsstrahlung is the necessity of using bulky targets in order to obtain useful yields. This requires particularly modification of the target chemistry. Presently some emphasis is put on medium long-lived isotopes with a clear potential for bio-medical application, e.g. ^{67}Cu and ^{52}Fe.

The isotope ^{67}Cu ($t_{\frac{1}{2}}$ = 62 h) is the longest-lived radionuclide of copper; it has certain advantages over ^{64}Cu ($t_{\frac{1}{2}}$ = 12.4 h). Production of ^{67}Cu is used as a pilot study for future work on different radionuclides. It was produced from ZnO targets by the photonuclear reaction $^{68}Zn(\gamma,p)^{67}Cu$ with Bremsstrahlung generated by 110 - 140 MeV electrons. After acid

dissolution of the ZnO (≈ 20 g) the radiocopper is retrieved in a very selective way by passage through a Chelex-100 column. A subsequent one-step anion-exchange purification is sufficient to obtain a radiochemically pure product. The measured cross section σ_q = 8 mb is in fair agreement with the expectations. It was shown that yields of many millicuries can readily be obtained.

The isotope ^{52}Fe ($t_{\frac{1}{2}}$ = 8.2 h) is a β^+ emitter; it is the parent of ^{52m}Mn ($t_{\frac{1}{2}}$ = 21 m). Carrier-free production is most feasible by means of $Ni(\gamma,\alpha xn)^{52}Fe$ for which reaction a cross section σ_q = 15 μb was measured.

4.6 Labelling of organic compounds

(G.A. Brinkman, B.W. van Halteren, G.W.M. Visser (Free University of Amsterdam))

Several compounds were labelled with ^{18}F, using ^{18}F-F, produced by the $^{20}Ne(d,\alpha)^{18}F$ reaction with 15 MeV deuterons from the cyclotron of the Free University. As fluorination of organic compounds proceeds fairly well controlled with CH_3COOF, this compound was used in CH_3COOH solvent for the replacement by fluorine of the H-group in arylmercury compounds.

Direct reaction with C_6H_5X results in a non-selective replacement of H by ^{18}F. Displacement of a HgCl or HgOAc group in substituted benzenes results in only one compound; see table 4.6.

In order to gain insight into the stability of CH_3COOF and the mechanism of the fluorination the reactions of $CH_3COO^{18}F$ with cyclohexene were investigated. By using reversed HPLC analysis we observed six products:

- two isomeric ^{18}F-cyclohexenes (total yield 4 %)

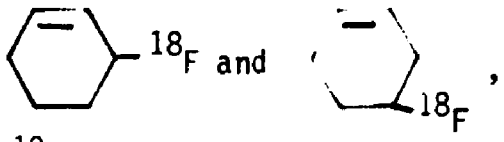

- cis and trans ^{18}F-acetoxycyclohexanes (total yield 18 %)

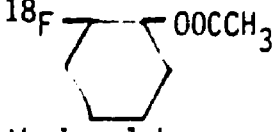

- cis and trans ^{18}F-methylcyclohexanes (total yield 11 %)

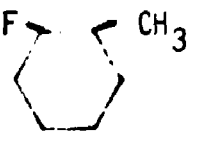

The last group of compounds must be formed by the addition of ^{18}F and CH_3 at the double bond requiring the decomposition of $CH_3COO^{18}F$ via $CH_3...COO..^{18}F$.

Table 4.6 Fluorinated aryl compounds from the displacement of a mercury group using MeCOOF.

Substrate	Yield [a] (%)	Ratio of fluoro products [b]			
		o	m	p	α
Anisole	85	3	-	1	-
p-$MeOC_6H_4HgOAc$	65	-	-	1	-
Acetanilide	67	2	-	1	-
p-$MeCONHC_6H_4HgOAc$	60	-	-	1	-
Phenol	75	3	-	2	-
o-HOC_6H_4HgCl	53	1	-	-	-
p-HOC_6H_4HgCl	47	-	-	1	-
Toluene	14	8	1	4	1
MeC_6H_4HgCl [c]	57	3	1	13	-
Benzene	18				
PhHgOAC	58				
PhHgCl	55				

a) Based on MeCOOF (MeCOOF was prepared from F_2 in 80 - 90 % chemical yield, so the radiochemical yields based on $[^{18}F]F_2$ are 20 - 30 %): the standard deviation is ca 5 %.

b) Identified by g.c.-mass spectroscopy and by comparison of the retention times in reversed phase h.p.l.c. with those of authentic samples.

c) Mixture consisting of 18 % o-, 6 % m-, and 76 % p-MeC_6H_4HgCl.

Some 18 % of the ^{18}F activity is unaccounted for. Experiments with bulk amounts of CH_3COOF with a GCMS for mass analysis revealed the presence of 15 - 20 % of an unlabelled compound, identified as 2-acetoxycyclohexene  $OOCCH_3$. The ^{18}F activity disappears in this reaction.

4.7 Reference

1. E. Roduner, W. Strub, P. Burkhard, J. Hochmann, P.W. Percival, H. Fischer, Chem. Phys. 67 (1982) 275

5 TECHNICAL DEVEPOPMENTS

Groupleaders: H. Arnold, P.J.T. Bruinsma, M. van Gelderen (until May 2, 1984), A.P. Kaan, E. Kwakkel, G. Luijckx, T.W. van der Raay)

5.1 Introduction

Over the past year, a total of 4800 beam hours has been scheduled, including some 600 h for accelerator studies and energy-upgrading activities. The weekly efficiencies for accelerator performance and data are displayed in fig. 5.1a and 5.1b, respectively.

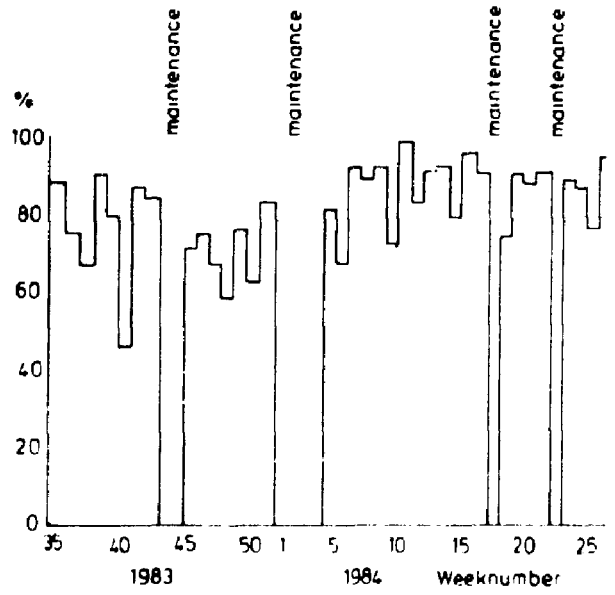

Fig. 5.1a

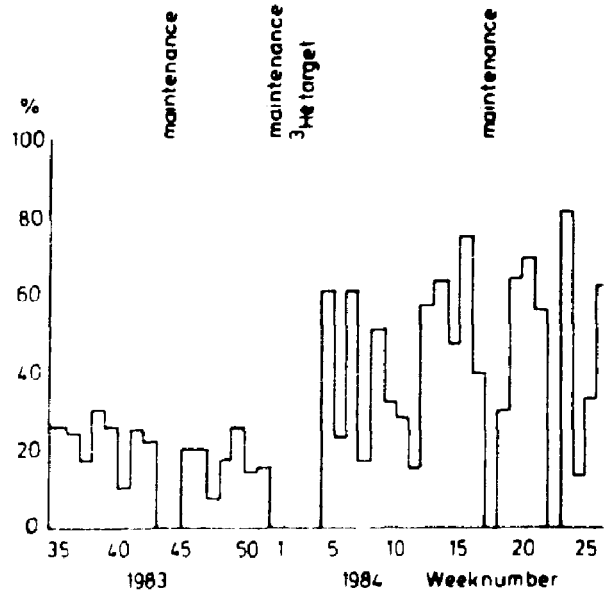

Fig. 5.1b

The second half of 1983 the efficiency was affected largely by difficulties with the implementation of the 4 MW mode of operation which was needed for the scheduled experiments increasingly requiring the highest available energies. These difficulties have largely been overcome so that since January 1984 nominally 400 MeV energy could be delivered to the experimental halls. The data-taking efficiency has reached an appreciably higher level during the first half of 1984.

The duty factor was deliberately restricted to 1 % although the

machine is capable to go up to 2 %. Reasons for the restriction were mainly energy costs and reliability.

All experimental halls (LEF, LECH, EMIN, PIMU) are operational such that the technical departments were mainly concerned with the maintenance of the rather complex equipment. For the PIMU hall the design and construction of a new pion converter has been taken up in order to improve the pion yield and electron contamination considerably.

In the LEF hall a MWDC detector has been designed and installed to improve the overall resolution to better than 1×10^{-3}. The different technical activities for accelerator, beam handling systems and experimental halls are discussed in section 5.2 through 5.4. Section 5.5 deals with the project 'UPDATE', section 5.6 with work for third parties and section 5.7 with general activities which serve to keep the know-how up to date.

5.2 The accelerator MEA and its beam lines

5.2.1 Operations

In the second half of 1983 beam production was unsatisfactory because operation of the klystrons at full power (4 MW) caused internal arc-over of the klystrons resulting in damage to the modulators. Excellent performance has been established since January 1984 due to the replacement of critical components and the introduction of special processing procedures. In view of overall accelerator performance attention has been paid to several subsystems, e.g. the 1 % stability of the klystron focussing power supplies has been improved to 0.1 % by the installation of redesigned amplifiers.

The present beam specification are listed in table 5.1. It has been decided not to increase the repetition rate above 250 pps (pulse length 40 μs) in order to improve the reliability during actual data taking hours (see section 5.1).

Table 5.1 Beam specification MEA

	Design value	Presently available
Energy (max)	50 - 500	50 - 480
Duty factor at 500 MeV (%)	2.5	max. 2
Duty factor at 250 MeV (%)	10	max. 2
Energy spectrum (%)	0.5	0.1
Target current (μA)	200	50 - 100

5.2.2 Major accelerator systems

Modulators. Initially high-voltage transients occurred during the 4 MW mode of operation due to klystron arc-overs. These transients damaged several components of the PFN circuits. Meanwhile semiconductor diodes have been replaced by higher-duty types, the end-of-line circuit has been modified to withstand higher currents and transient suppressors have been installed at critical positions. The 1000 volt main rectifiers have also been equipped with filter diodes to prevent oscillations at the higher power levels. These measures helped greatly to improve the reliability of the modulators.

Mechanical wear of some potentiometers caused erratic behaviour of the klystron focussing power supplies. They are gradually being replaced. The scheduled replacement of the filament transformers, important for increasing the duty factor, has not yet been completed.

Klystrons. The high duty factor klystrons perform well (see fig. 5.2a); 18 klystrons have been operating on a circulation scheme in the 13 sockets (12 at the accelerator and 1 in the test facility). The accumulated numbers of high-voltage hours per klystron are displayed in fig. 5.2b. In total over 150,000 high-voltage hours have been accumulated. The mean time between failures (MTBF) now is 25,000 hours. The newly developed body-current protection circuits proved essential in the successful 4 MW RF processing of the klystrons. On the other hand at the cathode voltage levels involved (> 120 kV), it has become apparent that after an internal arc-over considerable time should be allowed for reprocessing.

Cooling systems. The freon cooling capacity of all modulators has been doubled by applying vapour condensors instead of liquid-to-air heat exchangers. Another attractive feature of the new systems is the reduction of freon losses from 10,000 l/year to a negligible amount. The modification is shown in fig. 5.3.

Injector. The new fiberoptics system (Hewlett Packard HFBR-2001) performs well. Future high-current operation of the linac requires precise timing control (< 100 ns) in order to compensate for transient beam-loading effects. A design has been completed to modify the existing hot-deck electronic circuits. By replacing the bipolar drive transistors through power FET's timing accuracies better than 100 ns will be obtained.

Computer control. Work has been started to improve the performance of the local computer control system, which since ten years has been

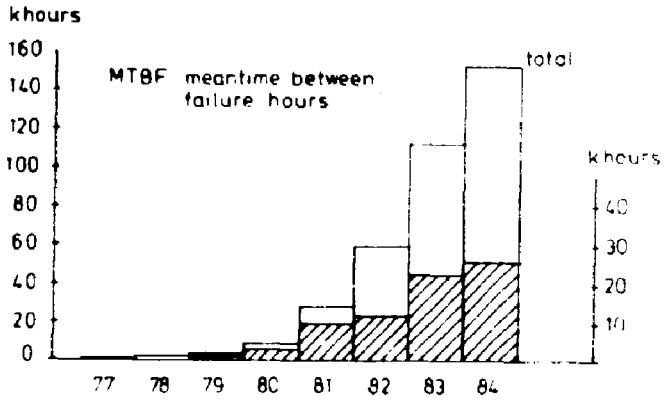

Fig. 5.2a Total accumulated high voltage hours (18 klystrons).

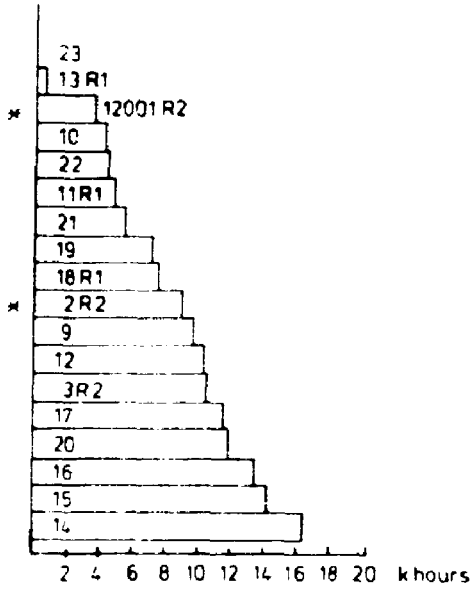

Fig. 5.2b Accumulated high voltage hours (July 1984) per specified klystron; * under repair.

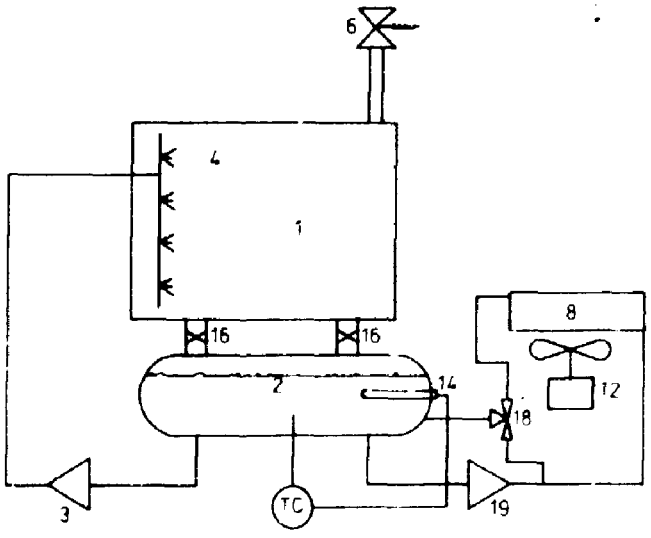

Former FREON cooling arrangement

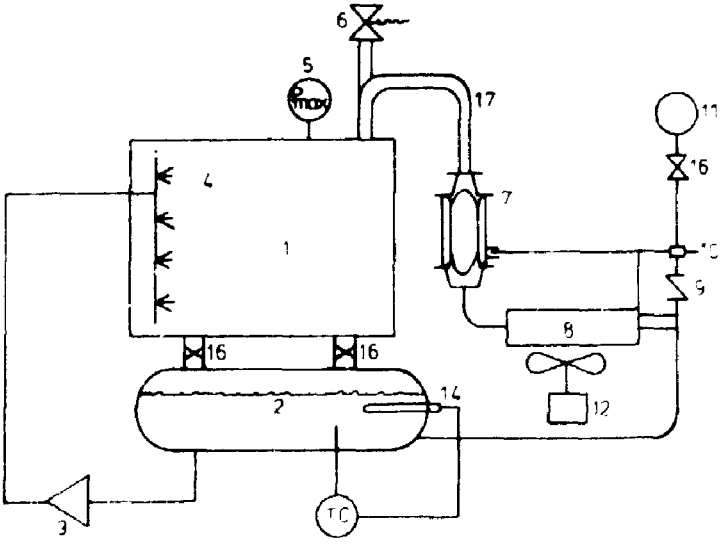

Modified FREON cooling arrangement

1 Modulator housing
2 Freon tank
3 Spray pump
4 Spraying nozzles
5 Max. pressure switch
6 Relief valve
7 Control valve
8 Air cooler
9 Check valve
10 Liquid separator
11 Exhaust line
12 Ventilator
13 Liquid return line
14 Electrical heater
15 Temperature switch
16 Valves
17 Vapour line
18 3-way valve
19 Cooling pump

Fig 5.3 Modulator freon cooling.

provided by Alpha LSI-2 minicomputers. A Capro-68K (from INCAA) system in CAMAC, containing a MC 68000 processor and 512 kb of memory, has been acquired. A portable version of the Fenix real-time operating system (now written in C) has been implemented in this hardware. It allows incorporation of the Capro-68K for accelerator control purposes in the existing IKO-net. The Capro-68K processor system requires the design of a Camac adapter for the existing modulator control unit Dig II, presently directly interfaced to the Alpha I/O bus. The design of a new control unit DIG III according to a more modular concept is in progress. The new unit should facilitate maintenance and require fewer and cheaper spare parts. At the same time the new design must provide an easier operator control of the individual PFN units of the modulator.

The central console computer (an Alpha-LSI-2) has been replaced by a MIK-11/2, and console facilities have been expanded by installing two or more of these systems.

The disk drives of the General Service Computers have been replaced by fast 330 Mb Winchester drives, resulting in higher reliability and less interaction between linac control and experimental analysis.

5.2.3 Accelerator research

In order to increase the number of beam hours, tuning procedures are constantly being improved. Tables, stored in the control computer, have been compiled which allow quick setting of most of the machine parameters. The beam-spot size and beam-position stability have been improved to 0.02 mm.mrad at 400 MeV. For those electron-scattering experiments requiring a very high resolution, the electron energy can now be maintained within 0.1 % during long operation periods without operator interaction.

Experiments show that, although the injector delivered peak beam currents up to 35 mA (corresponding to 350 μA at 1 % duty factor), stable linac operation at high current is presently not possible. This is due to the related stringent stability requirement on several beam-steering systems.

5.2.4 Upgrading program

Klystrons. In view of the project 'UPDATE' (see section 5.5) experiments have been made to increase the r.f. peak output of the klystrons beyond 4 MW. A modulator improvement program to raise the RF peak power output to 5.5 MW is in progress.

Kickermagnets. Initial beam tests have been performed with the low-energy kickermagnet system. The computer-control program has been adapted and protection systems modified. As a result beam-sharing between the LECH and AFBU beam lines on a pulse-to-pulse basis has been shown possible. With MEA operating at 250 Hz, 50 pps were available in LECH to be used for experiments and 10 pps were available in AFBU for tuning purposes. The main limitations so far are 20 ms rise and fall times of the present kickermagnet.

Magnet design. Based on aluminium tape wound coils, magnets have been designed and fabricated. Main features are low cost (simple production methods, cheap materials), reduced power consumption (more freedom in optimizing coil dimensions) and better cooling properties. Further studies have started to apply these techniques to septum, quadrupole and bending magnets of the proposed stretcher ring.

Monitors. The coupling loops in the traveling-wave beam-position monitors were redesigned in order to improve on absolute accuracy. A commercially available DCCT instrument has been tested as a non-interfering dc beam monitor. A sensitivity of 100 nA may be feasible provided rigorous magnetic and acoustic shielding is applied. This type of monitor could be an alternative to high power Faraday cups.

5.2.5 Beam switch yard system

A new collimator protection system (see fig. 5.4) has been installed in the 400 beam line. At the exit of the first bending magnet a non-cooled collimator-compton battery combination (C2) limits the spill of high energy filling-time electrons to 20 W, while low energy filling-time electrons, to a maximum of 300 W, are collected by a conduction-cooled collimator (C1). In front of the bending magnet a non-cooled collimator-compton battery system (C3) limits the out-of-range electron beam to 130 W.

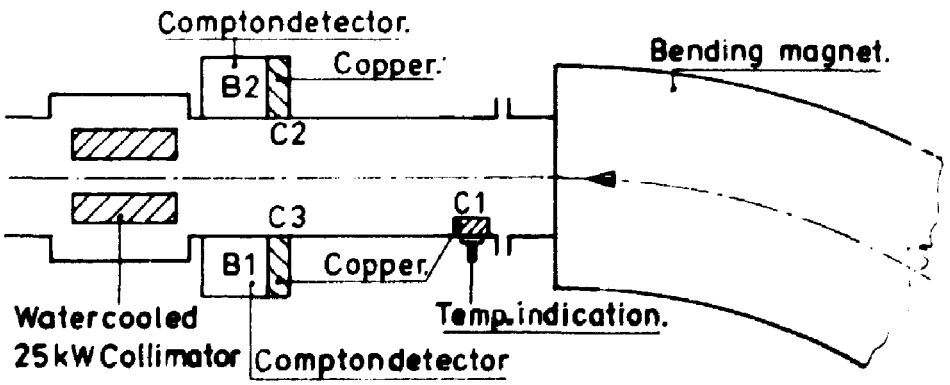

Fig. 5.4

5.3 Experimental equipment

A detailed description of the equipment in the different experimental halls can be found in earlier reports. Several papers [1,2,3,4,5] describing most of the equipment in the electron-scattering halls (EMIN and LEF) have appeared in the literature. In this report we only emphasize the important improvement in the past year.

5.3.1 The EMIN hall

In the past year about 3600 h have been scheduled for electron-scattering experiments; data-taking efficiency was around 35 %. The main addition to the experimental facility consists of a further extension of the detector systems with

- a Bira microprocessor to store the Camac information (ADC and TDC), as part of the event descriptor. This feature was applied in the $^{3}He(e,e'p)^{2}H$ experiment to enable proton-deuteron identification,
- a fine tuning of the look up table of the time-interpolation converter. The converter constructs a channel number from the hit lines in the wire chamber. The addition of the fine tuning improved the channel-channel response.
- a wire chamber gas safety and flow control to guarantee safe and stable operating chambers.

The instruments including their supporting mechanical, vacuum and electronic hardware showed little or no failures. Unfortunately the angle positioning of the spectrometers still requires manual control as the supplier of the remote controlled version was unable to deliver a reliably operating system.

5.3.2 The LEF hall

The 180^{0} electron-scattering equipment has hardly undergone any changes since 1982. An interface to adapt the NRL (USA) refrigerated gas target (Nucl. Instr. and Meth. 77 (1970) 136) to the LEF target box has been tested. Because of an accident with a high-pressure reducing valve in this system a new and safer one has been constructed with the following features (see fig. 5.5)

- the pressure is continuously adjustable between 0 and 10 bar by varying mechanically the height of a liquid nitrogen dewar, which cools a spiralised cooling tube,

- complete recovery of the expensive gas is possible by means of a gas-return trap-out tube,
- the pressure can be read out in units of 0.01 bar in the control room.

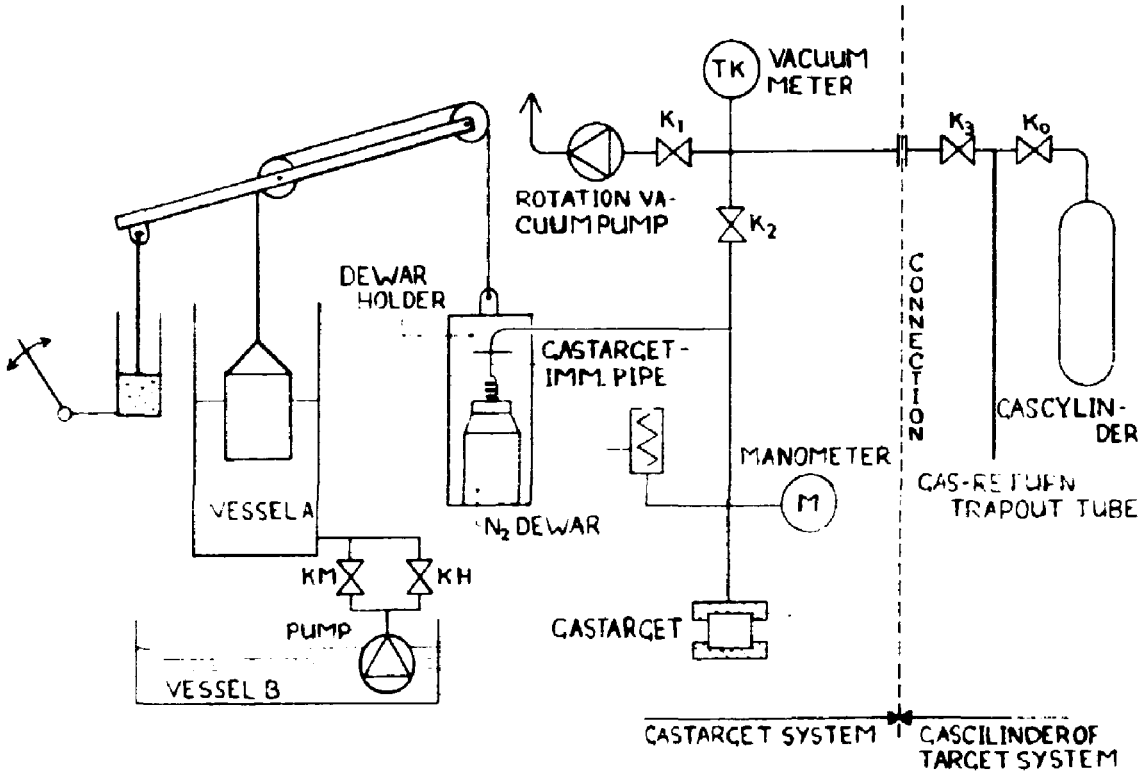

Fig. 5.5

As the first step to improve the resolution of the 180° electron-scattering facility, a multiwire proportional chamber (MWPC) has been constructed. The wire chamber is based on a design used at MIT (Nucl. Instr. and Meth. 141 (1977) 457). It consists of 16 measuring wires separated from each other by three field-shaping wires at distances of 2 mm. The distance between the measuring wires is 8 mm and the gap is 10.8 mm. The implementation of the wire chamber with its intrinsic resolution of better than 10^{-4} will improve the overall resolution from 1.25×10^{-3} down to 7×10^{-4} (see fig. 5.6). Further improvement of the resolution to $\leq 5 \times 10^{-4}$ requires the energy-loss technique to be implemented in the beam-handling system.

The wire chamber has been tested with a ^{106}Ru source and is now ready for installation in the focal plane of the Penner spectrometer.

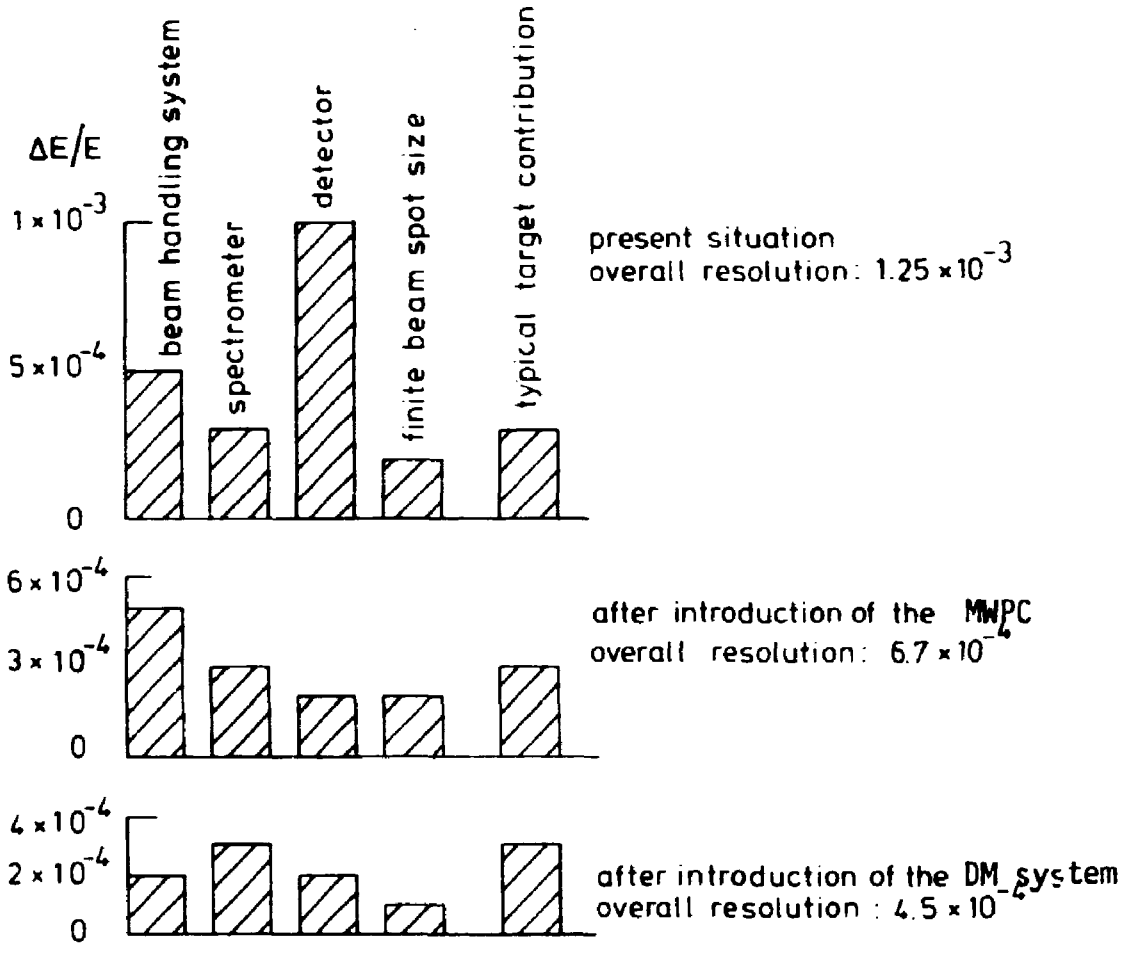

Fig. 5.6 Contributions to the overall resolution before and after installation of the MWPC and future dispersion matching (DM) system.

5.3.3 The PIMU hall

The pion-production target. After the successful installation of the new beam dump (see preceding annual report) it was decided to further improve the secondary beam intensity by developing a new pion-production target system. The design made is based on a SLAC type radiator and a LASL pyrolytic graphite target which target material has been chosen to produce a low Z material of high density combined with an outstanding heat transfer comparable with the heat transfer in metals. This choice also enables the use of a stationary water-cooled target instead of the present rotating graphite wheels. Calculations show that the temperature of the target will not exceed 1000 ^{o}C at an incident beam power of 100 kW. The technique required to solder the graphite to the copper cooling tubes has been mastered. The brazing alloy used is 70 % Ti, 15 % Cu and 15 % Ni. The brazing temperature of the alloy is 950 ^{o}C. The targets will be brazed

in the furnace of the FOM Institute for Plasma Physics 'Rijnhuizen'. The radiator would originally have been made from a sintered WRe compound which is much stronger than pure tungsten. In a trial irradiation it turned out that the rhenium-oxyde was knocked out of the target causing a rhenium contamination of the surroundings. To compare the residual radioactivity of a W and a Au radiator (which is a much better heat conductor) irradiations will have to be done to enable the best choice for the high Z radiator material. Fig. 5.7 shows the W (or Au) radiator and 5 blocks of 10 mm thick pyrolytic graphite, soldered onto the copper pipes of the cooling systems. From this arrangement, presently under construction, the pion beam intensity is expected to increase by a factor of more than two, whereas the electron background will decrease by a factor of four.

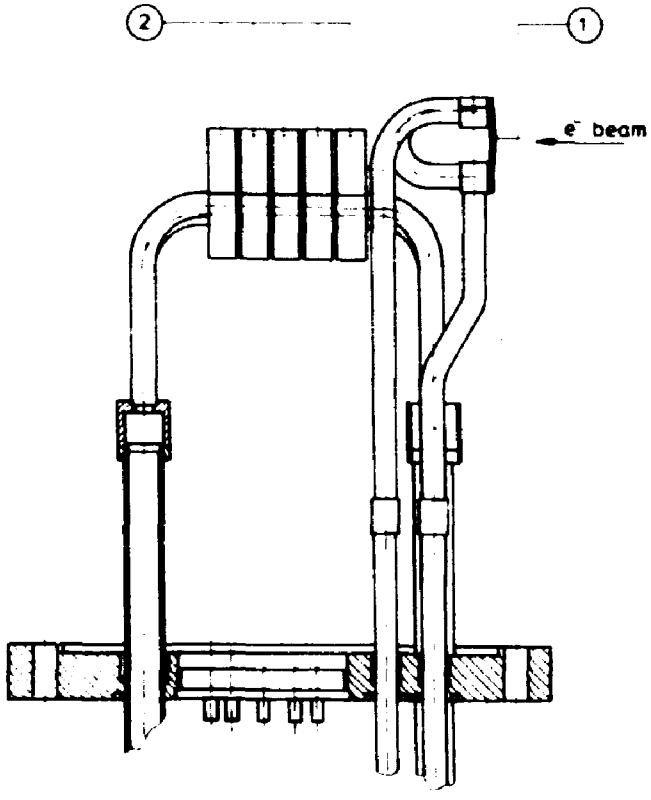

① Tungsten radiator (15mm thick).
② Pyrolytic graphite (5 plates 10mm thick)

Fig. 5.7 SLAC-LASL type pion converter.

The beam handling system. Using coils wound from aluminium tape glued on a copper plate, a new magnet has been built. After installation the heat transfer of one of the coils showed to be inadequate due to a too thick layer of insulating epoxy (1.5 instead of 0.5 mm). The manufacturer

has been given instruction how to avoid too thick a layer of insulation while repairing the coil. Aluminium band coils have also been ordered to modernise three quadrupole magnets from the shut-down cyclotron beam lines for use in the pion and muon beam systems.

5.4 Computer facilities

The three major tasks of the Computer Systems Group were:

a) enhancement, extension and renovation of the IKOnet accelerator and experiment control computer network,
b) management of the network and central computing facilities,
c) replacement of the central computing facility.

5.4.1 IKOnet accelerator and experiment control computer network

The most heavily used Experiment Control Machine (EMIN) has been replaced by a PDP-11/44 with 2 Mb of memory and a fast 330 Mb Winchester disk drive; a substantial improvement of data-taking and on-line data analysis capabilities resulted.

The disk drives of the General Service Machines A & B have been replaced by fast 300 Mb Winchester disks, resulting in higher reliability and much larger capacity, especially for the dumping and analysis of experimental data from physical experiments. A new Experiment Control Machine based on the BIRA-11/23 has been installed at the new chemical laboratory, and has been connected to the IKOnet. The task of the Message Switching Machine has been distributed over two machines (MSA-A and MSM-B) to achieve a higher reliability and throughput. Also malfunctioning of communication channels in the experiment control part of the network will no longer disturb the accelerator control part, and vice versa. THe central console computer (an Alpha LSI-2) has been replaced by a MIK-11/2, and console facilities have been expanded by installing two additional systems: CO2 as an additional central operator console machine, and E04 as a local console in the EMIN control room.

Software improvements. The Terminet system has been completed and installed on all major network computers. This system allows users to make a connection with an arbitrary computer from each computer terminal, in a transparant way. Three simultaneous connections (either with the same or with different computers) may be maintained from a single terminal. Two

screen editors have been made available to the user community;

1) a substantially enhanced version of the Rand editor, especially suitable for novice users,
2) a version of the Berkeley 'vi' editor, to provide compatibility with the new Gould computer (see below).

Various changes and extensions of the central accelerator control software resulted in increased reliability and improved operator response times. Experiment control software has also been enhanced and extended to provide more functionality. A subset of the Graphical Kernel System (GKS) has been installed and adapted to the needs of the physicists.

Software conversion. Various software conversion projects have been started to ease the transition of used software from DEC-System-10 to Gould 32/9705; these included an inventory management system for the Digital Electronics Group and a drawing administration system for the Mechanical Engineering Group.

5.4.2 Management of the network and central computing facilities

Management of computers in the open-shop fashion as currently practised at NIKHEF-K, centers around fool-proof backup procedures, simple boot procedures and sufficient documentation. All these items seem to have developed in the past few years up to a satisfactory level of usability (also by non-experts). Facilities to simplify the increasing amount of file backup (cf. increased amount of on-line disk storage) have been developed and put into operation. The transition to the new Gould 32/9705 central computer (see below) required many additional system management activities. The central computer room has been equipped with a new airconditioning system (the former one was more than 15 years old).

5.4.3 Replacement of the central computing facility

After an EEC advertisement by the KMC an extensive Request for Proposal was sent to 12 suppliers of computer equipment. Five suppliers responded with proposals, which have been evaluated by a NIKHEF-K selection committee. In addition, computational and interactive benchmarks have been performed on the various configurations offered.

A final choice was made for a Gould 32/9705 computer system, running under the UTX-32 operating system, a derivative of BSD 4.1c Unix and System V Unix. After obtaining approval from the CRIVA, the system was

ordered.

The system arrived two month behind schedule in May 1984, and various problems prevented the complete teansition from DEC-System-10 to Gould before the scheduled data of July 1, 1984.

When the transition is completed, Unix will be the standard operating system for all experiment and general service computers at NIKHEF-K (with the exception of one machine).

5.5 Project 'UPDATE'

On July 1, 1984 NIKHEF-K has put forward an official proposal called UPDATE, aiming at an increase of beam duty factor to 90 % by adding a pulse-stretching magnetic device to MEA while increasing the maximum energy to 700 MeV. Referring for full information to the proposal[6], we restrict ourselves here to a brief general description.

The lay-out of the pulse-stretcher (PS) with respect to MEA and Beam Transport System (BTS) (see fig. 5.8) enables beam extraction from the PS through the existing BTS towards the present experimental halls. The west arc and the north straight section of the PS will be located within existing buildings. A new tunnel has to be dug to accommodate the south straight section and the east arc. The total length of the PS is 280 m (the linear sections are 100 m long); this length corresponds to a revolution time τ = 0.93 μs. At three-turn injection, with a repetition rate f = 365 Hz and a MEA peak current of 40 mA, the average extracted current becomes I = 40 μA. As the r.f. filling time of the linac is $\tau_f \sim 1.3$ s, the r.f. duty cycle will become 1.5×10^{-3}.

A high-duty factor (≈ 90 %) beam will be generated by slowly extracting electrons from the PS during the time between the injection pulses At f = 365 Hz, this time is 2.74 ms, which corresponds to 2900 revolutions.

When the electrons traverse the bending magnets of the PS, part of their energy will be radiated away as synchrotron radiation; at E = 700 MeV, the loss is 6.44 keV/rev. An electron that stays in the machine for 2900 revolutions therefore would lose 18.7 MeV, which is 2.7 % of its energy. An 2856 MHz cavity system requiring ≳ 2.5 kW r.f. power will be installed to replenish the synchrotron radiation losses.

At the present facility it has been demonstrated that the overall momentum resolution in (e,e') experiments is of the order of 5×10^{-5}. This could only be achieved by properly matching the quality of the MEA

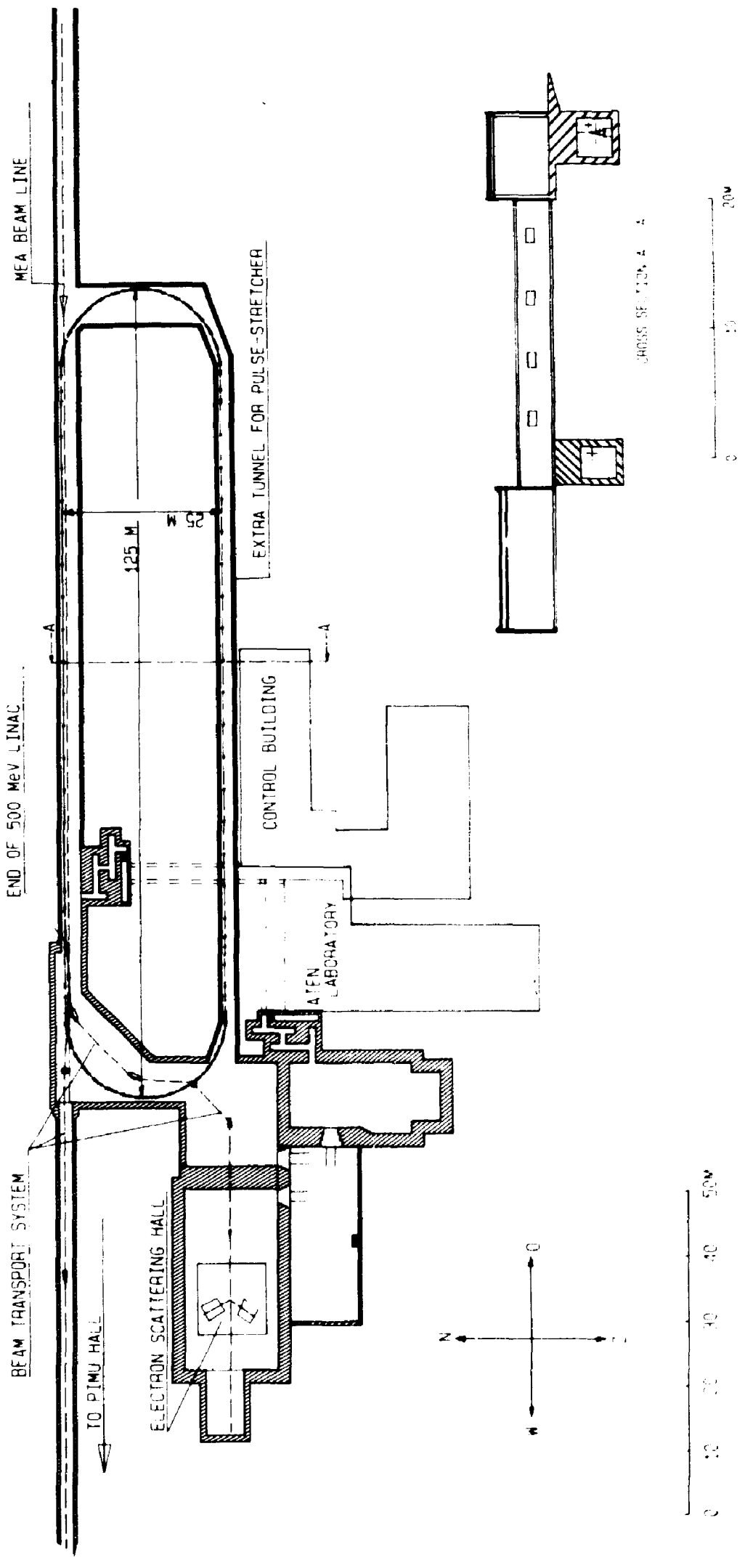

Fig. 5.8 Lay-out pulse stretcher facility with respect to the existing buildings.

emittance (0.07 mm.mrad at 700 MeV) with the optical quality of BTS, spectrometers and detectors. The emittance of the extracted beam from the PS should therefore be comparable to that of the present MEA beam. Study of the extraction mechanism shows that this is indeed possible.

The present MEA parameters are compared with those requested for the pulse-stretcher mode of operation in table 5.2.

Table 5.2 Main beam parameters

		Present MEA	MEA for PS mode
E_{max}	(MeV)	500	700
Beam pulse length	(μs)	40	2.8
Repetition rate	(Hz)	500	365
Beam duty factor	(%)	2	0.1
I_{peak}	(mA)	10	40
I_{target}	(μA)	$\geq$ 100	40

The present mode of operation which we will call High Current (> 100 μA), 2 % duty factor Mode (HCM) remains available also after the construction of the PS with the low current (40 μA), 90 % duty factor Mode of operation (PSM). It is foreseen that for certain experiments (e.g. with secundary beams) HCM operation will be preferred over PSM operation. The peak beam current in the accelerator has to be increased in the PSM operation from 10 mA to 40 mA in order to reach - at the considerably reduced MEA beam duty factor (0.10 %) - an average current of 40 μA for the experiments. The energy increase from 500 to 700 MeV will be achieved by installing four additional klystron-modulator units working each at 20 MW r.f. peak (0.15 % d.f.). In addition the present klystron-modulator units have to be updated from 4 MW, 2 % duty factor to 5 MW, 0.7 % d.f.

Test performed with MEA have shown that the new parameters requested for the PS mode of operation are well within the possibilities.

5.6 Work for third parties

The know-how obtained during the construction of MEA and its adjacent instrumentation could be put to use also for third parties. We report here in particular on the design and construction of beam handling

equipment for Daresbury (complete beam line) and CERN (septum magnet) and on the application of the NIKHEF-K cooling system design for a TF-R Tokamak in France.

5.6.1 Synchrotron radiation beam line at Daresbury (UK)

On behalf of Z.W.O., the Organisation for the Advancement of Pure Research, NIKHEF designed, built and tested equipment for experiments with synchrotron radiation at the Daresbury Laboratory. This equipment consists of two experimental stations, one for EXAFS and one for SAD/SAS experiments, beam transport lines and X-ray optics. A full description of the project can be found in the previous Annual Report. Part of the beam transport line, the front-end, was already delivered in May 1983. The remaining part of the hardware of the beam lines and most of the optics and the equipment for the experimental areas were shipped to Daresbury late 1983 and early 1984.

The lines contain a number of high precision instruments such as beam-defining slits, focussing mirrors and monochromators. These instruments have to operate in high vacuum and are remotely tuneable. They are housed in complex multiport vacuum vessels. Functional units of instruments are assembled on stiff but adjustable frames.

The conception of the experimental areas involved quite some effort. Because these areas have to serve many users they have to be as flexible as possible. In the SAD/SAS area, for instance, the positions of samples and detectors can shift over some six meters along the beam axis depending on the required beam spot size and the required detector image. The whole experimental bench has to swivel over an angle of 20^{o} horizontally and a few degrees vertically, depending on the chosen wave length. The settings have to be reproducable and stable within tenths of a mm. Because of the size of the project and the tight time schedule NIKHEF had to subcontract the manufacturing of some of the components; all assembly work and tests were done, however, by in-house manpower. Only the high resolution EXAFS monochromator was fully designed, manufactured and assembled by TPD (Technisch Physische Dienst) an organisation in Delft. Meanwhile, the front-end, the EXAFS and SAD beam lines with experimental areas have been installed by technicians of the Daresbury Laboratory. The beam pipes and vacuum vessels have been lead cladded for shielding purposes; commissionning of vacuum and safety control progressed such that shutters could be opened for the first time in May 1984. Synchrotron light was transmitted

successfully through the beam lines up to the beryllium windows; it appeared that all components were correctly aligned and that the full beam could be transported.

The high-resolution monochromator made by the TPD was tested with a conventional low power X-ray source by scanning through the Cu K_α spectrum lines. Two of the three crystal units showed the required energy resolution. The third unit, containing a doubly bend crystal is still outside specifications but will first be tested with full beam power. Commissioning of the experimental stations is planned during Fall 1984. It is expected that the first experiments will start end of this year. NIKHEF will continue to provide maintenance on the existing lines and also will assist Dutch users in preparing their equipment.

5.6.2 Septum magnet

For the second-generation antiproton collector project of CERN, a septum magnet has been designed (see fig. 5.9) with the following main features: maximum magnetic field of 1.1 Tesla to be achieved in a volume 1.6 m long by 0.11 m wide by 0.09 m high. In order to reduce the dissipated electric power from 250 kW to 500 W the magnet is to be used in pulsed operation (0.04 pps at 5 ms pulse width). The construction of the yoke has been simplified by employing rectangular stampings which will be glued together. A thin wedge will provide a rigid support for the coils under pulsed operating conditions. As a result of the design work a contract has been signed with CERN to fabricate the prototype septum magnet.

5.6.3 NIKHEF-K cooling system application

Based on the successful operation of the MEA cooling system a design has been made for FOM-Jutphaas involved in the Electron-Cyclotron Resonance Heating Project. The design dealt with the cooling system required for three 60 GHz gyrotrons (350 kW power level) and their associated modulators and transformer tanks. The ECRH project is associated with the TF-R Tokamak project at Fontenay-aux-Roses in France.

5.6.4 Mechanical design for ESRP

On invitation a NIKHEF-K technician has spent half a year at CERN to participate in the mechanical design study for the European

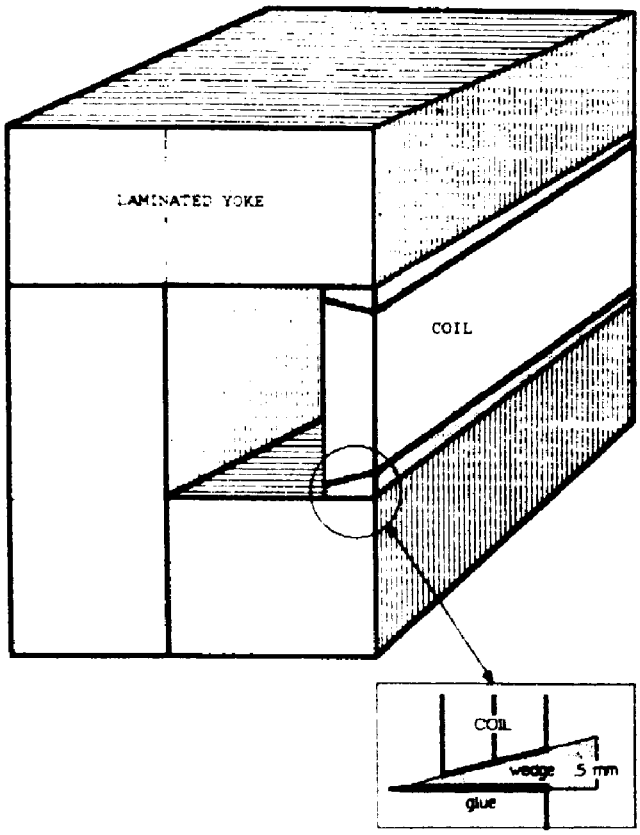

Fig. 5.9 Septum magnet.

Synchrotron Radiation Project (ESRP). Related with this work interest has been shown by ESRP for the NIKHEF-K computer program for designing large vacuum systems (see also section 5.7).

5.7 General technical activities

The technical departments are to a large extent involved in the work described in sections 5.2 through 5.6. A small part of their activities, however, is related with research requested to keep up to date with the latest technological developments. Some aspects of these activities are described below.

A computer program for designing large vacuum systems has been developed and tested on the Daresbury beam-line vacuum system. This program was also applied on the vacuum design of the European Synchrotron Radiation Machine. The results will be published in an ESRP-report. The program is based on the finite element method. Each vacuum part in the beam line (P_i, see fig. 5.10) is considered to be a system with its own pumping

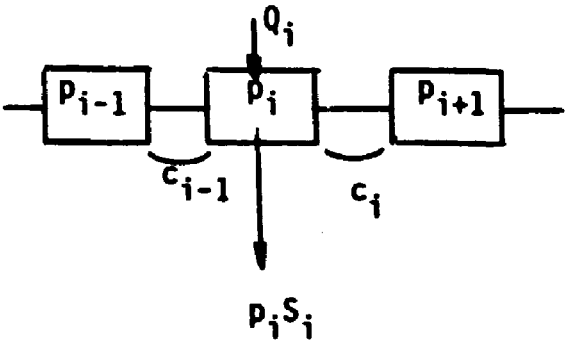

Fig. 5.10 Schematic set-up of the system.

speed, specific degassing potential (as a function of time) and conductance while also the influence of the neighbouring cells, P_{i-1} and P_{i+1} is considered. By combining these elements and correcting the conductances and pumping speeds as a function of the allowed residual gas composition, the total process from pump down to the final vacuum value of a total system can be simulated and optimized. A typical result is shown in fig. 5.11. Several laboratories (DESY, SLAC, CERN, Daresbury and Frascati) have shown their interest in the computer program.

A special proportional counter for the detection of electrons using a 20 µm thick stainless steel foil has been constructed. The cylindrical detector (Ø 10 x 200 mm) is butt welded by a pulsed microplasma apparatus. This welding technique is now also available for thin targets and thin exit foils required in the experimental halls.

A LISA personal workstation (from Apple), with bitmap graphics and mouse, has been installed. An experimental operator interface to the

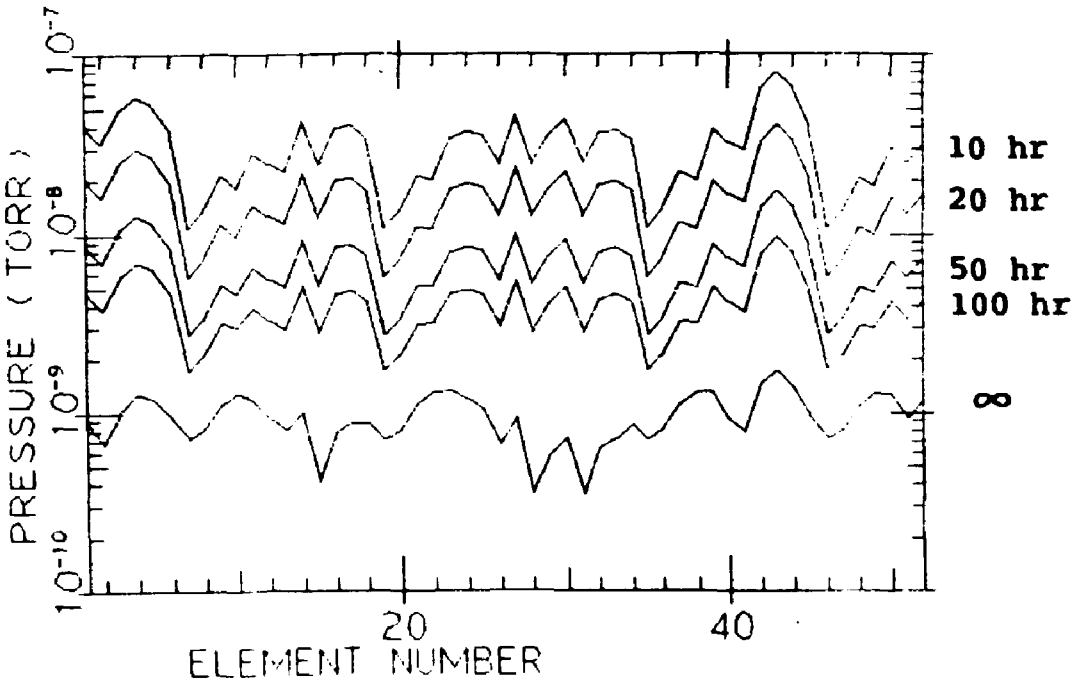

Fig. 5.11 Pressure contributions as a function of time as follows from the NIKHEF-K computer program for large vacuum systems.

accelerator control system has been developed in order to gain experience with modern ideas on man-machine interaction. This has resulted in a proposal for upgrading the operator console facility with systems based on the experimental version.

A start has been made with software support for the control of the accelerator on a pulse-to-pulse basis. As part of the accelerator hardware experiments, the independent control of two beams has been made possible.

In order to acquire experience with the application of the 8051 microcontroller this chip was used in the control electronics of an existing angle measurement demo system on a synchro-to-digital converter. Adaption of the synchro-output and the required scale, display, etc. are handled by software stored in the chips read only memory. Software development is done on the Intel PDS system.

The first multilayer printed circuit board of the time digitizer for time measurements with 0.5 ns resolution has been assembled and tested. The intensive use of computer simulation proved to be successful: no design or lay-out errors were found. The rather critical 100 k ECL impedance specifications were met. The second board allowing the first time resolution measurement is being produced; see fig. 5.12.

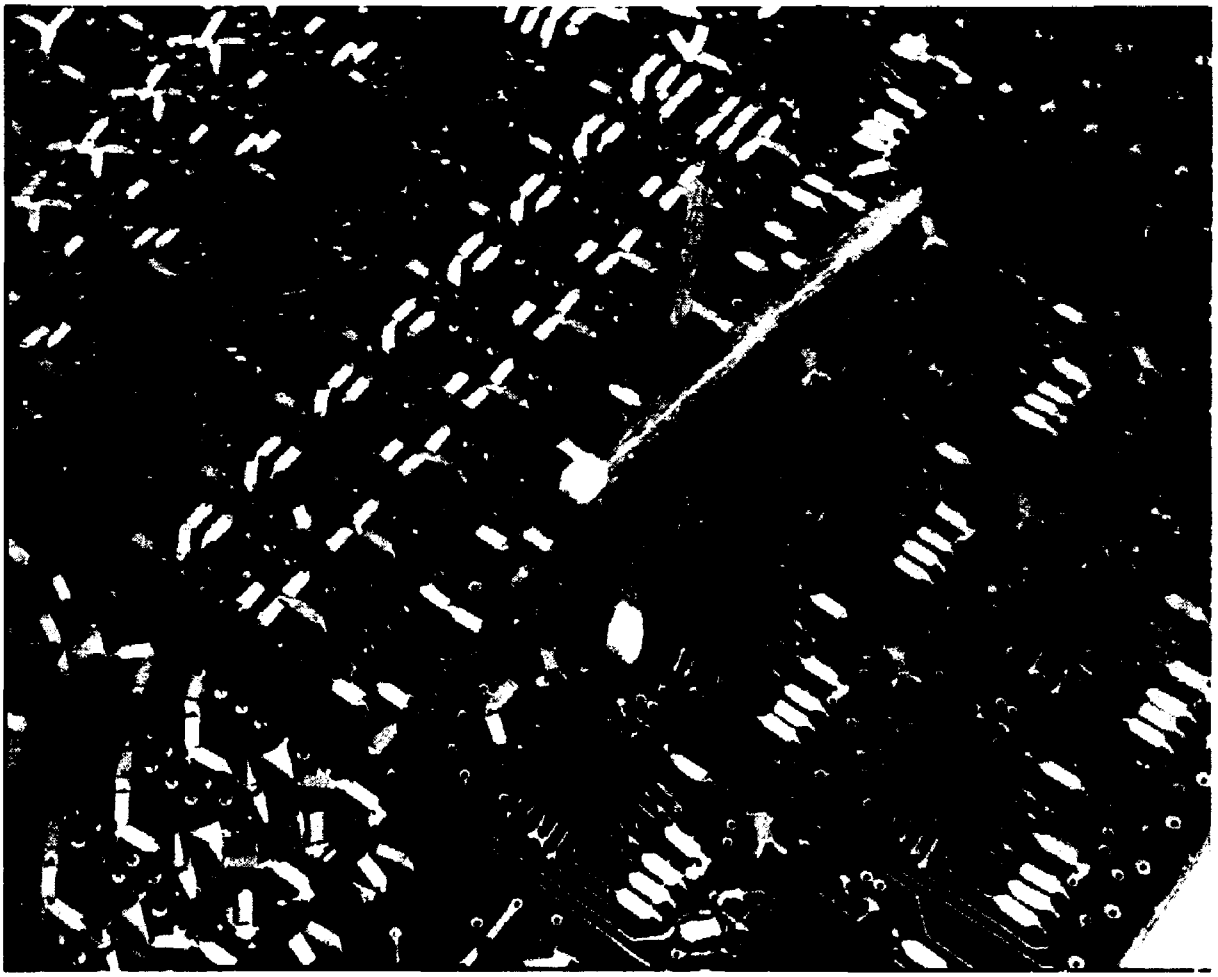

Fig. 5.12 Multilayer printed circuit board.

5.8 References

1. A.J.H. Donné *et al.*, Nucl. Instr. Meth. 224 (1984) 97
2. C. de Vries *et al.*, Nucl. Instr. Meth. 223 (1984) 1
3. J.H.J. Distelbrink *et al.*, Nucl. str. Meth. 220 (1984) 433
4. P.C. Dunn, Nucl. Instr. Meth. 224 (1984) 106
5. H. Postma, Nucl. Instr. Meth. 219 (1984) 292
6. NIKHEF-K proposal for UPDATE MEA, Amsterdam, July 1984

6 PUBLICATIONS

P. Barreau, M. Bernheim, J. Duclos, J.M. Finn, Z. Meziani, J. Morgenstern, J. Mougey, D. Royer, R. Saghai, D. Tarnowski, S. Turch-Chieze, M. Brussel, G.P. Capitani, E. De Sanctis, S. Frullani, F. Garibaldi, D.B. Isabelle, E. Jans, I. Sick, P.D. Zimmerman,
Deep-inelastic electron scattering from carbon,
Nucl. Phys. A402 (1983) 515

S.K. Platchkov, J.M. Cavedon, J.C. Clemens, B. Frois, D. Goutte, M. Huet, P. Leconte, X.-H. Phan, S. Williamson, I. Sick, P.K.A. de Witt Huberts, L. Lapikās, B. Desplanques, J.F. Mathiot,
The magnetic form factor of ^{51}V at very high momentum transfer,
Phys. Lett. 131B (1983) 301

H. Postma, J.P. Boogaard, P.H.M. Keizer, L. Prins, P.K.A. de Witt Huberts,
A higher power liquid ^{3,4}He target system for electron scattering experiments,
Nucl. Instr. and Meth. 219 (1984) 292

J.H.J. Distelbrink, E. Kok, H. Blok, J.L. Visschers, P.K.A. de Witt Huberts,
A fast and flexible focal-plane detection system for electron scattering experiments,
Nucl. Instr. and Meth. 220 (1984) 433

C. de Vries, C.W. de Jager, P.K.A. de Witt Huberts,
Dieper graven in de kernmaterie,
FOM Jaarboek 1982. Stichting voor Fundamenteel Onderzoek der Materie, 167

C. de Vries, C.W. de Jager, L. Lapikās, G. Luijckx, R. Maas, H. de Vries, P.K.A. de Witt Huberts,
The 500 MeV electron-scattering facility at NIKHEF-K,
Nucl. Instr. and Meth. 223 (1984) 1

L.T. van der Bijl, H. Blok, H.P. Blok, R. Ent, J. Heisenberg, O. Schwentker, A. Richter, P.K.A. de Witt Huberts,
Electro-excitation of the 1^+ state at E_x = 3.486 MeV in ^{88}Sr,
Nucl. Phys. A423 (1984) 365

A.J.H. Donné, G. van Middelkoop, L. de Vries, L. Lapikās, J.B. van der Laan, C. de Vries, J.G. Noomen,
The 180° electron-scattering facility at NIKHEF-K,
Nucl. Instr. and Meth. 224 (1984) 97

P.C. Dunn,
A charged-pion detection system with large electron suppression,
Nucl. Instr. and Meth. 224 (1984) 106

C.J. Martoff, J.A. Bistirlich, C.W. Clawson, K.M. Crowe, M. Koike, J.P. Miller, S.S. Rosenblum, W.A. Zajc, H.W. Baer, A.H. Wapstra, G. Strassner, R. Truöl,
Spin flip-transitions in ^{13}C and ^{19}F probed with the (π^-,γ) reaction,
Phys. Rev. C27 (1983) 1621

J.F.M. d'Achard van Enschut, J.B.R. Berkhout, W. Duinker, C.W.E. van Eijk, W.H.A. Hesselink, T. Johansson, T.J. Ketel, J.H. Koch, J. Konijn, C.T.A.M. de Laat, W. Lourens, G. van Middelkoop, W. Poeser,
Anomalous strong interaction shifts and widths of the 3d state in pionic Pt and Au,
Phys. Lett. 136B (1984) 24

F.W.N. de Boer, R. van Dantzig, M. Daum, J. Jansen, P.J.S. Watson, L. Felawka, C. Grab, A. van der Schaaf, T. Kozloswki, J. Martino, A.I. Smirnov,
Search for bound states of neutrons and negative pions,
Phys. Rev. Lett. 53 (1984) 423

J.H. Koch, E.J. Moniz,
Coherent π^0 photoproduction at intermediate energy,
Phys. Rev. C27 (1983) 751

A. Suzuki, Y. Nogami, N. Ohtsuka,
Pion-nucleon scattering: the P_{11} channel,
Nucl. Phys. A395 (1983) 301

H. Sagawa, Nguyen Van Giai,
Transition charge and current densities of collective isoscalar quadrupole states in ^{208}Pb,
Phys. Lett. 127B (1983) 393

T. de Forest, Jr.,
The relative Coulomb sum rule for electron scattering in the independent-particle model,
Nucl. Phys. A414 (1984) 347

J.H. Koch, E.J. Moniz, N. Ohtsuka,
Nuclear photoabsorption and Compton scattering at intermediate energy,
Ann. Phys. 154 (1984) 99

C. Gaarde, J.S. Larsen, H. Sagawa, N. Ohtsuka, J. Rapaport, T.N. Taddeucci, C.D. Goodman, C.C. Foster, C.A. Goulding, D. Horen, T. Masterson, E. Sugarbaker,
Spin-dipole strength in ^{12}N,
Nucl. Phys. A422 (1984) 189

T. de Forest, Jr.,
Electromagnetic interactions in the σ-ω model,
Phys. Rev. Lett. 53 (1984) 895

H.J. Broxterman, A. van Langevelde, C.N.M. Bakker, H. Boer, J.G. Journée de Korver, F.M. Kaspersen, H.M. Kakebeeke-Kemme, E.K.J. Pauwels,
Incorporation of (^{125}I)-5-Iodo-2-thiouracil in cultured hamster, rabbit and human melanoma cells,
Cancer Research 43 (1983) 1316

G.A. Brinkman,
Chemistry of energetic chlorine atoms,
Int. J. Appl. Rad. Isot. 34 (1983) 985

J.Th. Veenboer, G.A. Brinkman,
The effect of high radiation doses on the reactions of recoil Cl atoms with arenes,
Radiochimica Acta 33 (1983) 1

G.W.M. Visser, E.L. Diemer,
Inorganic astatine chemistry: Formation of complexes of astatine,
Radiochimica Acta 33 (1983) 145

D. de Jong, G.A. Brinkman, B.W. van Halteren,
Reactions of energetic $^{76,77,82}Br$ atoms with (halo)methanes,
Int. J. Appl. Rad. Isot. 34 (1983) 1597

E. Roduner, G.A. Brinkman, P.W.F. Louwrier,
Rate constants for the reactions of cyclohexadienyl type radicals with quinones,
Hyperfine Interactions 17-19 (1984) 797

J. Visser,
Radioactiviteit. Radioactiviteit als natuurkundig verschijnsel. Feiten en misverstanden. Gevaarlijk of niet?
Aula Pocket 730. Het Spectrum, Utrecht 1984

D. de Jong, G.A. Brinkman, B.W. van Halteren,
Chemical effects of the $^{76,77}Kr \rightarrow {}^{76,77}Br$ decay in gaseous propane and cyclopropane,
Radiochimica Acta 34 (1984) 93

B.S.M. Rao, G.A. Brinkman, J.Th. Veenboer,
Reactions of recoil T atoms with chloroanilines,
Radiochimica Acta 35 (1984) 57

B.S.M. Rao, G.A. Brinkman, J.Th. Veenboer,
Reactions of recoil Cl atoms with chloroanilines,
Radiochimica Acta 35 (1984) 61

P. Polak, L. Lindner,
Liquid scintillation beta spectroscopy on ^{32}Si,
Radiochimica Acta 35 (1984) 23

E. Roduner, G.A. Brinkman, P.W.F. Louwrier,
Muonium-substituted organic free radicals in liquids. Isomer distributions and end-of-track radiolytical processes determined from studies of cyclohexadienyl radicals derived from substituted benzenes,
Chem. Phys. 88 (1984) 143

G.W.M. Visser, B.W. van Halteren, J.D.M. Herscheid, G.A. Brinkman, A. Hoekstra,
Reaction of acetyl hypofluorite with aromatic mercury compounds: a new selective fluorination method,
J. Chem. Soc., Chem. Commun. (1984) 655

J. Korsse, P.W.F. Louwrier, J.N. Louwen, A. Oskam,
Redox potentials of the aquo, cyano and EDTA complexes of some transition metal ions by CNDO calculations,
Inorganica Chimica Acta 88 (1984) 67

E. Roduner, G.A. Brinkman, P.W.F. Louwrier,
Relative rate constants for the formation of muonic radicals in liquid aromatic systems,
Hypefine Interactions 17-19 (1984) 803

G. Bortels, G.A. Brinkman, W.B. Mann,
Preface in 'Alpha-particle-spectrometry techniques and applications'.
Proc. of a seminar on the Int. committee for Radionuclide Metrology (ICRM),
Geel (Belgium), October 14, 1981,
Int. J. Appl. Rad. Isot. 35 (1984) v

J. Visser,
Two papers in daily newspaper 'De Volkskrant'

P.J.T. Bruinsma, F.B. Kroes, L.H. Kuijer, J.G. Noomen, J.B. Spelt, A.G.C. Vogel,
The 500 MeV, 2½ % duty factor linear electron accelerator (MEA),
IEEE Trans. Nucl. Sci. NS-30 (1983) 3599

7 PH.D. THESES

None.

8 INVITED TALKS

Summerschool on Symmetries in Nuclear Structure, Dronten, August 16-28, 1982,
J.M. Bailey,
Parity non-conservation in muonic helium atoms

International School of Intermediate Energy Nuclear Physics, San Miniato,
August 19-29, 1983,
J.H. Koch,
The delta-hole approach to intermediate energy photonuclear reactions

International Symposium on Highly Excited States and Nuclear Structure,
Orsay, September 5-8, 1983,
L. Lapikás, P.K.A. de Witt Huberts,
Excitation of nuclear hole states by the (e,e'p) reaction

Workshop on Perspectives in Nuclear Physics at Intermediate Energies,
Triëste, October 13-15, 1983,
C. de Vries,
High precision (e,e') and (e,e'p) experiments at Amsterdam

Miniconference on 'Coincidence reactions with electromagnetic probes',
Amsterdam, November 14-15, 1983,
T. de Forest, Jr.,
Ambiguities in the reaction mechanism for (e,e'N)

P.K.A. de Witt Huberts,
On-going work at NIKHEF-K

Séminaire Générale, Saclay, January 13, 1984,
P.K.A. de Witt Huberts,
Progress in high-resolution (e,e'p) experiments

International School on Nuclear Physics, Erice, April 8-20, 1984,
P.K.A. de Witt Huberts,
High momentum components and (e,e'p) reactions

Journées d'Etudes sur la Chimie des Radiations, Mont Sainte-Odile, June 12-15, 1984,
P.W.F. Louwrier,
Spectroscopie de muons

Europhysics Conference on Nuclear Reactions, Crete, June 24-July 1, 1984,
C. de Vries,
High-resolution coincidence experiments with intermediate energy electron beams

Gordon Conference on Photonuclear Reactions, Helderness, New Hampshire, July 16-20, 1984,
E. Jans,
High-resolution (e,e'p) experiments at NIKHEF

BUGT Workshop, MIT, Cambridge, July 23-25, 1984,
P.K.A. de Witt Huberts,
High resolution (e,e'p) experiments at NIKHEF-K

T. de Forest, Jr.,
Nuclear medium effects and (e,e'N)

9 CONTRIBUTIONS TO CONFERENCES

Proceedings of the Nuclear Chemistry and Radiochemistry Symposium, Banares Hindu University, Varanasi, November 3-7, 1981,
G.A. Brinkman, P.W.F. Louwrier,
Reactions of muonium with aromatic compounds

Workshop on medium-energy interactions in nuclear physics, Pavia, September 28-30, 1982,
P. Barreau *et al.*, Nuovo Cim. 76A (1983) 288,
Exclusive electrodisintegration of few-body nuclear systems

P. Barreau *et al.*, Nuovo Cim. 76A (1983) 361
Coulomb sum rule on ^{12}C

The 5th Nordic Meeting on Intermediate and High Energy Nuclear Physics, Geilo, January 10-14, 1983,
J.P. Bocquer *et al.*,
Production of hypernuclei in $\bar{p}$ annihilation at rest

The 7th International Congress of Radiation Research, Amsterdam, July 3-8, 1983,
J. Korsse, G.A.J. Leurs, P.W.F. Louwrier,
Radiolysis of H_4EDTA and $CuEDTA^{2-}$ in aqueous solution

J.Th. Veenboer, G.A. Brinkman,
Selectivity in ^{32m}Cl-for-Cl exchange in substituted chlorobenzenes

International Conference on Nuclear Physics, Florence, Aug. 29-Sept. 3, 1983,
P. David *et al.*,
Prompt and delayed muon induced fission in ^{238}U and ^{237}Np

R.J.M. Bonnie *et al.*,
Electron scattering of $^{104,106,108,110}Pd$ and ^{196}Pt and the interacting boson approximation

A.J.H. Donné *et al.*,
Elastic magnetic electron scattering from ^{19}F and ^{49}Ti

C.W. de Jager *et al.*,
An electron scattering study of ^{39}K

International Symposium on Highly Excited States and Nuclear Structure, Orsay, Sept. 5-8, 1983,
L.T. van der Bijl *et al.*,
Electro-excitation of the 1^+ state at 3.486 MeV in ^{88}Sr

Ninth International Vacuum Congress and Fifth International Conference on Solid Surfaces, Madrid, Sept. 26-30, 1983,
A.P. Kaan,
The vacuum system of MEA

Netherlands Chemical Society Meeting, section Radiochemistry and Radiation Chemistry, Groningen, 28 oct. 1983,
L. Lindner,
Chronologie van meteorieten

P. Polak,
^{32}Si vervalskarakteristieken

Netherlands' Physical Society Meeting, Petten, Nov. 11, 1983,
P. David *et al.*,
Prompt and delayed muon-induced fission of ^{235}U, ^{238}U, ^{237}Np, ^{242}Pu and ^{244}Pu

Netherlands' Physical Society Meeting, Amsterdam, April 26, 1984,
P.C. Dunn *et al.*,
The photopion reaction $^{13}C(\gamma,\pi^-)^{13}N$ at pion kinetic energy of 50 MeV

S. Müller *et al.*,
High-resolution inelastic electron scattering and the isoscalar nature of the M1-transition to the 5.846 MeV state in ^{208}Pb

R.J.M. Bonnie *et al.*,
Electroexcitation of natural parity states in ^{11}B

H.P. Blok *et al.*,
Electroexcitation of the Yrast 2^+, 4^+, 6^+ states in ^{50}Ti

W.T.A. Borghols *et al.*,
Electron scattering from ^{196}Pt

H. d'Achard van Enschut *et al.*,
Anomalous shifts and widths in pionic atoms of Mg, Al, Pt, Au

W. Duinker *et al.*,
An anti-Compton multi-detector system for gamma-ray spectroscopy

J. van den Brand *et al.*,
High-resolution (e,e'p) coincidences experiments at NIKHEF-K

A.J.H. Donné *et al.*,
Elastic magnetic electron scattering from ^{19}F and ^{49}Ti

R. Ent *et al.*,
Excitation of stretched states in the $^{51}V(^{3}He,d)^{52}Cr$ reaction

International Workshop on Interacting Boson-Boson and Boson-Fermion Systems,
Gull Lake, Michigan, May 28-30, 1984
C.W. de Jager,
Inelastic electron scattering as a test of the IBA

10 SEMINARS AT NIKHEF-K

Th. Bauer (SIN, Villigen),
The pion, the delta and the nucleus

G.A. Brinkman (NIKHEF-K),
Gestopte π^-, μ^- in verbindingen

B.A. Brown (Michigan State University),
Corrections to M1 and Gamov-Teller operators

R. van Dantzig (NIKHEF-K),
On anomalous nuclear systems

P. Decowski (KFA, Jülich),
Fast nucleon emission in high-energy alpha scattering from heavy nuclei

W.H. Dickhoff (University Tübingen),
Pions, nucleons and isobars: a selfconsistent treatment

W. Duinker (NIKHEF-K),
Pionic atoms: absorption and double charge exchange

H.L. Hagedoorn (TH, Eindhoven),
Versnelling, energievariatie en energiedefinitie in circulaire versnellers

W.H.A. Hesselink (Free University, Amsterdam),
Neutron emission following nuclear muon capture

R.S. Hicks (University of Massachusetts),
Isospin mixing determination from inelastic pion scattering and the charge-dependence of the strong interaction

Ch.E. Hyde-Wright (MIT, Cambridge),
Inelastic electron scattering to stretched particle-hole states in ^{16}O

C.W. de Jager (NIKHEF-K),
Electron scattering tests of the IBA and magnetic M1 transitions

J. de Kam (Fokker B.V.),
The special role of the pion

T.J. Ketel (NIKHEF-K; Free University, Amsterdam),
Experiments with hypernuclei

J.C. Kluyver (NIKHEF-H),
Antiproton physics at LEAR

J. Konijn (NIKHEF-K),
Recent experiments with pionic atoms

A. Landé (State University, Groningen),
Theory of quantum fluids and why they are of interest to nuclear physics

B. Metsch (Erlangen),
Pion production in proton-nucleus collisions: a microscopic model

T. Miczaika (University Bonn),
Polarization experiments with photons in the nucleon resonance region

P.J. Mulders (MIT, Cambridge),
Hitting quarks in the nucleus

A.M. Nathan (University of Illinois),
Photon scattering studies at Illinois

Nguyen Van Giai (Orsay),
Response function method applied to giant resonances

B. Norum (University of Virginia),
The continuous electron beam accelerator facility

A.M. Selig (NIKHEF-K),
An (e,e'p) study of effective operators in the 1f/2p shell

O. Scholten (Michigan State University),
Microscopic calculations for the IBA-model

T. Suzuki (NIKHEF-K),
Magnetic properties of nuclei and the Landau-Migdal parameter

T. Takaki (NIKHEF-K),
The delta-nucleon interaction and pion-nucleus inelastic scattering

L. Tiator (University Mainz),
Pion photoproduction on light nuclei

J. Verbaarschot (University Heidelberg),
Chaos and randomness in nuclear physics

A.H. Wapstra (NIKHEF-K),
De eerste Nobelprijzen in astrofysica

A.H. Wapstra (NIKHEF-K),
Atoommassatabellen 1983

11 SEMINARS PRESENTED BY STAFF MEMBERS OUTSIDE NIKHEF-K

H.P. Blok, KVI,
Quenching of transverse excitations in inelastic electron scattering

H.P. Blok, Kyushu University, Fukuoka,
Two-step processes in the $^{208}Pb(p,t)^{206}Pb$ reaction and new results from (e,e'p) and (e,e'd) experiments at NIKHEF-K

H.P. Blok, Institute for Physical and Chemical Research, Tokyo, and Laboratory of Nuclear Science, Tohoku University, Sendai,
Recent (e,e') and (e,e'p) results at the Amsterdam electron accelerstor

C.W. de Jager, University of Illinois, Urbana,
Inelastic electron scattering as a test of the IBA

C.W. de Jager, University of Mainz,
Inelastic electron scattering as a test of the shell model and the interacting boson approximation

J.H. Koch, University of Utrecht,
Nuclear photoabsorption and Compton scattering at intermediate energy

J.H. Koch, University of Groningen,
Photonuclear reactions at intermediate energies

L. Lindner, University of Utrecht,
Over meteorieten; een inleiding

L. Lindner, Teylers Museum, Haarlem,
Meteorieten: herkenning, herkomst, ontstaan en belang voor de wetenschap

G. van Middelkoop, University of Groningen and University of Utrecht,
Het binnenste van atoomkernen

A.M. Selig, RPI, Troy; NBS, Washington; University of Saskatchewan; University of Massachusetts; MIT, Cambridge,
An (e,e') study of effective electromagnetic operators in the 1f-20 shell